

# New non-arithmetic complex hyperbolic lattices

Martin Deraux, John R. Parker, Julien Paupert

May 15, 2015

## Abstract

We produce a family of new, non-arithmetic lattices in  $\mathrm{PU}(2, 1)$ . All previously known examples were commensurable with lattices constructed by Picard, Mostow, and Deligne–Mostow, and fell into 9 commensurability classes. Our groups produce 5 new distinct commensurability classes. Most of the techniques are completely general, and provide efficient geometric and computational tools for constructing fundamental domains for discrete groups acting on the complex hyperbolic plane.

## 1 Introduction

The general context of this paper is the study of lattices in semisimple Lie groups and their classification. In what follows,  $X$  denotes an irreducible symmetric space of non-compact type, and  $G$  denotes its isometry group. Recall that  $X$  is a homogeneous space  $G/K$  with  $K$  a maximal compact subgroup of  $G$ , and up to scale, it carries a unique  $G$ -invariant Riemannian metric.

A subgroup  $\Gamma \subset G$  is called a lattice if  $\Gamma \backslash G$  has finite Haar measure (equivalently, if  $\Gamma \backslash X$  has finite Riemannian volume for the invariant metric on  $X$ ). Mostow-Prasad rigidity says that, for most symmetric spaces, a given lattice  $\Gamma$  in  $G$  admits a unique discrete faithful representation into  $G$  (unique in the sense that all such representation are conjugate in  $G$ ). In order for this to hold, the only case to exclude is  $X = \mathbf{H}_{\mathbb{R}}^2$  (equivalently  $G = \mathrm{PSL}_2(\mathbb{R})$ ), where lattices are known to admit pairwise non-conjugate continuous deformations.

The discreteness assumption in the statement of the Mostow-Prasad rigidity theorem cannot be removed, since Galois automorphisms sometimes produce non-discrete representations that are clearly faithful and type-preserving (see the non-standard homomorphisms constructed in [Mos80], and also Section 6.2 of the present paper). This is related to the notion of arithmeticity of lattices, which we now briefly recall.

There is a general construction of lattices, obtained by taking integer matrices in the set of real points of linear algebraic groups defined over  $\mathbb{Q}$ ; this is a special case of the more general notion of arithmetic group, where one considers lattices commensurable with the image of an integral group under surjective homomorphisms with compact kernel (see [Mar91] for instance). Recall for further reference that subgroups  $\Gamma_1$  and  $\Gamma_2$  of a group  $G$  are commensurable if there is a  $g \in G$  such that  $\Gamma_1 \cap g\Gamma_2g^{-1}$  has finite index in both  $\Gamma_1$  and  $g\Gamma_2g^{-1}$ .

Arithmetic groups are classified, and they can be understood (up to commensurability) from purely number-theoretical data (see [Wei60], [Tit66]). Indeed, it follows from rigidity that any lattice in a simple real Lie group not isomorphic to  $\mathrm{PSL}_2(\mathbb{R})$  is defined over a number field, and semisimple groups over arbitrary number fields can be classified in a way similar to the well known classification of semisimple groups over  $\mathbb{Q}$  (one uses Dynkin diagrams

with a symmetry corresponding to the action of the Galois group of the number field). The arithmeticity condition says that the lattice is given up to commensurability by taking the corresponding  $\mathbb{Z}$ -points in the group, hence there are only countably many arithmetic lattices (since there are only countably many number fields).

It follows from work of Margulis [Mar75], together with work of Corlette [Cor92] and Gromov-Schoen [GS92], that most lattices are arithmetic; given the discussion in the previous paragraph, this means that there is a satisfactory classification of lattices in *most* semisimple Lie groups. More specifically, if the isometry group  $G$  of a symmetric space  $X = G/K$  of non-compact type contains a non-arithmetic lattice, then  $X$  can only be  $\mathbf{H}_{\mathbb{R}}^n$  or  $\mathbf{H}_{\mathbb{C}}^n$  for some  $n$ ; in other words, up to index 2,  $G$  can only be  $\mathrm{PO}(n, 1)$  or  $\mathrm{PU}(n, 1)$ .

Real hyperbolic space  $\mathbf{H}_{\mathbb{R}}^n$  is the model  $n$ -dimensional negatively curved space form, i.e. it is the unique complete simply connected Riemannian manifold of constant negative curvature (we may assume that constant is  $-1$ ). Similarly,  $\mathbf{H}_{\mathbb{C}}^n$  is the model negatively curved *complex* space form, in the sense it is the unique complete, simply connected Kähler manifold whose holomorphic sectional curvature is a negative constant, which we may assume is  $-1$ . With that normalization, the real sectional curvatures of  $\mathbf{H}_{\mathbb{C}}^n$  vary between  $-1$  and  $-1/4$ . This makes complex hyperbolic spaces very different from real hyperbolic ones (apart from the coincidence that  $\mathbf{H}_{\mathbb{C}}^1$  is isometric to  $\mathbf{H}_{\mathbb{R}}^2$ ).

In the real hyperbolic case, the hybridization procedure described by Gromov and Piatetski-Shapiro [GPS88] allows the construction of (infinitely many commensurability classes of) non-arithmetic lattices in  $\mathrm{PO}(n, 1)$  for any  $n \geq 2$ . In  $\mathrm{PU}(n, 1)$ , it is not clear how to make sense of the construction of such hybrids, and the construction of non-arithmetic lattices in the complex hyperbolic setting is a longstanding challenge.

In fact, for  $n \geq 2$ , only a handful of examples are known. The first ones were constructed by Mostow [Mos80], who showed that some complex reflection groups are non-arithmetic lattices in  $\mathrm{Isom}(\mathbf{H}_{\mathbb{C}}^2)$  (the analogous statement was well known for real reflection groups in  $\mathrm{Isom}(\mathbf{H}_{\mathbb{R}}^n)$  for low values of  $n$ , see [Vin68]).

Complex hyperbolic manifolds are of special interest in complex geometry, because of the extremal properties of their ratios of Chern numbers. Indeed, compact complex hyperbolic manifolds are complex manifolds of general type (i.e. their Kodaira dimension is maximal), and they have the same ratios of Chern numbers as complex projective space  $\mathbf{P}_{\mathbb{C}}^n$ , which is the compact symmetric space dual to  $\mathbf{H}_{\mathbb{C}}^n$  (this is explained by the Hirzebruch proportionality principle). In fact, any compact complex manifold of general type that realizes equality in the Miyaoka-Yau inequality  $(-1)^n c_1^n \leq (-1)^n \frac{2n+2}{n} c_1^{n-2} c_2$  is biholomorphic to a quotient of  $\mathbf{H}_{\mathbb{C}}^n$  (this is a corollary of the Calabi conjecture, proved by Aubin and Yau). In the special case  $n = 2$ , the corresponding equality reads  $c_1^2 = 3 c_2$ , and it plays an important role in so-called surface geography.

In principle, this characterization should give a simple way to produce many complex hyperbolic manifolds, but so far this has been successful in very few cases, only in dimension 2. A spectacular example was obtained by Mumford, using sophisticated techniques from algebraic geometry to produce a fake projective plane, i.e. a compact surface with the same Betti numbers as  $\mathbf{P}_{\mathbb{C}}^2$  but not biholomorphic to it. The fundamental group of any such surface is infinite, and admits a faithful and discrete representation into  $\mathrm{PU}(2, 1)$ , even though it took a long time for this representation to be made somewhat explicit for Mumford's example (see [Kat08]). It is now well known that fake projective planes must be arithmetic (see [Kli03] and [Yeu04]), and this was used to classify them (see [PY07] and [CS10]).

Hirzebruch systematically explored coverings of  $\mathbf{P}_{\mathbb{C}}^2$  branched along configurations of lines,

and found all the ball quotients that could be produced in this way, see [Hir83], [BHH87]. The arithmetic properties of Hirzebruch ball quotients were studied later (see [Shv92]). It turns out that all the non-arithmetic examples can also be obtained from the Deligne-Mostow construction [DM86].

Our construction is closer in spirit to Mostow's approach in [Mos80]. We start with some well-chosen complex reflection groups in  $\mathrm{PU}(2,1)$  and show that they are lattices by constructing explicit fundamental domains (the domains are shown to be fundamental domains by applying the Poincaré polyhedron theorem).

The application of this general strategy in the context of complex hyperbolic space is difficult and subtle, as can be seen in the difficulties in Mostow's proof that were analyzed in [Der05]. It has been successfully carried out in several places, but always for groups closely related to Mostow's (see [DFP05], [Par06], [FP06], [Zha12]). For the groups we consider in this paper, the previously used techniques seem difficult to implement (for instance, the Dirichlet domains we studied in [DPP11] have extremely complicated combinatorial structure).

Mostow's lattices turn out to be closely related to monodromy groups of hypergeometric functions studied a century earlier by Picard [Pic81]. The hypergeometric interpretation was extended by Deligne and Mostow [DM86], who showed that these monodromy groups produce a handful of non-arithmetic lattices in  $\mathrm{PU}(2,1)$ , and a single one in  $\mathrm{PU}(3,1)$  (which is currently the only known non arithmetic lattice in  $\mathrm{PU}(n,1)$  with  $n \geq 3$ ).

Note that the above hypergeometric monodromy groups can also be interpreted as modular groups for moduli spaces of weighted points on  $\mathbf{P}_{\mathbb{C}}^1$ , or equivalently moduli spaces of flat metrics on the sphere with prescribed cone angle singularities (see [Thu98]). The few other examples of moduli spaces that are known to admit a complex hyperbolic uniformization (see [ACT02], [Kon00] for instance) produce arithmetic lattices.

The commensurability relations between Deligne-Mostow lattices were studied in detail in [Sau90] and [DM93], then more recently in [KM12] and [McM13]. In particular, it turns out that non-arithmetic Deligne-Mostow lattices in  $\mathrm{PU}(2,1)$  fall into exactly nine commensurability classes.

The main result of this paper produces five new commensurability classes of non-arithmetic lattices in  $\mathrm{PU}(2,1)$ . They are the first such groups to be constructed since the work of Deligne and Mostow.

We consider groups generated by two isometries, namely a complex reflection and a regular elliptic element of order 3. For historical reasons (see [Mos80]), these two isometries will be denoted respectively by  $R_1$  and  $J$ ; we will also denote  $R_2 = JR_1J^{-1}$  and  $R_3 = JR_2J^{-1}$ . It turns out that conjugacy classes of such groups are parametrized by the pair  $(\psi, \tau)$ , where  $\psi$  is the rotation angle of  $R_1$  and  $\tau$  is the trace of  $R_1J$ . There are restrictions on the pair  $(\psi, \tau)$  for a group with a given angle/trace pair to exist (see the discussion in [PP09]); when it exists, we denote the corresponding group by  $\Gamma(\psi, \tau)$ .

Following previous work on complex reflection groups (see [Mos80], [Sch02], [Der06], [Tho10]), one expects such groups to be lattices only when well-chosen short words in the generators are elliptic. For instance, for (4,4,4)-triangle groups, Schwartz conjectured that the discreteness was controlled by the word  $1232$ , in the sense that the group should be discrete if and only if  $R_1R_2R_3R_2$  is loxodromic, parabolic, or elliptic of finite order (here the  $R_j$  denote the generating complex reflections). The (4,4,4)-triangle group where  $R_1R_2R_3R_2$  is elliptic of order  $n$  (more specifically has eigenvalues  $1, e^{\pm 2\pi i/n}$ ) is referred to as the  $(4,4,4;n)$ -triangle group. This seems to have infinite covolume for  $n > 5$ , see for instance the group in [Sch03], which is the  $(4,4,4;7)$ -triangle group. On the other hand, it was observed in [Der06] that

the  $(4, 4, 4; 5)$ -triangle group is a lattice. When considering  $(4, 4, 4; n)$ -triangle groups, an important distinction between  $n = 5$  and  $n \geq 6$  is the type of the isometry  $R_1 R_2 R_3 = (R_1 J)^3$ , which is loxodromic for  $n \geq 6$ , but elliptic of order 10 when  $n = 5$ . It is then natural to expect the ellipticity of the words 123 and 1232 to control the property of triangle groups to be a lattice. This is confirmed for some other triangle groups by the results in [Tho10].

This motivated us to study groups  $\Gamma(\psi, \tau)$  where  $R_1 R_2$  and  $R_1 J$  are both elliptic of finite order (in fact we allow  $R_1 R_2$  to be parabolic as well, but not  $R_1 J$ ). The groups  $\Gamma(\psi, \tau)$  satisfying these conditions were listed by the last two authors (see [Par08] and [PP09]); the key ingredient in their arguments is a result of Conway and Jones [CJ76] that classifies rational relations between roots of unity.

We proved in [DPP11] that only finitely many of these groups can be lattices. We also gave a conjectural list of ten groups that we strongly suspected to be lattices, corresponding to three special choices of  $\tau$ , namely

$$\sigma_1 = -1 + i\sqrt{2}, \quad \bar{\sigma}_4 = \frac{-(1 + i\sqrt{7})}{2}, \quad \sigma_5 = e^{-\pi i/9} \frac{i\sqrt{3} + \sqrt{5}}{2},$$

for some well-chosen rotation angles  $\psi$ . The main result of this paper is the following:

**Theorem 1.1** *Let  $\tau = -(1 + i\sqrt{7})/2$ , and let  $p \in \mathbb{Z}$ . Then  $\Gamma(2\pi/p, \tau)$  is a lattice in  $\text{PU}(2, 1)$  if and only if  $p = 3, 4, 5, 6, 8$  or  $12$ , and that lattice is*

1. *cocompact if and only if  $p = 3, 5, 8$  or  $12$ ;*
2. *arithmetic if and only if  $p = 3$ ;*

*Moreover, the six lattices lie in distinct commensurability classes, and they are not commensurable to any Deligne-Mostow lattice.*

The values of  $p$  in the theorem may seem mysterious, but one can rephrase the theorem as an integrality condition, in the vein of the Picard integrality condition (see [DM86] for instance). Indeed (see section 4.3),  $(R_1 R_2)^2$  is a complex reflection with angle  $2\pi/c$ , and  $(R_1 R_2 R_3 R_2^{-1})^3$  is a reflection with angle  $2\pi/d$ , where:

$$c = 2p/(p - 4); \quad d = 2p/(p - 6).$$

The values of  $p$  in the theorem are precisely those for which both  $c$  and  $d$  are integers (or infinite).

Non-arithmeticity of these groups was proved in [Pau10]. For completeness, we prove that the five commensurability classes are new *and distinct* in Section 6, and recall the proof of non-arithmeticity in Section 6.2; see also [Pau10]. The fact that the groups are non-discrete for all other integer values of  $p$  was proved in [DPP11].

We prove that the six groups that appear in Theorem 1.1 are lattices by constructing explicit fundamental polyhedra for their respective actions on  $\mathbf{H}_{\mathbb{C}}^2$ , using Theorem 3.2. By this method we obtain presentations of the lattices:

**Theorem 1.2** *Let  $\tau = -(1 + i\sqrt{7})/2$ . For  $p = 3, 4, 5, 6, 8, 12$  the group  $\Gamma(2\pi/p, \tau)$  has the presentation:*

$$\left\langle R_1, R_2, R_3, J \mid \begin{array}{l} R_1^p = J^3 = (R_1 J)^7 = id, \quad R_2 = J R_1 J^{-1}, \quad R_3 = J^{-1} R_1 J, \\ (R_1 R_2)^2 = (R_2 R_1)^2, \quad (R_1 R_2)^{4p/(p-4)} = (R_1 R_2 R_3 R_2^{-1})^{6p/(p-6)} = id \end{array} \right\rangle.$$

*If an exponent is infinite or negative then the relation should be omitted.*

Moreover, from the detailed analysis of the polyhedra and the groups, we obtain the orbifold Euler characteristic  $\chi$  of the quotient orbifolds (hence their complex hyperbolic volume which is  $8\pi^2\chi/3$ ):

**Theorem 1.3** *Let  $\tau = -(1 + i\sqrt{7})/2$ . Let  $\chi(2\pi/p, \tau)$  be the orbifold Euler characteristic of the orbifold  $\Gamma(2\pi/p, \tau)\backslash\mathbf{H}_{\mathbb{C}}^2$ . Then  $\chi(2\pi/p, \tau)$  has the following values*

$p$	3	4	5	6	8	12
$\chi(2\pi/p, \tau)$	2/63	25/224	47/280	25/126	99/448	221/1008

These statements prove our conjecture from [DPP11] for five groups out of ten. The corresponding statement about lattices with  $\tau = \sigma_1$  and  $\tau = \sigma_5$  would follow from similar techniques, but some of the verifications are too tedious to be written up here.

For a fixed value of  $\tau$  the number of sides of the domain is the same, and the combinatorial structure is very similar. For each of the groups presented in the paper, the domain has 28 sides, but there are only two isometry types of sides (the domain is invariant under a regular elliptic element of order 7, and sides are paired isometrically). This decreases the complexity enough to make it possible to present most of the proof in detail on paper.

For  $\sigma_1$  (resp.  $\sigma_5$ ), our construction would produce a polyhedron with 64 (resp. 130) sides, and there would be four (resp. three) isometry types of sides. This makes some of the verifications longer, but not more difficult in any essential way. One important place where the arguments would be more painful is the verification that the bounding pyramids glue to build a copy of  $S^3$ , see section 4.7 of the present paper. In these more complicated cases, one could resort to the solution of the Poincaré conjecture, and check only that the bounding 3-complex is a manifold with trivial fundamental group; that argument can easily be automatized, but the computation would be difficult to write down on paper.

Our main results are proved using a standard application of the Poincaré polyhedron theorem, but we also provide new, useful techniques for studying fundamental domains for lattices in  $\text{PU}(2, 1)$ .

We apply systematic techniques for producing a fundamental domain with fairly simple combinatorics and with sides contained in bisectors (as other nice features, all vertices are fixed by specific isometries in the group, and all 1-faces of our polyhedron are chosen to be geodesic arcs). These techniques, which were in part inspired by the construction in [Sch03], will be briefly summarized in section 4.4.

Another novel aspect is the provision of efficient computational tools in Section 4.8 for certification of the combinatorics of a polyhedron bounded by (finitely many) bisectors. We summarize these techniques, since they have not systematically been used in the literature.

The determination of the combinatorics amounts to solving a system of (finitely many) quadratic inequalities in the real and imaginary parts of ball coordinates, for which no standard computational techniques are known. The main difficulty is to determine which pairs of bisectors contain a non-empty 2-face, and to give a precise list of the vertices and edges adjacent to that 2-face.

Using geometric properties of bisectors and bisector intersections (see Section 2.3), we can give parameters for any intersection  $\mathcal{B}_1 \cap \mathcal{B}_2$  of bisectors, and write explicit equations for the intersection  $\mathcal{B}_1 \cap \mathcal{B}_2 \cap \mathcal{B}_3$  for any third bisector  $\mathcal{B}_3$ . For well-chosen parametrizations, these equations are given by polynomials in two variables, quadratic in each variable. This is a consequence of the fact that the (hyperbolic cosine of the) distance between two points in

$\mathbf{H}_{\mathbb{C}}^2$  is given by a quadratic polynomial in the real and imaginary part of affine coordinates for the points. The coefficients of these polynomial equations are algebraic numbers (in fact, they lie in the adjoint trace field), which allows for arbitrary precision calculations.

The determination of the combinatorics is then reduced to the minimization of finitely many polynomials in two variables on finitely many polygonal regions, where the polygons are bounded by plane curves of degree at most two. We perform this minimization by computing the critical points of the above polynomials, which can be done by exact computations since the coefficients are known exactly. Even though these verifications can in principle be performed by hand, it is most reasonable to use a computer, given the large number of computations. Open source software that performs the necessary checks is available on the first author’s web page.

Most of these techniques are completely general, and can be used to reduce the certification of fundamental domains for discrete subgroups of  $\mathrm{PU}(2, 1)$  to a finite number of verifications. Note that the determination of fundamental domains is clearly important in the context of the search of non-arithmetic lattices, but it is also important for arithmetic ones, where discreteness comes for free. For instance, the determination of explicit group presentations for small covolume arithmetic lattices in  $\mathrm{PU}(2, 1)$  allowed Cartwright and Steger to complete the classification of fake projective planes (see [PY07] and [CS10]).

The paper is organized as follows. In Sections 2 and 3 we give well-known background material. Section 4 starts by establishing basic notation for the specific groups we study in the paper. We then sketch the general procedure that was used in order to produce the combinatorial model for our fundamental polyhedron (Sections 4.3 and 4.4).

The details of the combinatorial model  $\widehat{E}$  for the groups that appear in this paper (incidence properties of facets of various dimensions) are discussed in Section 4.6, and the strategy to show that it is homeomorphic to its geometric realization  $E$  is outlined in Section 4.6.2. To that end, an important point is to show that the 3-skeleton of  $\widehat{E}$  is homeomorphic to  $S^3$ , which is proved in section 4.7. We then show that the geometric realization of  $\widehat{E}$  is embedded, see Section 4.8; apply the Poincaré polyhedron theorem to  $E$  in order to show that our groups are lattices, Section 5; and finally we show that these lattices are non-arithmetic and not commensurable to each other or to any Deligne-Mostow lattice, Section 6.

**Acknowledgements:** The authors would like to thank the following institutions for their support during the preparation of this paper, in chronological order: the University of Utah, Université de Fribourg, Durham University, Université de Grenoble, Arizona State University. The authors acknowledge support from the ANR through the program “Structures Géométriques et Triangulations”, NSF grants DMS 1107452, 1107263, 1107367 (the GEAR Network) and ICERM at Brown University. The third author was also partially supported by SNF grant 200020-121506/1 and NSF grant DMS 1007340/1249147. The authors would also like to thank Bernard Parisse and Fabrice Rouillier for useful assistance on the computational aspects of this project, as well as the referee for several suggestions which improved the exposition of the paper.

## 2 Complex hyperbolic geometry

We define complex hyperbolic space, introduce totally geodesic subspaces and bisectors, and review properties of bisector intersections. Most of this material may be found in [Gol99].

## 2.1 Complex hyperbolic space

We define  $\mathbf{H}_{\mathbb{C}}^n$  to be the subset of  $\mathbf{P}_{\mathbb{C}}^n$  consisting of negative complex lines in  $\mathbb{C}^{n,1}$ . Here  $\mathbb{C}^{n,1}$  denotes  $\mathbb{C}^{n+1}$  equipped with a Hermitian form of signature  $(n, 1)$ , and a negative line is one spanned by a vector  $\mathbf{u} \in \mathbb{C}^{n,1}$  with  $\langle \mathbf{u}, \mathbf{u} \rangle < 0$ . There is a natural action on  $\mathbf{H}_{\mathbb{C}}^n$  of the unitary group of the Hermitian form, which is denoted by  $U(n, 1)$ . We shall often work with  $SU(n, 1)$ , which is an  $(n + 1)$ -fold cover of the projective group  $PU(n, 1)$ .

Up to scaling,  $\mathbf{H}_{\mathbb{C}}^n$  carries a unique  $U(n, 1)$ -invariant Riemannian metric, which makes it a symmetric space. It is well known that  $\mathbf{H}_{\mathbb{C}}^n$  is a complex space form, in fact the holomorphic sectional curvature of the above metric is equal to  $-1$ . This implies that real sectional curvatures are pinched between  $-1$  and  $-1/4$  (when  $n = 1$  the curvature is in fact constant).

It is a standard fact that the group of holomorphic isometries of  $\mathbf{H}_{\mathbb{C}}^n$  is precisely  $PU(n, 1)$ . The full group  $\text{Isom}(\mathbf{H}_{\mathbb{C}}^n)$  contains  $PU(n, 1)$  with index 2, the other component consisting of all anti-holomorphic isometries (an example of which is complex conjugation in affine coordinates, provided that the Hermitian form has real entries).

The only metric information we will need in this paper is the following distance formula:

$$\cosh\left(\frac{d(u, v)}{2}\right) = \frac{|\langle \mathbf{u}, \mathbf{v} \rangle|}{\sqrt{\langle \mathbf{u}, \mathbf{u} \rangle \langle \mathbf{v}, \mathbf{v} \rangle}}, \quad (1)$$

where  $\mathbf{u}, \mathbf{v}$  denote lifts of  $u, v$  to  $\mathbb{C}^{n+1}$ . The standard choice of a Hermitian form of signature  $(n, 1)$  is the Lorentzian form

$$\langle \mathbf{u}, \mathbf{v} \rangle = -u_0 \bar{v}_0 + u_1 \bar{v}_1 + \cdots + u_n \bar{v}_n. \quad (2)$$

In the affine coordinates  $(z_1, \dots, z_n) = (u_1/u_0, \dots, u_n/u_0)$  for the chart  $\{u_0 \neq 0\}$  of  $\mathbf{P}_{\mathbb{C}}^n$ , complex hyperbolic space corresponds to the unit ball  $|z_1|^2 + \cdots + |z_n|^2 < 1$ . We will denote  $\bar{\mathbf{H}}_{\mathbb{C}}^n = \mathbf{H}_{\mathbb{C}}^n \cup \partial \mathbf{H}_{\mathbb{C}}^n$  the corresponding closed ball.

We will use the standard classification of isometries of negatively curved spaces into elliptic, parabolic and hyperbolic isometries, with the following refinements. An elliptic element of  $PU(n, 1)$  is called **regular elliptic** if any of its lifts to  $U(n, 1)$  has distinct eigenvalues. In particular, regular elliptic isometries have isolated fixed points in  $\mathbf{H}_{\mathbb{C}}^n$  (given by the single negative eigenspace). When  $n = 2$ , non-regular elliptic isometries of  $\mathbf{H}_{\mathbb{C}}^2$  have two distinct eigenvalues, one simple and one double eigenvalue. These elements are called **complex reflections** in points or in lines, depending on the sign of the simple eigenspace.

## 2.2 Totally geodesic subspaces

If  $V \subset \mathbb{C}^{n,1}$  is any complex linear subspace where the restriction of the Hermitian form has signature  $(k, 1)$ , then the set of negative complex lines in  $V$  gives a copy of  $\mathbf{H}_{\mathbb{C}}^k$ , which can easily be checked to be totally geodesic. In terms of the ball model, they correspond to the intersection with the unit ball of complex affine subspaces in  $\mathbb{C}^n$ . When  $k = n - 1$ , the subspaces  $V$  as above are simply obtained by taking the orthogonal complement of a positive vector  $\mathbf{n}$ , which we refer to as a **polar vector** to the corresponding complex hyperplane. When  $k = 1$ , the complex totally geodesic submanifolds described above are called **complex lines**, or **complex geodesics**. Note that there is a unique complex line joining any two distinct points in  $\mathbf{H}_{\mathbb{C}}^n$ .

Similarly, some  $\mathbb{R}$ -linear subspaces can be used to produce totally geodesic submanifolds, namely those where the Hermitian form restricts to a quadratic form of hyperbolic signature.

These yield copies of  $\mathbf{H}_{\mathbb{R}}^k$ ,  $k \leq n$  (with real sectional curvature  $-1/4$ ). For  $k = 1$  these are precisely the real geodesics, and for  $k = 2$ , they are called  **$\mathbb{R}$ -planes**.

It is a standard fact that every complete totally geodesic submanifold is in one of the two families described above (see [Gol99], Section 3.1.11). Note that in particular, there are no totally geodesic real hypersurfaces in complex hyperbolic spaces.

### 2.3 Bisectors

The basic building blocks for our fundamental domains are **bisectors**, which are hypersurfaces equidistant from two given points. Their geometric structure has been analyzed in great detail in [Mos80], [Gol99], we only recall a few facts that will be needed in the paper.

Given two distinct points  $p_0, p_1 \in \mathbf{H}_{\mathbb{C}}^n$ , write

$$\mathcal{B}(p_0, p_1) = \{u \in \mathbf{H}_{\mathbb{C}}^n : d(u, p_0) = d(u, p_1)\}$$

for the bisector equidistant from  $p_0$  and  $p_1$ .

There is some freedom in choosing the pair of points  $p_0, p_1$ , but perhaps surprisingly, the possible choices are much more constrained than in constant curvature geometries. Indeed, the points  $q_0$  for which there exists a  $q_1$  with  $\mathcal{B}(q_0, q_1) = \mathcal{B}(p_0, p_1)$  all lie on the complex line through  $p_0$  and  $p_1$ ; thus the complex line through the two points is canonically attached to the bisector, and is called its **complex spine**.

The **real spine** is the intersection of the complex spine with the bisector itself, which is a (real) geodesic; it is the locus of points inside the complex spine which are equidistant from  $p_0$  and  $p_1$ . It consists of points  $z \in \mathbf{H}_{\mathbb{C}}^n$  associated to negative vectors  $\mathbf{u} \in \mathbb{C}^{n,1}$  that are in the complex span of  $\mathbf{p}_0$  and  $\mathbf{p}_1$  and that satisfy

$$|\langle \mathbf{u}, \mathbf{p}_0 \rangle| = |\langle \mathbf{u}, \mathbf{p}_1 \rangle|, \tag{3}$$

where  $\mathbf{p}_0$  and  $\mathbf{p}_1$  denote lifts of  $p_0$  and  $p_1$  to  $\mathbb{C}^{n,1}$  with the same norm (e.g. one could take  $\langle \mathbf{p}_0, \mathbf{p}_0 \rangle = \langle \mathbf{p}_1, \mathbf{p}_1 \rangle = -1$ ). The nonzero vectors in  $\text{Span}_{\mathbb{C}}(\mathbf{p}_0, \mathbf{p}_1)$  satisfying (3), but that are not necessarily negative, span a real projective line in  $\mathbf{P}_{\mathbb{C}}^n$ , which we call the **extended real spine** of the bisector.

We will sometimes describe bisectors by giving two points of their extended real spines; as mentioned in Section 2.2, we can think of a real geodesic as a real 1-dimensional hyperbolic space. Hence, we can describe it as the projectivization of a totally real 2-dimensional subspace of  $\mathbb{C}^{n,1}$ , i.e. we take two vectors  $\mathbf{v}$  and  $\mathbf{w}$  in  $\mathbb{C}^{n,1}$  with  $\langle \mathbf{v}, \mathbf{w} \rangle \in \mathbb{R}$ , and consider their real span. The simplest way to guarantee that the span really yields a geodesic in  $\mathbf{H}_{\mathbb{C}}^n$  is to require moreover that  $\mathbf{v}$  and  $\mathbf{w}$  form a Lorentz basis, i.e.  $\langle \mathbf{v}, \mathbf{v} \rangle = -1$ ,  $\langle \mathbf{w}, \mathbf{w} \rangle = 1$  and  $\langle \mathbf{v}, \mathbf{w} \rangle = 0$ .

Recall that bisectors are *not* fixed point sets of any isometric involution, since they are not totally geodesic. According to the discussion in Section 2.2, there are two kinds of maximal totally geodesic submanifolds contained in a given bisector. The complex ones are called **complex slices** of  $\mathcal{B}$ ; they are the preimages of points of the real spine under orthogonal projection onto the complex spine. They can also be described as hyperplanes with polar vectors  $\mathbf{n} \in \mathbb{C}^{n,1}$  satisfying  $\langle \mathbf{n}, \mathbf{n} \rangle > 0$  and  $|\langle \mathbf{n}, \mathbf{p}_0 \rangle| = |\langle \mathbf{n}, \mathbf{p}_1 \rangle|$ , see equation (3). The totally real submanifolds that are contained in  $\mathcal{B}$  are precisely those containing the real spine and are called **real slices** of  $\mathcal{B}$ .



## 2.4 Bisectors and geodesics

Several times in the paper, we will need to determine when a geodesic arc is contained in a bisector. Recall that bisectors in  $\mathbf{H}_{\mathbb{C}}^2$  are not convex: given two distinct points  $p, q$  in a bisector  $\mathcal{B}$ , the geodesic through  $p$  and  $q$  is in general not contained in  $\mathcal{B}$ . This is stated more precisely in the following (see Theorem 5.5.1 of [Gol99]).

**Lemma 2.1** *Let  $\alpha \subset \mathbf{H}_{\mathbb{C}}^2$  be a real geodesic, and let  $\mathcal{B}$  be a bisector. Then  $\alpha$  is contained in  $\mathcal{B}$  if and only if it is contained either in a real slice or in a complex slice of  $\mathcal{B}$ .*

In particular, we have:

**Lemma 2.2** *Let  $u$  and  $v$  be distinct points of a bisector  $\mathcal{B}$ , such that  $u$  is on the real spine of  $\mathcal{B}$ . Then the geodesic through  $u$  and  $v$  is contained in  $\mathcal{B}$ .*

Indeed, if  $v$  is in the complex slice through  $u$  this is obvious. Otherwise, taking lifts  $\mathbf{u}, \mathbf{v}$  of  $u, v$ , the point  $v$  is in a slice  $\mathbf{w}^{\perp}$  with  $\langle \mathbf{u}, \mathbf{w} \rangle \neq 0$  in which case  $\mathbf{u}, \mathbf{v}, \mathbf{w}$  are linearly independent. Since  $\langle \mathbf{v}, \mathbf{w} \rangle = 0$ , we can normalize  $\mathbf{u}, \mathbf{v}, \mathbf{w}$  to have pairwise real inner products, so they span a copy of  $\mathbf{H}_{\mathbb{R}}^2$  which contains the real spine of  $\mathcal{B}$ , i.e. they span a real slice of  $\mathcal{B}$ .

The following result will also be useful (see also Lemma 2.2 of [DFP05] for a related statement).

**Lemma 2.3** *Let  $\mathcal{B}$  be a bisector and let  $C$  be a complex line orthogonal to a complex slice of  $\mathcal{B}$ . Then  $C \cap \mathcal{B}$  is a real geodesic contained in a real slice of  $\mathcal{B}$ .*

PROOF. In the unit ball, we may normalize the real spine  $\sigma$  of  $\mathcal{B}$  to be the set of points of the form  $(x_1, 0)$ , with  $x_1 \in \mathbb{R}$ , the slice of  $\mathcal{B}$  to be  $\{z_1 = 0\}$ , and  $C$  to be of the form  $\{z_2 = \beta\}$  for some  $\beta$  (with  $|\beta| < 1$ ). Since orthogonal projection onto  $\{z_2 = 0\}$  is just the usual projection onto the first coordinate axis, and a bisector is the preimage of its real spine under orthogonal projection onto its complex spine,  $C \cap \mathcal{B}$  is given by  $(x_1, \beta)$  with  $x_1 \in \mathbb{R}$  (and  $|x_1| < \sqrt{1 - |\beta|^2}$ ). The latter curve is a geodesic; in fact it is the intersection  $C \cap L$  where  $L$  is obtained from the real ball  $B_{\mathbb{R}}^2 \subset B_{\mathbb{C}}^2$  by applying the isometry  $(z_1, z_2) \mapsto (z_1, \frac{\beta}{|\beta|} z_2)$ .  $\square$

## 2.5 Coequidistant bisector intersections

It is well-known that bisector intersections can be somewhat complicated, see the detailed analysis in [Gol99]. In what follows, for simplicity of notation, we restrict ourselves to the case of complex dimension  $n = 2$ .

A simple way to get these intersections to be somewhat reasonable is to restrict to **coequidistant** pairs, i.e. intersections  $\mathcal{B}_1 \cap \mathcal{B}_2$  where  $\mathcal{B}_1, \mathcal{B}_2$  are equidistant from a common point  $p_0 \in \mathbf{H}_{\mathbb{C}}^n$ . We write  $\Sigma_1, \Sigma_2$  for the complex spines of  $\mathcal{B}_1, \mathcal{B}_2$  respectively, and  $\sigma_1, \sigma_2$  for their real spines.

In view of the discussion in Section 2.3, it should be clear that this is a restrictive condition, which implies that  $\Sigma_1, \Sigma_2$  intersect inside  $\mathbf{H}_{\mathbb{C}}^n$ . Since complex lines with two points in common coincide, there are two possibilities for coequidistant pairs  $\mathcal{B}_1, \mathcal{B}_2$ ; either the complex spines coincide or they intersect in a single point.

When the complex spines coincide, the bisectors are called **cospinal**, and the intersection is easily understood; it is non-empty if and only if the real spines  $\sigma_1$  and  $\sigma_2$  intersect, and

in that case the intersection  $\mathcal{B}_1 \cap \mathcal{B}_2$  consists of a complex line (namely the complex line orthogonal to  $\Sigma_1 = \Sigma_2$  through  $\sigma_1 \cap \sigma_2$ ).

Now suppose  $\Sigma_1$  and  $\Sigma_2$  intersect in a point which lies outside of the real spines  $\sigma_1$  and  $\sigma_2$ , so that  $\mathcal{B}_1 \cap \mathcal{B}_2$  can be written as the equidistant locus from three points  $p_0, p_1, p_2$  which are not contained in a common complex line. The following important result is due to G. Giraud [Gir21] (see also Theorem 8.3.3 of [Gol99]).

**Proposition 2.4** *Let  $p_0, p_1, p_2$  be distinct points in  $\mathbf{H}_{\mathbb{C}}^2$ , not all contained in a complex line. When it is non empty, the intersection  $\mathcal{B}(p_0, p_1) \cap \mathcal{B}(p_0, p_2)$  is a (non-totally geodesic) smooth disk. Moreover, it is contained in precisely three bisectors, namely  $\mathcal{B}(p_0, p_1)$ ,  $\mathcal{B}(p_0, p_2)$  and  $\mathcal{B}(p_1, p_2)$ .*

**Definition 2.5** *We define a **Giraud disk** to be a bisector intersection as in Proposition 2.4 and we denote it by  $\mathcal{G}(p_0, p_1, p_2)$ .*

Given a Giraud disk  $\mathcal{G} = \mathcal{B}_1 \cap \mathcal{B}_2 \cap \mathcal{B}_3$ , the complex slices of the three bisectors  $\mathcal{B}_j$  intersect  $\mathcal{G}$  in hypercycles, so that  $\mathcal{G}$  has three pairwise transverse foliations by arcs.

**Parametrizing Giraud disks:** Let  $\mathbf{p}_j$  denote a lift of  $p_j$  to  $\mathbb{C}^3$ . By rescaling the lifts, we may assume that the three square norms  $\langle \mathbf{p}_j, \mathbf{p}_j \rangle$  are equal, and also that  $\langle \mathbf{p}_0, \mathbf{p}_1 \rangle$  and  $\langle \mathbf{p}_0, \mathbf{p}_2 \rangle$  are real and positive.

Now for  $j = 1, 2$ , consider  $\tilde{\mathbf{v}}_j = \mathbf{p}_0 - \mathbf{p}_j$  and  $\tilde{\mathbf{w}}_j = i(\mathbf{p}_0 + \mathbf{p}_j)$  (note that  $\tilde{\mathbf{v}}_j$  corresponds to the midpoint of the geodesic segment between  $p_0$  and  $p_j$ ), and normalize these to unit vectors  $\mathbf{v}_j = \tilde{\mathbf{v}}_j / \sqrt{-\langle \tilde{\mathbf{v}}_j, \tilde{\mathbf{v}}_j \rangle}$  and  $\mathbf{w}_j = \tilde{\mathbf{w}}_j / \sqrt{\langle \tilde{\mathbf{w}}_j, \tilde{\mathbf{w}}_j \rangle}$ .

Here recall that  $\mathbf{u} \boxtimes \mathbf{v}$  is the Hermitian cross product of  $\mathbf{u}$  and  $\mathbf{v}$  associated to the Hermitian form  $H$  (see p. 43 of [Gol99]). By definition,  $\mathbf{u} \boxtimes \mathbf{v}$  is  $\mathbf{0}$  if  $\mathbf{u}$  and  $\mathbf{v}$  are collinear, and spans their  $H$ -orthogonal complement otherwise. In other words, it is the Euclidean cross product of the vectors  $\mathbf{u}^* H$  and  $\mathbf{v}^* H$ , where  $H$  is the matrix defining the Hermitian form (the cross product makes sense because the vector space of homogeneous coordinates has dimension three).

Then the extended real spine of  $\mathcal{B}(p_0, p_j)$  is given by real linear combinations of  $\mathbf{v}_j$  and  $\mathbf{w}_j$ , so (lifts of) points in  $\mathcal{B}_1 \cap \mathcal{B}_2$  are given by negative vectors of the form

$$V(t_1, t_2) = (\mathbf{w}_1 + t_1 \mathbf{v}_1) \boxtimes (\mathbf{w}_2 + t_2 \mathbf{v}_2), \quad (4)$$

with  $t_1, t_2 \in \mathbb{R}$ . The only linear combinations we are missing with this parametrization of the extended real spines are  $\mathbf{v}_1$  and  $\mathbf{v}_2$ , but these are negative vectors so the projectivization of their orthogonal complement does not intersect  $\mathbf{H}_{\mathbb{C}}^2$ . We will call  $t_1, t_2$  **spinal coordinates** for  $\mathcal{G}$ .

We will use this parametrization repeatedly; for now, note that, given three points  $p_0, p_1$  and  $p_2$ , it is easy to determine whether the intersection  $\mathcal{B}(p_0, p_1) \cap \mathcal{B}(p_0, p_2)$  is empty or not. Indeed, negative vectors in  $\mathbb{C}^{2,1}$  are characterized by the fact that their orthogonal complement is a positive definite complex 2-plane, so the condition that  $(\mathbf{w}_1 + t_1 \mathbf{v}_1) \boxtimes (\mathbf{w}_2 + t_2 \mathbf{v}_2)$  is negative is equivalent to requiring that  $g(t_1, t_2) > 0$  where

$$g(t_1, t_2) = \det \begin{bmatrix} \langle \mathbf{w}_1 + t_1 \mathbf{v}_1, \mathbf{w}_1 + t_1 \mathbf{v}_1 \rangle & \langle \mathbf{w}_1 + t_1 \mathbf{v}_1, \mathbf{w}_2 + t_2 \mathbf{v}_2 \rangle \\ \langle \mathbf{w}_2 + t_2 \mathbf{v}_2, \mathbf{w}_1 + t_1 \mathbf{v}_1 \rangle & \langle \mathbf{w}_2 + t_2 \mathbf{v}_2, \mathbf{w}_2 + t_2 \mathbf{v}_2 \rangle \end{bmatrix}. \quad (5)$$

## 2.6 Cotranchal bisectors

We will encounter more complicated intersections than coequidistant ones. Two bisectors are called **cotranchal** if they have a common complex slice; the intersection of cotranchal bisectors is completely understood; see Thm 9.2.7 in [Gol99].

**Theorem 2.6 (Goldman)** *Let  $\mathcal{B}_1, \mathcal{B}_2$  be distinct bisectors, with real spines  $\sigma_1, \sigma_2$ . Assume that  $\mathcal{B}_1$  and  $\mathcal{B}_2$  share a complex slice  $C_0$ .*

- (1) *If  $\sigma_1$  and  $\sigma_2$  intersect, then  $\mathcal{B}_1 \cap \mathcal{B}_2$  is equal to  $C_0$ ;*
- (2) *If  $\sigma_1$  and  $\sigma_2$  lie in a common  $\mathbb{R}$ -plane  $L$  and are ultraparallel, then  $\mathcal{B}_1 \cap \mathcal{B}_2 = C_0 \cup L$ ;*
- (3) *If  $\sigma_1$  and  $\sigma_2$  do not lie in a totally geodesic plane, then either  $\mathcal{B}_1 \cap \mathcal{B}_2 = C_0$ , or  $\mathcal{B}_1 \cap \mathcal{B}_2 = C_0 \cup R$  where  $R$  is diffeomorphic to a disk and  $R \cap C_0$  is a hypercycle.*

Goldman's proof also gives a way to distinguish between the two very different possibilities that are described in case (3), working with Heisenberg coordinates for the vertices of the bisectors (which are the endpoints in  $\partial\mathbf{H}_{\mathbb{C}}^2$  of their real spines). We briefly review this in terms of our notation.

Let  $C$  be a complex line with polar vector  $\mathbf{n}$ . Note that this implies  $\langle \mathbf{n}, \mathbf{n} \rangle > 0$ . Let  $\mathbf{v}_1$  and  $\mathbf{v}_2$  be two vectors in  $\mathbf{n}^\perp$  with  $\langle \mathbf{v}_j, \mathbf{v}_j \rangle < 0$ . Hence  $\mathbf{v}_j$  projects to a point  $v_j$  in  $\mathbf{H}_{\mathbb{C}}^2$ , which of course is in  $C$ . Consider bisectors  $\mathcal{B}_1$  and  $\mathcal{B}_2$  so that the extended real spine of  $\mathcal{B}_j$  contains  $\mathbf{n}$  and  $\mathbf{v}_j$ . (Note that we have to be careful when choosing the lift  $\mathbf{v}_j$  in  $\mathbb{C}^{2,1}$  of the corresponding points  $v_j$  in  $C$  since we want the extended spine to be the real span of  $\mathbf{n}$  and  $\mathbf{v}_j$ ; choosing a different lift of  $\mathbf{v}_j$  rotates  $\mathcal{B}_j$  around  $C$ .) We want to decide when the intersection of  $\mathcal{B}_1$  and  $\mathcal{B}_2$  is precisely  $C$ ; see [Gol99], [Hsi03].

**Proposition 2.7** *Let  $\mathcal{B}_1, \mathcal{B}_2$  be cotranchal bisectors with common slice  $C$ . Let  $\mathbf{n}$  be a polar vector for  $C$  and let  $\mathbf{v}_1, \mathbf{v}_2$  be negative vectors with  $\langle \mathbf{v}_j, \mathbf{n} \rangle = 0$  so that the extended real spine of  $\mathcal{B}_j$  is the real span of  $\mathbf{n}$  and  $\mathbf{v}_j$ . Then the intersection of  $\mathcal{B}_1$  and  $\mathcal{B}_2$  is precisely  $C$  if and only if*

$$\langle \mathbf{v}_1, \mathbf{v}_1 \rangle \langle \mathbf{v}_2, \mathbf{v}_2 \rangle \geq (\Re \langle \mathbf{v}_1, \mathbf{v}_2 \rangle)^2.$$

PROOF. By assumption  $C$  is a slice of  $\mathcal{B}_1$  and  $\mathcal{B}_2$ . The other slices are parametrized by the polar vectors  $t_j \mathbf{n} + \mathbf{v}_j$  subject to  $\langle t_j \mathbf{n} + \mathbf{v}_j, t_j \mathbf{n} + \mathbf{v}_j \rangle > 0$ . In other words,

$$t_j^2 > \frac{-\langle \mathbf{v}_j, \mathbf{v}_j \rangle}{\langle \mathbf{n}, \mathbf{n} \rangle}. \quad (6)$$

Hence we want to find conditions under which the corresponding slices are disjoint, for all  $t_1$  and  $t_2$  satisfying this inequality.

Two complex lines  $\mathbf{a}^\perp$  and  $\mathbf{b}^\perp$  are disjoint if and only if the restriction of the Hermitian form to the span of  $\mathbf{a}$  and  $\mathbf{b}$  is indefinite, so the above condition is equivalent to the following inequality being satisfied for all  $t_1$  and  $t_2$  in the range (6):

$$\begin{aligned} 0 &\leq |\langle t_1 \mathbf{n} + \mathbf{v}_1, t_2 \mathbf{n} + \mathbf{v}_2 \rangle|^2 - \langle t_1 \mathbf{n} + \mathbf{v}_1, t_1 \mathbf{n} + \mathbf{v}_1 \rangle \langle t_2 \mathbf{n} + \mathbf{v}_2, t_2 \mathbf{n} + \mathbf{v}_2 \rangle \\ &= -t_1^2 \langle \mathbf{n}, \mathbf{n} \rangle \langle \mathbf{v}_2, \mathbf{v}_2 \rangle + t_1 t_2 \langle \mathbf{n}, \mathbf{n} \rangle 2\Re \langle \mathbf{v}_1, \mathbf{v}_2 \rangle - t_2^2 \langle \mathbf{n}, \mathbf{n} \rangle \langle \mathbf{v}_1, \mathbf{v}_1 \rangle \\ &\quad + |\langle \mathbf{v}_1, \mathbf{v}_2 \rangle|^2 - \langle \mathbf{v}_1, \mathbf{v}_1 \rangle \langle \mathbf{v}_2, \mathbf{v}_2 \rangle. \end{aligned} \quad (7)$$

First, note that the constant term is non-negative since

$$1 \leq \cosh^2 \left( \frac{d(v_1, v_2)}{2} \right) = \frac{|\langle \mathbf{v}_1, \mathbf{v}_2 \rangle|^2}{\langle \mathbf{v}_1, \mathbf{v}_1 \rangle \langle \mathbf{v}_2, \mathbf{v}_2 \rangle}.$$

Therefore, the expression in (7) is always non-negative if and only if its quadratic part is positive semi-definite. (Recall  $\langle \mathbf{n}, \mathbf{n} \rangle > 0$  and  $\langle \mathbf{v}_j, \mathbf{v}_j \rangle < 0$ .) This is equivalent to

$$\langle \mathbf{v}_1, \mathbf{v}_1 \rangle \langle \mathbf{v}_2, \mathbf{v}_2 \rangle \geq (\Re \langle \mathbf{v}_1, \mathbf{v}_2 \rangle)^2.$$

Finally, note that the range (6) is irrelevant in the argument as we may rescale  $t_1$  and  $t_2$  without affecting the sign of the quadratic form.  $\square$

## 2.7 Computational issues

As described in the previous sections, bisector intersections can be studied by checking the sign of various functions, sometimes defined in a somewhat complicated compact region.

This will be facilitated by the fact that all geometric objects we introduce are defined over specific number fields. For general computational tools in number fields, see [Coh93]. Throughout this section, we denote by  $k$  a number field, and we assume complex hyperbolic space is given as the set of lines in projective space that are negative with respect to a Hermitian inner product *defined over  $k$* .

**Definition 2.8** *A point  $p \in \mathbf{P}_{\mathbb{C}}^2$  will be called  $k$ -rational if it can be represented by a vector in  $k^3$ . A real geodesic will be called  $k$ -rational if it can be parametrized by vectors of the form  $\mathbf{v} + t\mathbf{w}$  ( $t \in \mathbb{R}$ ) with  $\mathbf{v}, \mathbf{w} \in k^3$ . A bisector will be called  $k$ -rational if its real spine is  $k$ -rational.*

Note that a real geodesic through two  $k$ -rational points is automatically  $k$ -rational. Indeed, if  $v \neq w$  are two  $k$ -rational points in  $\mathbf{H}_{\mathbb{C}}^2$ , then they have lifts to  $\mathbf{v}, \mathbf{w} \in k^3$  such that  $\langle \mathbf{v}, \mathbf{w} \rangle$  is real and positive (given any two lifts, multiply  $\mathbf{w}$  by  $\langle \mathbf{v}, \mathbf{w} \rangle$ , which is in  $k$  because the Hermitian form is defined over  $k$ ). The real geodesic segment from  $v$  to  $w$  is then parametrized by vectors of the form  $\mathbf{v} + t(\mathbf{w} - \mathbf{v})$ ,  $t \in [0, 1]$ , where  $\mathbf{v}$  and  $\mathbf{w}$  are  $k$ -rational. In these circumstances, we will also say that the geodesic segment  $[v, w]$  is  $k$ -rational.

Note also that a bisector is  $k$ -rational if and only if it can be written as  $\mathcal{B}(p, q)$  for some  $k$ -rational points  $p, q$ .

**Proposition 2.9** *Let  $[p, q]$  be a geodesic segment defined by  $k$ -rational endpoints. Let  $\mathcal{B}$  be a  $k$ -rational bisector. The following statements can be checked by performing arithmetic in  $k$ :*

- $p$  is in  $\mathcal{B}$  (resp.  $p$  is not in  $\mathcal{B}$ );
- $[p, q]$  is contained in  $\mathcal{B}$ ;
- $[p, q]$  is in a specific component of  $\mathbf{H}_{\mathbb{C}}^2 \setminus \mathcal{B}$ .
- $p$  is in  $\mathcal{B}$  and  $[p, q]$  is tangent to  $\mathcal{B}$ .

PROOF. We parametrize the geodesic segment by vectors  $\mathbf{z}_t = \mathbf{v} + t(\mathbf{w} - \mathbf{v})$ ,  $t \in [0, 1]$ . If  $\mathcal{B} = \mathcal{B}(q_0, q_1)$  and  $\mathbf{q}_0, \mathbf{q}_1 \in k^3$  are corresponding lifts, the intersection of the extended real geodesic with (the extension to  $\mathbf{P}_{\mathbb{C}}^2$  of)  $\mathcal{B}$  is described by the following equation,

$$\frac{|\langle \mathbf{z}_t, \mathbf{q}_0 \rangle|^2}{\langle \mathbf{q}_0, \mathbf{q}_0 \rangle} = \frac{|\langle \mathbf{z}_t, \mathbf{q}_1 \rangle|^2}{\langle \mathbf{q}_1, \mathbf{q}_1 \rangle}, \quad (8)$$

which has degree at most two in  $t$ .

The geodesic is contained in  $\mathcal{B}$  if and only if this equation is identically zero; checking whether this holds amounts to checking whether  $a = b = c = 0$  where

$$\begin{aligned} a &= |\langle \mathbf{w} - \mathbf{v}, \mathbf{q}_0 \rangle|^2 / \langle \mathbf{q}_0, \mathbf{q}_0 \rangle - |\langle \mathbf{w} - \mathbf{v}, \mathbf{q}_1 \rangle|^2 / \langle \mathbf{q}_1, \mathbf{q}_1 \rangle \\ b &= \Re( \langle \mathbf{v}, \mathbf{q}_0 \rangle \langle \mathbf{q}_0, \mathbf{w} - \mathbf{v} \rangle / \langle \mathbf{q}_0, \mathbf{q}_0 \rangle - \langle \mathbf{v}, \mathbf{q}_1 \rangle \langle \mathbf{q}_1, \mathbf{w} - \mathbf{v} \rangle / \langle \mathbf{q}_1, \mathbf{q}_1 \rangle ) \\ c &= |\langle \mathbf{v}, \mathbf{q}_0 \rangle|^2 / \langle \mathbf{q}_0, \mathbf{q}_0 \rangle - |\langle \mathbf{v}, \mathbf{q}_1 \rangle|^2 / \langle \mathbf{q}_1, \mathbf{q}_1 \rangle. \end{aligned}$$

This can be decided with arithmetic in  $k$ .

In order to check that the segment is on a specific side of  $\mathcal{B}$ , we need to check that a strict inequality holds between the two sides of (8). A natural way to do this is to find the solutions of (8), and to check that they are all negative (resp. positive); the latter requires extracting square-roots, which is not quite arithmetic in  $k$ . Alternatively, one can simply check that there is no sign change between the endpoints, in conjunction with a computation of the value of the polynomial at the point where its derivative vanishes.

Suppose  $p \in \mathcal{B}$  and  $q \notin \mathcal{B}$ . Then the geodesic is tangent to  $\mathcal{B}$  if and only if

$$\Re\{ \langle \mathbf{w}, \mathbf{q}_0 \rangle \langle \mathbf{q}_0, \mathbf{v} \rangle \} / \langle \mathbf{q}_0, \mathbf{q}_0 \rangle = \Re\{ \langle \mathbf{w}, \mathbf{q}_1 \rangle \langle \mathbf{q}_1, \mathbf{v} \rangle \} / \langle \mathbf{q}_1, \mathbf{q}_1 \rangle.$$

This condition is checked by arithmetic in  $k$ , since the vectors  $\mathbf{v}, \mathbf{w}, \mathbf{q}_0, \mathbf{q}_1$  are rational, and the Hermitian form is defined over  $k$ .  $\square$

## 3 Discrete groups and lattices

### 3.1 Lattices and arithmeticity

A given lattice  $\Gamma \subset \mathrm{SU}(n, 1)$  can be conjugated in complicated ways, but it is a classical fact that one can always represent it as a subgroup of some  $\mathrm{GL}(N, k)$  where  $k$  is a number field (of course one needs to require  $n > 1$  to exclude lattices in  $\mathrm{SU}(1, 1) \simeq \mathrm{SL}(2, \mathbb{R})$ ). For a general result along these lines, see Theorem 7.67 in [Rag72]. The smallest field one can use is given by the field  $\mathbb{Q}(\mathrm{tr} \mathrm{Ad} \Gamma)$  generated by traces in the adjoint representation, see Proposition (12.2.1) of [DM86] and also Section 6.1.

In this manner,  $\Gamma$  determines a  $k$ -form of  $\mathrm{SU}(n, 1)$ , and the  $k$ -forms of  $\mathrm{SU}(n, 1)$  are known to be obtained as  $\mathrm{SU}(H)$  for some Hermitian form  $H$  on  $F^r$ , where  $F$  is a division algebra with involution over a quadratic imaginary extension  $\mathbb{L}$  of the totally real field  $k$  (see [Wei60], [Tit66]). For dimension reasons,  $r$  must divide  $n + 1$ ; in fact  $n + 1 = rd$ , where  $d$  is the degree of  $F$ . In particular, if  $n = 2$  then  $r$  can only be 1 or 3. This gives two types of lattices in  $\mathrm{PU}(2, 1)$ , those related to Hermitian forms over number fields ( $d = 1$ , hence  $r = 3$ ) and those related to division algebras ( $d = 3$ ,  $r = 1$ ). These are often referred to as arithmetic lattices of the first and second type, respectively.

Note that the groups we construct in the present paper are clearly not arithmetic of the second type, because they contain Fuchsian subgroups. For the relationship between Fuchsian subgroups and groups of the second type, see [Rez95], [Sto12] (and also [McR06]). For lattices preserving a Hermitian form over a number field, there is a fairly simple arithmeticity criterion, which we now state for future reference. The following result is essentially Mostow's Lemma 4.1 of [Mos80] (following Vinberg [Vin68], see also Corollary 12.2.8 of [DM86]). We refer to this statement as the **Mostow–Vinberg arithmeticity criterion**.

**Proposition 3.1** *Let  $\mathbb{L}$  be a purely imaginary quadratic extension of a totally real field  $k$ , and  $H$  a Hermitian form of signature  $(n, 1)$  defined over  $\mathbb{L}$ . Suppose  $\Gamma \subset \mathrm{SU}(H; \mathcal{O}_{\mathbb{L}})$  is a lattice. Then  $\Gamma$  is arithmetic if and only if for all  $\varphi \in \mathrm{Gal}(\mathbb{L})$  not inducing the identity on  $\mathbb{Q}(\mathrm{tr} \mathrm{Ad} \Gamma)$ , the form  ${}^{\varphi}H$  is definite.*

Note that when  $\Gamma$  is as in Proposition 3.1 and it is not arithmetic, the whole group of integral matrices  $\mathrm{SU}(H; \mathcal{O}_{\mathbb{L}})$  is non discrete in  $\mathrm{SU}(H)$ , and in particular  $\Gamma$  must have infinite index in  $\mathrm{SU}(H; \mathcal{O}_{\mathbb{L}})$ .

### 3.2 The Poincaré polyhedron theorem

Various versions of the Poincaré polyhedron theorem for complex hyperbolic space have been given (see for example [Mos80], [DFP05], [FP06], [Par06]). For the purpose of the present paper, just as in [Mos80], we need to consider fundamental polyhedra for coset decompositions, where the polyhedron is invariant under a non-trivial subgroup.

Since the hypotheses as well as the conclusions of the theorem require quite a bit of notation, we now give a detailed statement of the Poincaré polyhedron theorem. A detailed proof can be found in [Par]. For simplicity, we only state this theorem for finite-sided polyhedra, as this is sufficient when considering lattices (for a more general statement that applies to locally finite polyhedra, see [Par]).

**Polyhedra:** For the purpose of the present paper, we only consider finite CW complexes which are regular, in the sense that every attaching map is an embedding. In particular, the closure of each cell is homeomorphic to a closed ball of the appropriate dimension, with embedded boundary sphere. A **(finite-sided) polyhedron** is the geometric realization in  $\overline{\mathbf{H}}_{\mathbb{C}}^n$  of such a complex with a single top-dimensional cell of dimension  $2n$ .

We will refer to closed cells of a polyhedron as facets, and denote by  $\mathcal{F}_k(E)$  the set of codimension  $k$  facets of  $E$ . We give special names to facets of each codimension: facets of codimension one, two, three and four will be called **sides**, **ridges**, **edges** and **vertices**, respectively. Because the focus of the present paper is mainly about lattices, we will assume  $E \cap \partial \mathbf{H}_{\mathbb{C}}^n$  consists of finitely many vertices, which we call **ideal vertices**.

Given a facet  $f$ , we denote by  $f^{\circ}$  the relative interior of  $f$  (equivalently,  $f^{\circ}$  is the set of points that are on  $f$  but not in any other facet of the same codimension). It follows from the regularity assumption that for each  $k$ -cell  $f$ , the  $(k-2)$ -cells in  $\partial f$  are contained in precisely two  $(k-1)$ -cells of  $\partial f$ . In particular, in the above terminology, a ridge of a polyhedron is on precisely two sides.

In the context of complex hyperbolic space, there is no canonical choice of hypersurfaces that can be used to bound polyhedra. Indeed, as mentioned in Section 2, there are no totally geodesic real hypersurfaces in  $\mathbf{H}_{\mathbb{C}}^n$ ,  $n \geq 2$ . In fact the polyhedra that appear in this paper are bounded exclusively by bisectors, and they actually have piecewise smooth boundary

(one can relax this to allow for more general faces, see [Mos80] and [Par] for a specific set of hypotheses).

**Side pairings:** A map  $\sigma : \mathcal{F}_1(E) \rightarrow \text{Isom}(\mathbf{H}_{\mathbb{C}}^n)$  is called a **side pairing** for  $E$  if it satisfies the following conditions:

1. For each side  $s \in \mathcal{F}_1(E)$  there is another side  $s^-$  in  $\mathcal{F}_1(E)$  so that  $S = \sigma(s)$  maps  $s$  onto  $s^-$  preserving the cell structure. Moreover,  $\sigma(s^-) = S^{-1}$ . In particular, if  $s = s^-$  then  $S = S^{-1}$  and so  $S$  is an involution. We call  $S^2 = id$  a **reflection relation**. (In fact  $s \neq s^-$  in all the cases we consider in this paper.)
2. If  $s \in \mathcal{F}_1(E)$  and  $\sigma(s) = S$  then  $S^{-1}(E) \cap E = s$  and  $S^{-1}(E^\circ) \cap E^\circ = \emptyset$ .
3. If  $w \in s^\circ$  then there is an open neighborhood  $U(w)$  of  $w$  contained in  $E \cup S^{-1}(E)$ .

We say that  $S = \sigma(s)$  is the **side-pairing map** associated to the side  $s \in \mathcal{F}_1(E)$ .

We suppose the polyhedron  $E$  is preserved by a finite group  $\Upsilon < \text{Isom}(\mathbf{H}_{\mathbb{C}}^n)$ , which acts by cell-preserving automorphisms. We assume moreover that we have a presentation of  $\Upsilon$  in terms of generators and relations (in the examples treated in this paper,  $\Upsilon$  will simply be a finite cyclic group).

Let  $\Gamma < \text{Isom}(\mathbf{H}_{\mathbb{C}}^n)$  be the group generated by  $\Upsilon$  and the side-pairing maps. In what follows, we will need to consider  $\Upsilon$ -orbits of sides and ridges. We suppose that the side pairing  $\sigma$  is **compatible with**  $\Upsilon$  in the following sense: for all  $s \in \mathcal{F}_1(E)$  and all  $P \in \Upsilon$  we have  $\sigma(Ps) = P\sigma(s)P^{-1}$ .

**Ridge cycles:** Consider a ridge  $\rho_1 \in \mathcal{F}_2(E)$ . We know that  $\rho_1$  is contained in exactly two sides of  $E$ , so we can write  $\rho_1 = s_1 \cap s_1'$  where  $s_1, s_1' \in \mathcal{F}_1(E)$ . Let  $S_1 = \sigma(s_1)$  be the side pairing map associated to  $s_1$ . Then we know that  $S_1(s_1)$  is another side  $s_1^-$  of  $E$ . Since the side pairing maps are bijections preserving the cell structure, it must be the case that  $\rho_2 = S_1(\rho_1)$  is a ridge contained in  $s_1^-$ . In other words, there is a side  $s_2 \in \mathcal{F}_1(E)$  so that  $\rho_2 = s_2 \cap s_1^-$ . Let  $S_2 = \sigma(s_2)$  be the side pairing map associated to  $s_2$ . We repeat the above process and thereby obtain a sequence of ridges  $\rho_i$ , sides  $s_i$  and side pairing maps  $S_i$  so that  $\rho_i = s_i \cap s_{i-1}^-$  and  $S_i = \sigma(s_i)$ .

If  $\rho_2 = \rho_1$ , we set  $m = 0$ ; otherwise let  $m > 0$  be the smallest positive integer such that  $\rho_{m+1}$  is in the same  $\Upsilon$ -orbit as  $\rho_1$  (there must exist such an  $m$ , since the set of ridges is finite).

Note that there is then a unique  $P \in \Upsilon$  such that  $P\rho_{m+1} = \rho_1$  (or else there would be a non-trivial element of  $\Upsilon$  fixing  $\rho_1$  pointwise and preserving the pair of sides containing it). We then have  $\rho_1 = s_1 \cap Ps_m^-$ , and the other side  $s_1'$  containing  $\rho_1$  must be  $Ps_m^-$ .

We say that  $(\rho_1, \dots, \rho_{m+1})$  is the **ridge cycle** of  $\rho_1$  and we define the **cycle transformation**  $T = T(\rho_1)$  of  $\rho_1$  to be  $T = P \circ S_m \circ \dots \circ S_1$ . Then  $T$  maps  $\rho_1$  to itself:

$$T(\rho_1) = P \circ S_m \circ \dots \circ S_2 \circ S_1(\rho_1) = \dots = P \circ S_m(\rho_m) = P(\rho_{m+1}) = \rho_1.$$

Note that  $T$  may not act as the identity on  $\rho_1$  and, even if it does, then it may not be the identity on the whole of  $\mathbf{H}_{\mathbb{C}}^n$ . We assume that  $T$  has finite order  $\ell$ . The relation  $T^\ell = id$  is called the **cycle relation** associated to  $\rho_1$ .

Note that the sequence  $\rho_1, \dots, \rho_m$  is entirely determined by  $\rho_1$  and the choice of the first side  $s_1$ . Observe that if we had started at another ridge in the cycle, say  $\rho_i$  then, using our hypothesis that the side pairings are compatible with  $\Upsilon$ , we would obtain the ridge

cycle  $(\rho_i, \rho_{i+1}, \dots, \rho_m, P^{-1}\rho_1, P^{-1}\rho_2, \dots, P^{-1}\rho_i)$ . Because  $\Upsilon$  is compatible with the side pairings, the cycle transformation of  $\rho_i$  is

$$\begin{aligned} T_i &= P \circ (P^{-1}S_{i-1}P) \circ \dots \circ (P^{-1}S_1P) \circ S_m \circ \dots \circ S_1 \\ &= S_{i-1} \circ \dots \circ S_1 \circ P \circ S_m \circ \dots \circ S_i. \end{aligned}$$

This is just a cyclic permutation of  $T$ . Likewise, if we had started at  $\rho_1$  but had chosen the first side pairing to be the one associated to the other side  $s'$  instead, we would have obtained (up to elements of  $\Upsilon$ ) the same sequence of sides in the reverse order, with the side pairing maps inverted. Furthermore, if  $Q \in \Upsilon$  then the ridge cycle of  $Q\rho_1$  is  $(Q\rho_1, \dots, Q\rho_{m+1})$  and the corresponding cycle transformation is  $QTQ^{-1}$ . Hence it suffices to consider the cycle associated to a single ridge in each  $\Upsilon$ -orbit of ridge cycles.

Writing out  $T$  in terms of  $P$  and the  $S_i$ , we let  $\mathcal{C} = \mathcal{C}(\rho_1)$  be the collection of suffix subwords of  $T^\ell$ , that is

$$\mathcal{C}(\rho_1) = \left\{ S_i \circ \dots \circ S_1 \circ T^j : 0 \leq i \leq m-1, 0 \leq j \leq \ell-1 \right\}$$

where  $i = 0$  means we write none of the  $S_i$  (this includes the case where  $m = 0$ ) and so  $i = j = 0$  corresponds to the identity map.

For  $i \in \{1, \dots, m\}$  we have  $\rho_i = s_i \cap s_{i-1}^-$ , where  $s_0^- = Ps_m^-$ . From the side pairing conditions,  $s_i = E \cap S_i^{-1}(E)$  and  $s_i^- = E \cap S_{i-1}(E)$  and so  $\rho_i \subset E \cap S_i^{-1}(E) \cap S_{i-1}(E)$ . Furthermore, for  $2 \leq i \leq m$  we have  $\rho_i = S_{i-1} \circ \dots \circ S_1(\rho_1)$ . Therefore

$$\begin{aligned} \rho_1 &= S_1^{-1} \circ \dots \circ S_{i-1}^{-1}(\rho_i) \\ &\subset S_1^{-1} \circ \dots \circ S_{i-1}^{-1}(S_i^{-1}(E) \cap E \cap S_{i-1}(E)) \\ &= \left( S_1^{-1} \circ \dots \circ S_i^{-1}(E) \right) \cap \left( S_1^{-1} \circ \dots \circ S_{i-1}^{-1}(E) \right) \cap \left( S_1^{-1} \circ \dots \circ S_{i-2}^{-1}(E) \right). \end{aligned}$$

Hence,  $\rho_1$  is contained in  $S_1^{-1} \circ \dots \circ S_{i-1}^{-1}(E)$  for all  $i$  between 1 and  $m$  where, as before,  $i = 1$  corresponds to the identity map. Note that, since  $P(E) = E$  we have

$$T^{-1}(E) = S_1^{-1} \circ \dots \circ S_m^{-1} \circ P^{-1}(E) = S_1^{-1} \circ \dots \circ S_m^{-1}(E).$$

Hence we have shown that

$$\rho_1 \subset \bigcap_{C \in \mathcal{C}(\rho_1)} C^{-1}(E).$$

We say that  $E$  and  $\Gamma$  satisfy the **cycle condition** at  $\rho_1$  if this intersection is precisely  $\rho_1$  and all these copies of  $E$  tessellate around  $\rho_1$ . That is:

1.

$$\rho_1 = \bigcap_{C \in \mathcal{C}(\rho_1)} C^{-1}(E).$$

2. If  $C_1, C_2 \in \mathcal{C}(\rho_1)$  with  $C_1 \neq C_2$  then  $C_1^{-1}(E^\circ) \cap C_2^{-1}(E^\circ) = \emptyset$ .

3. For all  $w \in \rho_1^\circ$  there exists an open neighborhood  $U(w)$  of  $w$  so that

$$U(w) \subset \bigcup_{C \in \mathcal{C}(\rho_1)} C^{-1}(E).$$



**Consistent system of horoballs:** When  $E$  has cusps, we need an extra hypothesis, related to metric completeness of the quotient of the polyhedron under the side-pairing maps. Let  $\xi_1, \dots, \xi_m$  be the cusps of  $E$ . We will assume the existence of a **consistent system of horoballs**, which is a collection  $\{U_1, \dots, U_m\}$ , where each  $U_j$  is a horoball based at  $\xi_j$  which is preserved by the stabilizer of  $\xi_j$  in  $\Gamma$ . By shrinking if necessary, we may suppose that a consistent system is made up of pairwise disjoint horoballs. The existence of a consistent system of horoballs can be checked by verifying that all cycle transformations fixing a given cusp are non-loxodromic (since in that case they automatically preserve every horoball based at that ideal vertex).

Then the statement of the complex hyperbolic Poincaré polyhedron theorem (see [Mos80] or [Par]) is the following.

**Theorem 3.2** *Suppose  $E$  is a smoothly embedded finite-sided polyhedron in  $\mathbf{H}_{\mathbb{C}}^n$ , together with a side pairing  $\sigma : \mathcal{F}_1(E) \rightarrow \text{Isom}(\mathbf{H}_{\mathbb{C}}^n)$ . Let  $\Upsilon < \text{Isom}(\mathbf{H}_{\mathbb{C}}^n)$  be a group of automorphisms of  $E$ . Let  $\Gamma$  be the group generated by  $\Upsilon$  and the side-pairing maps. Suppose the cycle condition is satisfied for each ridge in  $\mathcal{F}_2(E)$ , and that there is a consistent system of horoballs at the cusps of  $E$  (if it has any).*

*Then the images of  $E$  under the cosets of  $\Upsilon$  in  $\Gamma$  tessellate  $\mathbf{H}_{\mathbb{C}}^n$ . That is*

1.

$$\bigcup_{A \in \Gamma} A(E) = \mathbf{H}_{\mathbb{C}}^n.$$

2. *If  $A \in \Gamma - \Upsilon$  then  $E^\circ \cap A(E^\circ) = \emptyset$ .*

*Moreover,  $\Gamma$  is discrete and a fundamental domain for its action on  $\mathbf{H}_{\mathbb{C}}^n$  is obtained by intersecting  $E$  with a fundamental domain for  $\Upsilon$ .*

*Finally, one obtains a presentation for  $\Gamma$  in terms of the generators given by the side pairing maps together with a generating set for  $\Upsilon$ ; the relations are given by the reflection relations, the cycle relations and the relations in a presentation for  $\Upsilon$ .*

**Finite volume:** Note that the statement of the Poincaré polyhedron theorem says nothing about the volume of the quotient  $\Gamma \backslash \mathbf{H}_{\mathbb{C}}^n$ , which is also the volume of  $E$ . This volume is of course finite when  $E$  is entirely contained in  $\mathbf{H}_{\mathbb{C}}^n$ , in which case  $\Gamma$  is a cocompact lattice in  $\text{PU}(n, 1)$ .

Some of the groups we study in this paper are not cocompact (namely, when  $p = 4, 6$ ). In that case,  $E$  has some ideal vertices, but one easily sees that the volume of  $E$  is finite by studying the structure of the stabilizer of the ideal vertices. Let  $x$  be an ideal vertex with stabilizer  $\Gamma_x$ . By the existence of a consistent system of horoballs, the ideal point corresponding to  $x$  in the quotient  $\Gamma \backslash \mathbf{H}_{\mathbb{C}}^n$  has a neighborhood diffeomorphic to  $(0, +\infty) \times H_x$ , where  $H_x$  is the quotient of any horosphere based at  $x$  by the action of  $\Gamma_x$ . It is well known that the fact that  $\Gamma_x$  acts cocompactly on  $\partial \mathbf{H}_{\mathbb{C}}^2 \setminus \{x\}$  (or equivalently, on horospheres based at  $x$ ) implies that cusp neighborhoods in the quotient have finite volume (see for example Lemma 5.2 in [HP96]). This is clear for our polyhedra, whose cusp cross-sections are compact (see Section 5.3, Figure 17 for their explicit description).

**Toy model:** To illustrate this theorem and to help understand our family of examples, it is instructive to work through a toy example with  $n = 1$ . Consider a triangle in the Poincaré disk  $\mathbf{H}_{\mathbb{C}}^1$  with vertices  $q_R$  with angle  $\pi/2$ ,  $q_J$  with angle  $\pi/3$  and  $q_P$  with angle  $\pi/7$  (see Figure 1).

Let  $R$ ,  $J$  and  $P$  be elements of  $\text{Isom}(\mathbf{H}_{\mathbb{C}}^1)$ , with orders 2, 3 and 7, fixing the respective points and satisfying  $P = RJ$ . Let  $\Gamma$  be the group generated by  $R$ ,  $J$  and  $P$ . The usual fundamental domain  $D$  for this group consists of this triangle together with its image under reflection in the side joining  $q_P$  and  $q_R$ . There is a natural  $P$ -invariant hyperbolic heptagon  $E$ , obtained as the union of the seven images of  $D$  under powers of  $P$ . This heptagon is a fundamental domain for the cosets of  $\Upsilon = \langle P \rangle$  in  $\Gamma$ .

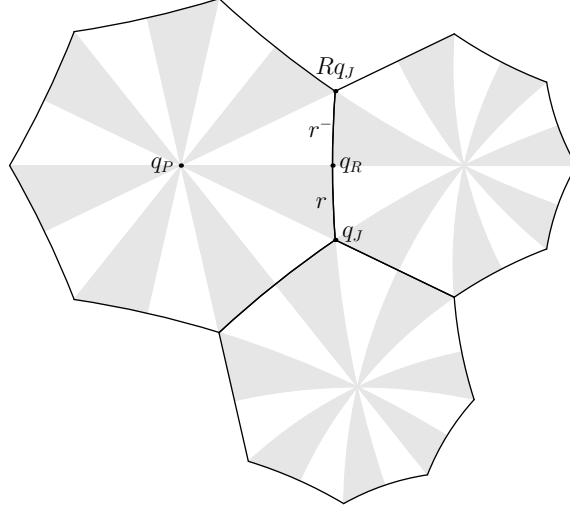


Figure 1: Toy model for fundamental domains for coset decompositions.

The vertices of the heptagon  $E$  are of the form  $P^k q_J$ , where  $k = 0, \dots, 6$ , and the midpoints of its sides are given by the points  $P^k q_R$ . Now let  $r$  be the edge from  $q_J$  to  $q_R$  and let  $r^-$  be the edge from  $q_R$  to  $Pq_J = Rq_J$ . Then we define the side pairing map  $R : r \rightarrow r^-$ , and extend this to the other sides in a way that is compatible with  $\Upsilon$ . Namely, we have side pairings  $P^k R P^{-k} : P^k r \rightarrow P^k r^-$ . We obtain two vertex cycles, which we write in terms of the edges and the vertices.

$R$	$r \cap r^-$ $r \cap r^-$	$q_R$ $q_R$
$R$ $P^{-1}$	$r \cap P^{-1}r^-$ $Pr \cap r^-$ $r \cap P^{-1}r^-$	$q_J$ $Rq_J$ $q_J$

It is easy to check local tessellation around the vertices and so Poincaré's theorem shows that the heptagons tile the Poincaré disk.

For  $r \cap r^-$ , the cycle transformation is  $R$ , and the cycle relation is  $R^2 = id$ . For  $r \cap P^{-1}r^-$ , the cycle transformation is  $P^{-1}R$  and the cycle relation is  $(P^{-1}R)^3 = id$ . Adding the generator  $P$  of  $\Upsilon$  and its relation  $P^7 = id$  gives the well known presentation

$$\Gamma = \langle R, P \mid R^2 = (P^{-1}R)^3 = P^7 = id \rangle.$$

Note that a fundamental domain for  $\Gamma$  is obtained by intersecting  $E$  with a fundamental domain for  $\Upsilon$  (one example of such a fundamental domain is of course given simply by  $D$ ).

We can also calculate the orbifold Euler characteristic  $\chi$  of  $\Gamma \backslash \mathbf{H}_{\mathbb{C}}^1$  as follows. We consider

each  $\Gamma$ -orbit of facets of  $E$  and we weight them by the reciprocal of the order of their stabilizer:

Facet	Stabilizer	Order
$q_R$	$\langle R \rangle$	2
$q_J$	$\langle P^{-1}R \rangle$	3
$r$	$id$	1
$E$	$\langle P \rangle$	7

Thus

$$\chi = \left( \frac{1}{2} + \frac{1}{3} \right) - 1 + \frac{1}{7} = \frac{-1}{42}.$$

We now briefly review standard techniques used to verify the hypotheses on ridge cycles.

**Tessellating around Giraud disks.** For cycles around Giraud ridges the conditions of the Poincaré polyhedron theorem are easily checked, as we now recall.

Let  $\mathcal{G} = \mathcal{G}(p_0, p_1, p_2)$  be a Giraud disk. Then  $\mathcal{G}$  defines three regions  $Y_0, Y_1$  and  $Y_2$  given, for indices  $j = 0, 1, 2$  taken mod 3, by:

$$Y_j = \{u \in \mathbf{H}_{\mathbb{C}}^2 : d(u, p_j) \leq d(u, p_{j+1}), d(u, p_j) \leq d(u, p_{j-1})\} \quad (9)$$

Any point in  $\mathbf{H}_{\mathbb{C}}^2$  is contained in (at least) one of these three regions according to the minimum of  $d(u, p_j)$  for  $j = 0, 1, 2$ . The interior  $Y_j^\circ$  of  $Y_j$  is the set of points where  $d(u, p_j)$  is strictly smaller than  $d(u, p_{j+1})$  and  $d(u, p_{j-1})$ . Clearly the interiors of these three regions are disjoint.

**Lemma 3.3** *Let  $E$  be a polyhedron bounded by bisectors and let  $\rho = s_1 \cap s_2$  be a Giraud ridge of  $E$  contained in the sides  $s_1$  and  $s_2$  of  $E$ . Let  $S_1 = \sigma(s_1)$  and  $S_2 = \sigma(s_2)$ . Let  $Y_0, Y_1$  and  $Y_2$  be the three regions given in (9), defined by the Giraud disk containing  $\rho$ . Suppose the  $Y_j$  each contain exactly one of  $E, S_1^{-1}(E)$  and  $S_2^{-1}(E)$  and that  $S_1^{-1}(E) \cap S_2^{-1}(E)$  is contained in the third bisector containing  $\rho$ . Then  $E, S_1^{-1}(E)$  and  $S_2^{-1}(E)$  tessellate a neighborhood of the interior of  $\rho$ .*

**PROOF.** Without loss of generality, suppose that  $E \subset Y_0, S_1^{-1}(E) \subset Y_1$  and  $S_2^{-1}(E) \subset Y_2$ . Since the  $Y_j$  have disjoint interiors, it is clear that  $E^\circ, S_1^{-1}(E^\circ)$  and  $S_2^{-1}(E^\circ)$  are disjoint.

We must show that the three copies of  $E$  cover a neighborhood of the interior of  $\rho$ . Suppose that  $w \in \rho^\circ$  and  $U(w)$  is a neighborhood of  $w$ . Then any point in  $U(w)$  is in (at least) one of  $Y_0, Y_1, Y_2$ . If the point is sufficiently close to  $\rho$  then it is in  $E, S_1^{-1}(E)$  or  $S_2^{-1}(E)$  respectively.  $\square$

**Tessellating around complex lines.** Cycles around ridges contained in complex lines can be more complicated than ridges contained in Giraud disks. However, by looking at complex lines orthogonal to the intersection, tessellation is reduced to an angle condition resembling the classical version of the Poincaré polyhedron theorem for the hyperbolic plane.

Let  $\mathcal{B}$  and  $\mathcal{B}'$  be two bisectors that intersect in a complex line  $C$ . Suppose  $E$  is a polyhedron contained in the intersection of two half-spaces defined by  $\mathcal{B}$  and  $\mathcal{B}'$  and that these bisectors contain sides  $s$  and  $s'$  of  $E$  intersecting in a simply connected ridge  $\rho$  in  $C$ . Using Lemma 2.3 any complex line  $C^\perp$  orthogonal to  $C$  intersects  $\mathcal{B}$  and  $\mathcal{B}'$  along geodesics, and  $C^\perp \cap E$  is contained in a wedge bounded by these geodesics, as  $\mathcal{B}$  and  $\mathcal{B}'$  both bound  $E$ . We must keep track of the angle subtended by this wedge. It is important to note that this

angle will depend on the point where  $C$  and  $C^\perp$  intersect, but that the total angle subtended over a ridge cycle will remain the same.

In particular, suppose  $T$  is the cycle transformation of  $\rho$ . By construction,  $T$  maps  $C$  to itself. There are two possibilities: either  $T$  fixes  $C$  pointwise, and so is a complex reflection in  $C$ , or  $T$  has a unique fixed point  $o$  in  $C$ . In the latter case, the point  $o$  must lie in  $\rho$  as  $T$  is a symmetry of  $\rho$ , which is simply connected. In either case, if  $o$  is a point of  $\rho$  fixed by  $T$  then the complex line  $C_o^\perp$  through  $o$  orthogonal to  $C$  is mapped to itself by  $T$ .

Suppose the cycle transformation is  $T = P \circ S_m \circ \cdots \circ S_1$ . The definition of a ridge cycle leads to ridges  $\rho_i = s_i \cap s_{i-1}^-$  where  $S_i = \sigma(s_i)$ . The intersection of  $C_o^\perp$  with  $S_1^{-1} \circ \cdots \circ S_{i-1}^{-1}(E)$  for  $1 \leq i \leq m$  is a wedge, say with angle  $\beta_i$ , bounded by the intersection of  $C_o^\perp$  with the sides  $S_1^{-1} \circ \cdots \circ S_{i-1}^{-1}(s_i)$  and  $S_1^{-1} \circ \cdots \circ S_{i-1}^{-1}(s_{i-1}^-)$ . These wedges fit together to give a larger wedge bounded by the intersection of  $C_o^\perp$  with a bisector and its image under  $T$ . In this larger wedge, the total angle at  $o$  subtended by copies of  $E$  under the cycle is  $\beta_1 + \cdots + \beta_m$ .

**Lemma 3.4** *Let  $E$  be a polyhedron bounded by bisectors and let  $\rho$  be a ridge of  $E$  contained in a complex line  $C$ . Let  $T$  be the cycle transformation of  $\rho$  and let  $o$  be a fixed point of  $T$  in  $\rho$ . Suppose that  $T$  has order  $\ell > 0$  and that  $T$  acts on  $C_o^\perp$  as a rotation by angle  $2\pi/\ell$ . Suppose that the total angle at  $o$  in  $C_o^\perp$  subtended by copies of  $E$  under the cycle is  $2\pi/\ell$ . Then any point  $w \in \rho^\circ$  has an open neighborhood tessellated by images of  $E$ .*

PROOF. For simplicity, we begin by supposing the ridge cycle has length one and  $T = P \circ S$  where  $S$  is the side-pairing map of  $s$  and  $P \in \Upsilon$ . This means we only have to show that  $E, T^{-1}(E), \dots, T^{-(\ell-1)}(E)$  tessellate around  $\rho$ . (This is the only case we need in the applications in this paper.)

First consider the action of  $T$  on  $C_o^\perp$ . Let  $\mathcal{B}$  and  $\mathcal{B}' = T(\mathcal{B})$  be the bisectors containing the sides  $s$  and  $s' = T(s)$  of  $E$ . Write  $b_o = \mathcal{B} \cap C_o^\perp$  and  $b'_o = \mathcal{B}' \cap C_o^\perp$ . Since  $T$  acts on  $C_o^\perp$  as a rotation by  $2\pi/\ell$  then  $b'_o = T(b_o)$  and the arcs  $b_o, b'_o$  bound a wedge with angle  $2\pi/\ell$  containing  $C^\perp \cap E$ . Applying powers of  $T$  we obtain  $\ell$  wedges containing images of  $E$  that tessellate a neighborhood of  $o$  in  $C_o^\perp$ .

When  $T$  is a complex reflection in  $C$ , this argument applies to all points of  $\rho$  and the result follows.

We now consider the case where the fixed point  $o$  of  $T$  is unique. For a general point  $u \in C \cap E$  consider  $C_u^\perp$ , the orthogonal complex line to  $C$  at  $u$ . Since  $T$  does not fix  $u$ , we see that  $T$  sends  $C_u^\perp$  to  $C_{Tu}^\perp$ . However, by continuity, the intersection of  $C_u^\perp$  with  $E$  is contained in some wedge with apex  $u$ . The angle may change as  $u$  varies but will always be positive since  $\mathcal{B} \cap \mathcal{B}'$  is  $C$ . Let  $k$  (which divides  $\ell$ ) be the smallest positive integer so that  $T^k$  is the identity on  $C$ . Then the angles of these wedges at all the images of  $C_u^\perp, T(C_u^\perp), \dots, T^k(C_u^\perp)$  add up to  $2k\pi/\ell$ . Since  $T^k$  is a complex reflection in  $C$  with angle  $2k\pi/\ell$  we see that the intersection of  $E, T(E), \dots, T^{\ell-1}(E)$  with  $C_u^\perp$  tessellate a neighborhood of  $u$  in  $C_u^\perp$ .

By carrying out this process for all points of  $C \cap E$ , we see that for any point  $u$  in the (relative) interior of  $C \cap E$  there is an open neighborhood of  $u$  tessellated by copies of  $E$ .

Now consider the general case where the length of the ridge cycle is  $m \geq 1$  and the cycle transformation is  $T = P \circ S_m \circ \cdots \circ S_1$ . In this case, we need to keep track of wedges in  $T^{-j} \circ S_1^{-1} \circ \cdots \circ S_i^{-1}(C_u^\perp)$  for  $0 \leq i \leq m-1$  and  $0 \leq j \leq \ell-1$ . Nevertheless, the same argument gives the result.  $\square$

## 4 Construction of the fundamental polyhedron

In section 4.1 and 4.2, we define the six groups that appear in Theorem 1.1, and establish basic notation that will be used throughout the paper.

In section 4.3, we study braiding properties of some complex reflections in our groups, which are used in an essential way in order to build our fundamental polyhedra, as explained in section 4.4. These braiding pairs of reflections are also important because they will correspond to the stabilizers of various vertices and complex ridges of our fundamental polyhedron, see section 5.3; this will allow us to compute the orbifold Euler characteristic, see section 5.5.

We define our polyhedra in section 4.5 by building the  $k$ -skeleton for increasing values of  $k$ . The general strategy for this definition is described in section 4.8; an important point for this inductive definition to make sense is that the boundary of every cell is a topological (piecewise smooth) sphere. The only difficult part of this verification is the one that concerns the boundary of the whole polyhedron. We show that the boundary of  $E$  is homeomorphic to  $S^3$  in section 4.7.

We then start from the combinatorial model of the polyhedron (this is described in section 4.6.2), and prove that the geometric realization is well-defined, and that it gives an embedding of the combinatorial model (sections 4.8.1 through 4.8.5).

### 4.1 Generators

In this section, we give explicit matrices that generate our groups. For more details on sporadic triangle groups, see [PP09] and [DPP11].

Recall from the introduction that our groups are generated by a complex reflection  $R_1$  and a regular elliptic element  $J$  of order three. We write

$$R_2 = JR_1J^{-1}, \quad R_3 = JR_2J^{-1}.$$

We write  $\mathbf{n}_j$  for polar vector to the mirror of the complex reflection  $R_j$  ( $j = 1, 2, 3$ ). Matrix representatives for  $R_j$  in  $SU(2, 1)$  will have eigenvalues  $a^2, \bar{a}, \bar{a}$  where

$$a = e^{2\pi i/3p}.$$

Since  $R_{j+1} = JR_jJ^{-1}$  we see that  $\mathbf{n}_{j+1} = J\mathbf{n}_j$  (with  $j \bmod 3$ ). In the cases that interest us,  $(\mathbf{n}_1, \mathbf{n}_2, \mathbf{n}_3)$  forms a basis for  $\mathbb{C}^3$ , which we will use throughout the paper. The matrix for  $J$  in this basis is then simply the permutation matrix:

$$J = \begin{bmatrix} 0 & 0 & 1 \\ 1 & 0 & 0 \\ 0 & 1 & 0 \end{bmatrix}$$

and the Hermitian form is given by a matrix of the form

$$H = \begin{bmatrix} \alpha & \beta & \bar{\beta} \\ \bar{\beta} & \alpha & \beta \\ \beta & \bar{\beta} & \alpha \end{bmatrix}.$$

It is convenient to choose

$$\alpha = 4 \sin^2(\pi/p) = 2 - a^3 - \bar{a}^3,$$

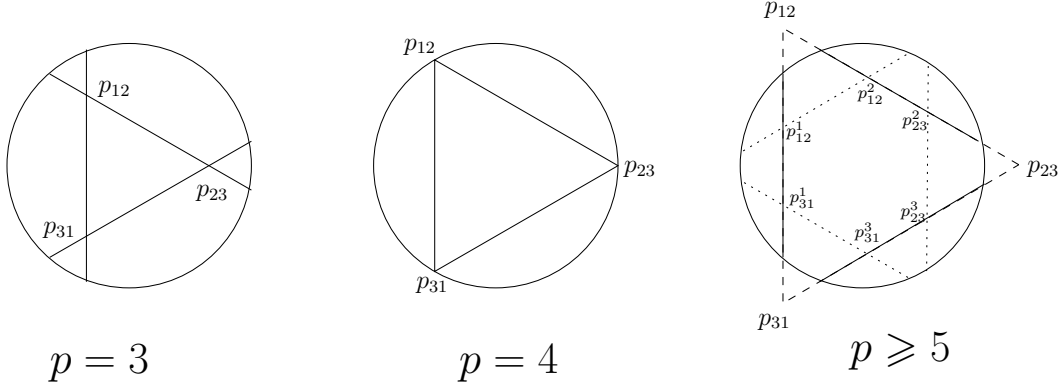


Figure 2: Relative positions of the mirrors of  $R_1$ ,  $R_2$ ,  $R_3$ . For  $p \geq 5$ , the dotted lines correspond to the lines polar to  $p_{jk}$ , or in other words the common perpendicular between the mirrors of  $R_j$  and  $R_k$ .

in which case the condition  $\text{tr}(R_1 J) = \tau$  imposes

$$\beta = (\bar{a}^2 - a)\tau.$$

The matrix of the reflection  $R_1$  (adjusted to have determinant 1, since we want to work with  $\text{SU}(2, 1)$ ), is easily seen to be

$$R_1 = \begin{bmatrix} a^2 & \tau & -a\bar{\tau} \\ 0 & \bar{a} & 0 \\ 0 & 0 & \bar{a} \end{bmatrix}$$

and  $R_2 = J R_1 J^{-1}$ ,  $R_3 = J^{-1} R_1 J$ .

The configuration of three complex lines given by the mirrors of  $R_1$ ,  $R_2$  and  $R_3$  varies with  $p$ . Note that the relative position of the mirrors of  $R_1$  and  $R_2$  is controlled by the restriction of the Hermitian form to  $\text{Span}(\mathbf{n}_1, \mathbf{n}_2)$ , i.e by the sign of the determinant of the  $2 \times 2$  matrix in the upper left corner of  $H$ . Using the specific value  $\tau = -(1 + i\sqrt{7})/2$  (in fact all we need is that  $|\tau|^2 = 2$ ), we have

$$\alpha^2 - |\beta|^2 = 8 \sin^2(\pi/p)(2 \sin^2(\pi/p) - 1) = -8 \sin^2(\pi/p) \cos(2\pi/p).$$

Hence the mirrors intersect inside complex hyperbolic space only for  $p = 3$ , they intersect at infinity when  $p = 4$ , and they are ultraparallel when  $p \geq 5$  (see Figure 2).

For future reference, we define

$$P = R_1 J$$

and

$$S_1 = P^2 R_1 P^{-2} R_1 P^2 \tag{10}$$

which will turn out to be key isometries when constructing our fundamental domains. Since  $P = R_1 J$  has trace  $\tau = -(1 + i\sqrt{7})/2 = e^{-2\pi i/7} + e^{-4\pi i/7} + e^{-8\pi i/7}$ , we immediately see that  $P$  is a regular elliptic map of order 7, with isolated fixed point

$$\mathbf{p} = \begin{bmatrix} a e^{-2\pi i/7} \\ 1 \\ \bar{a} e^{2\pi i/7} \end{bmatrix}. \tag{11}$$

For completeness we give an explicit matrix for  $S_1$ , which is also regular elliptic of order  $2p$ :

$$S_1 = \begin{bmatrix} -a & \bar{a}\bar{\tau} & -1 \\ 0 & -a\tau + \bar{a}^2\bar{\tau} & a^2\bar{\tau} - a^2 - \bar{a} \\ 0 & -1 - \bar{a}^3 + \bar{a}^3\tau & a\tau - \bar{a}^2\bar{\tau} \end{bmatrix}.$$

## 4.2 Word notation

We shall often use word notation and write  $j$  for  $R_j$  and  $\bar{j}$  for  $R_j^{-1}$ , so that a word in  $R_1, R_2, R_3$  and their inverses is described by a sequence of (possibly overlined) integers. Note that there is very little confusion possible between  $R_j^{-1}$  and the complex conjugate matrix  $\bar{R}_j$  (which we shall never use in this paper). For example,  $23\bar{2}$  denotes  $R_2R_3R_2^{-1}$ , and  $1\bar{3}23\bar{1}$  denotes  $R_1R_3^{-1}R_2R_3R_1^{-1}$ .

When an isometry given by a word  $w$  in  $1, 2, 3$  has an isolated fixed point, we denote this point by  $p_w$  or  $q_w$ . In particular, consider two reflections with distinct mirrors that can be expressed as words  $u, v$ . If  $w = uv$  is conjugate in  $\Gamma$  to  $12$  (this is a word, not a number!) then we denote by  $p_w$  the intersection point of their mirrors of reflections (or the intersection of the extension of their mirrors to projective lines, i.e. these points may be in  $\mathbf{P}_{\mathbb{C}}^2$  rather than  $\mathbf{H}_{\mathbb{C}}^2$ ). Similarly, if  $w = uv$  is conjugate to  $123\bar{2}$  then we denote the fixed point of  $w$  by  $q_w$ . The reason for using different letters of the alphabet is that points of the form  $p_w$  and those of the form  $q_w$  are in different group orbits. We will refer to vertices of our polyhedra that have the form  $p_w$  for some word  $w$  as  $p_*$ -vertices (and similarly for  $q_*$ -vertices).

Let  $\mathbf{n}_w$  denote a lift to  $\mathbb{C}^3$  of the corresponding point  $p_w$ . Of course, by definition, these lifts are only determined up to multiplication by a scalar; so we give some explicit formulae for future reference.

$$\mathbf{n}_{23\bar{2}} = R_2\mathbf{n}_3 = \begin{bmatrix} 0 \\ \tau \\ \bar{a} \end{bmatrix}, \quad \mathbf{n}_{123\bar{1}} = aR_1\mathbf{n}_{23} = \begin{bmatrix} a^6 + a^3 - a^3\tau + \bar{\tau} \\ a^2\bar{\tau} - \bar{a} \\ \bar{a}^2\tau - a \end{bmatrix},$$

$$\mathbf{n}_{123\bar{2}} = \begin{bmatrix} \bar{a}^2 + a\tau \\ \bar{a}^3 - a^3 - \bar{\tau} \\ \bar{a}^4\bar{\tau} + \bar{a} \end{bmatrix}, \quad \mathbf{n}_{1\bar{3}23} = \begin{bmatrix} a^2 + \bar{a}\bar{\tau} \\ a^4\tau + a \\ a^3 - \bar{a}^3 - \tau \end{bmatrix}, \quad \mathbf{n}_{1\bar{3}23\bar{1}} = aR_1R_3^{-1}\mathbf{n}_2 = \begin{bmatrix} a^2 \\ a \\ \bar{\tau} \end{bmatrix}.$$

We will also denote by  $m_w$  the mirror of the complex reflection corresponding to a word  $w$ , so that  $\mathbf{n}_w$  is a polar vector to  $m_w$  (in other words,  $m_w$  corresponds to  $\mathbf{n}_w^\perp$ ). We will also extend this notation to group elements that have a complex reflection as a power, so that (when  $p \geq 5$ )  $m_{23}$  denotes the mirror of  $(R_2R_3)^2$ , and (when  $p \geq 8$ )  $m_{123\bar{2}}$  denotes the mirror of  $(R_1R_2R_3R_2^{-1})^3$ .

## 4.3 Higher braiding

The key to the general procedure to build the fundamental domains for our groups (see section 4.4) is the following result from [PP09] (see also section 2.2 of [Mos80]).

**Proposition 4.1 (Proposition 4.4 of [PP09])** *Suppose that  $R_x$  and  $R_y$  are complex reflections in  $SU(2, 1)$  both with eigenvalues  $e^{2i\psi/3}, e^{-i\psi/3}, e^{-i\psi/3}$ . Let  $L_x$  and  $L_y$  be the  $e^{-i\psi/3}$  eigenspaces of  $R_x$  and  $R_y$ , respectively. Then  $L_x \cap L_y$  is an  $e^{-2i\psi/3}$  eigenspace of  $R_xR_y$ . Suppose  $R_xR_y$  is non-loxodromic and that its other eigenvalues are  $-e^{i\psi/3 \pm i\phi}$ . Then the group*

$\Gamma_{xy} = \langle R_x, R_y \rangle$  acts on the orthogonal complement of  $L_x \cap L_y$  as (the orientation preserving subgroup of) a  $(\psi/2, \psi/2, \phi)$  triangle group  $\Delta_{xy}$ .

Consider the action of  $\langle R_x, R_y \rangle$  on the projectivization of  $(L_x \cap L_y)^\perp$ , which we denote by  $m_{xy}$ . The space  $m_{xy}$  is a sphere, Euclidean plane or hyperbolic plane respectively, depending on whether  $m_x$  and  $m_y$  intersect, are asymptotic or are ultraparallel. Note that there is a close connection between the values of  $\psi$  and  $\phi$  and these three cases (see Figure 2). In what follows, we will suppose  $\psi = 2\pi/p$  and  $\phi = 2\pi/q$  (which will be the case in our examples). This means that the triangle associated to  $\Delta_{xy}$  has internal angles  $\pi/p, \pi/p, 2\pi/q$ . In particular,  $R_x R_y$  acts on  $m_{xy}$  as a rotation through angle  $2\phi = 4\pi/q$ . If  $q$  is even then  $\Delta_{xy}$  is a  $(p, p, q/2)$  triangle group. Therefore  $(R_x R_y)^{q/2}$  acts as the identity on  $m_{xy}$ . On the other hand, if  $q$  is odd this triangle can be divided into two  $(2, p, q)$  triangles, and  $\Delta_{xy}$  is a  $(2, p, q)$  triangle group. In this case a simple geometric argument in  $m_{xy}$  shows that  $(R_x R_y)^{(q-1)/2}(m_x \cap m_{xy}) = (m_y \cap m_{xy})$ . Since  $m_x$  and  $m_y$  are orthogonal to  $m_{xy}$  we immediately see that  $R_x$  and  $R_y$  satisfy a (generalized) braid relation. When  $q$  is even, this braid relation is

$$(R_x R_y)^{q/2} = (R_y R_x)^{q/2} \quad (12)$$

and when  $q$  is odd, it is

$$(R_x R_y)^{(q-1)/2} R_x = R_y (R_x R_y)^{(q-1)/2}. \quad (13)$$

Furthermore, by examining the eigenvalues we can see that  $(R_x R_y)^{q/2}$  (respectively  $(R_x R_y)^q$ ) has a repeated eigenvalue. Therefore it is either a complex reflection (in a line or a point), the angle depending on  $p$  and  $q$  or it is possibly parabolic. The latter case arises when  $p_{xy}$  lies on  $\partial \mathbf{H}_\mathbb{C}^2$ . In either case, a power of  $R_x R_y$  is in the center of  $\langle R_x, R_y \rangle$ .

The following result is clear from the analysis in [PP09], but it can also be checked by explicit computations (see also Section 9.2.1 of [DPP11], and Section 2.2 of [Mos80]). Geometrically, it corresponds to the relative positions of the mirrors of  $R_1$  and  $R_2$  described in Section 4.1 and illustrated in Figure 2. When we use the Poincaré polyhedron theorem in Section 5.4, we will derive these equations from the cycle relations, see Lemma 5.12.

**Proposition 4.2**  $(R_1 R_2)^2$  is a complex reflection with angle  $(p-4)\pi/p$  when  $p \neq 4$ , and it is parabolic when  $p = 4$ . For  $p = 3$ ,  $(R_1 R_2)^2$  is a complex reflection in the point  $p_{12}$  where the mirrors of  $R_1$  and  $R_2$  intersect. For  $p \geq 5$ , it is a complex reflection in the common perpendicular complex line  $m_{12}$  to the mirrors of  $R_1$  and  $R_2$ . Moreover, for any  $p$ , we have the higher braid relation

$$(R_1 R_2)^2 = (R_2 R_1)^2 \quad (14)$$

Note that it follows from (14) that  $R_1$  and  $R_2$  both commute with  $(R_1 R_2)^2$ , which implies the orthogonality statement about their mirrors. More specifically, we have

**Proposition 4.3** The group  $\langle R_1, R_2 \rangle$  is a central extension of a  $(2, p, p)$  orientation preserving triangle group with center  $\langle (R_1 R_2)^2 \rangle$  of order  $2p/|p-4|$  (which is infinite for  $p = 4$ ). In particular,  $\langle R_1, R_2 \rangle$  has order  $8p^2/(4-p)^2$  when  $p \leq 3$  and infinite order when  $p \geq 4$ .

PROOF. The first statement follows from the fact that  $R_1$  and  $R_2$  have order  $p$  and  $(R_1 R_2)^2$  is central with order  $2p/|p-4|$ . The second statement follows from the fact that, for  $p \leq 3$ , a  $(2, p, p)$  triangle group has order  $4p/(4-p)$  and for  $p \geq 4$  it is infinite.  $\square$



Geometrically, when  $p = 3$  the spherical  $(2, 3, 3)$  triangle group acts on the sphere of complex lines through  $p_{12}$ ; when  $p = 4$  the vertex  $p_{12}$  is on the ideal boundary and the Euclidean  $(2, 4, 4)$  triangle group acts on the horizontal factor of the Heisenberg group based at that vertex; when  $p \geq 5$  the hyperbolic triangle group  $(2, 5, 5)$  acts on the complex line  $m_{12}$ .

It is useful to have a formula for the mirror of  $(R_1 R_2)^2$  (when  $p \geq 5$ ), which is polar to

$$\mathbf{n}_{12} = \begin{bmatrix} a^2 \bar{\tau} - \bar{a} \\ \bar{a}^2 \tau - a \\ a^3 + \bar{a}^3 \end{bmatrix}.$$

The notation is set up to indicate that it is the intersection point of the mirrors of  $R_1$  and  $R_2$  (see also Section 4.3). When  $p = 3, 4$  the vector  $\mathbf{n}_{12}$  projects to  $p_{12}$ , which is in  $\mathbf{H}_{\mathbb{C}}^2$  or on its boundary respectively. The obvious extension of this notation allows us to describe the  $J$ -orbit of this vector, namely

$$\mathbf{n}_{23} = J\mathbf{n}_{12}, \quad \mathbf{n}_{13} = J\mathbf{n}_{23}.$$

Note that the higher braid relation holds of course between any pair of reflections  $R_j$  and  $R_k$  with  $j \neq k$ , since  $JR_k J^{-1} = R_{k+1}$ , so that

$$(R_2 R_3)^2 = (R_3 R_2)^2, \quad (R_3 R_1)^2 = (R_1 R_3)^2.$$

The following observation will be useful later.

**Proposition 4.4**  $P^2 S_1$  is a complex reflection, in fact

$$P^2 S_1 = R_2 R_3^{-1} R_2^{-1}. \quad (15)$$

PROOF. Using the identity (10), we see that  $P^2 S_1 = R_3^{-1} R_2^{-1} R_3^{-1} R_2 R_3$ , by repeatedly using  $P = R_1 J$  and  $JR_k J^{-1} = R_{k+1}$ . The equality (15) then follows from the braid relation  $(R_2 R_3)^2 = (R_3 R_2)^2$ .  $\square$

A similar analysis holds for  $R_1$  and  $R_2 R_3 R_2^{-1}$ . In fact, in this case we recover the braid relation (compare with the calculations in [DFP05], or in Section 2.2 of [Mos80], in or Section 6 of [Par06]).

**Proposition 4.5**  $(R_1 R_2 R_3 R_2^{-1})^3$  is a complex reflection with angle  $(p - 6)\pi/p$  when  $p \neq 6$ , and it is parabolic when  $p = 6$ . For  $p \leq 5$ ,  $(R_1 R_2 R_3 R_2^{-1})^3$  is a complex reflection in the point  $q_{123\bar{2}}$ . For  $p \geq 7$ , it is a complex reflection in the complex line  $m_{123\bar{2}}$  perpendicular to the mirrors of  $R_1$  and  $R_2 R_3 R_2^{-1}$ . Moreover, for any  $p \in \mathbb{N}^*$ , we have the braid relation

$$R_1 (R_2 R_3 R_2^{-1}) R_1 = (R_2 R_3 R_2^{-1}) R_1 (R_2 R_3 R_2^{-1}). \quad (16)$$

**Proposition 4.6** The group  $\langle R_1, R_2 R_3 R_2^{-1} \rangle$  is a central extension of a  $(2, 3, p)$  orientation preserving triangle group with center  $\langle (R_1 R_2 R_3 R_2^{-1})^3 \rangle$  of order  $2p/|p - 6|$  (which is infinite for  $p = 6$ ). In particular,  $\langle R_1, R_2 R_3 R_2^{-1} \rangle$  has order  $24p^2/(6 - p)^2$  when  $p \leq 5$  and infinite order when  $p \geq 6$ .

PROOF. Since  $R_1$  has order  $p$  and  $(R_1 R_2 R_3 R_2^{-1} R_1)^2 = (R_1 R_2 R_3 R_2^{-1})^3$  is central with order  $2p/|p - 6|$ , we obtain the first statement. The second statement follows since a  $(2, 3, p)$  triangle group has order  $12p/(6 - p)$  for  $p \leq 5$  and is infinite for  $p \geq 6$ .  $\square$

## 4.4 General procedure for building fundamental domains

In this section, we give a rough idea of the procedure that allowed us to produce the fundamental domains that appear in this paper.

The general context is that of triangle groups, i.e. groups generated by three complex reflections. An important example of such a group was studied in [Sch03], where Schwartz gave a fundamental domain for a group generated by complex reflections  $I_1, I_2, I_3$  of order 2 with pairwise products of order 4 and such that  $I_1 I_2 I_3 I_2$  has order 7. The combinatorial structure of Schwartz's fundamental domain inspired several subsequent constructions, see [Par06] and [Tho10], which in turn evolved into a fairly general procedure that applies to triangle groups. We now outline that procedure and relate it to Schwartz's construction.

In Section 4.3, we discussed the fact that some pairs of complex reflections in the group satisfy the (generalized) braid relations (12) and (13). In the present paper, we consider only  $q = 3$  or  $q = 4$  (for groups with  $\tau = \sigma_1$  or  $\sigma_5$  in the notation of [PP09], we would need to consider  $q = 5$  and  $q = 6$  as well).

We will now outline how to go from a pair of braiding complex reflections  $R_x$  and  $R_y$  to (the combinatorial model of) a side in our polyhedron. We first explain the construction in the simplest case, namely when  $L_x \cap L_y$  is negative for the Hermitian inner product, or equivalently,  $m_x \cap m_y = p_{xy} \in \mathbf{H}_{\mathbb{C}}^2$ .

### 4.4.1 Basic construction of pyramids using braiding

The mirrors  $m_x$  and  $m_y$  of  $R_x$  and  $R_y$  pass through  $p_{xy}$ . Now consider the images of the lines  $m_x$  and  $m_y$  under powers of  $R_x R_y$ . Using subscript notation, these can be written as  $m_x, m_{xy\bar{x}}, m_{xyx\bar{y}\bar{x}}, \dots, m_{\bar{y}xy}, m_y$ . It is not hard to see that there are exactly  $q$  of these lines, all lying in the pencil of complex lines through  $p_{xy}$ . (If  $q$  is odd then  $m_y$  is the image of  $m_x$  under  $(R_x R_y)^{(q-1)/2}$ . If  $q$  is even  $m_x$  and  $m_y$  are in distinct orbits, each orbit comprising  $q/2$  lines.) These  $q$  lines form our starting point when constructing a side of the polyhedron.

Consider now a third complex reflection  $R_z$  with mirror  $m_z$  and angle  $\psi = 2\pi/p$ . For simplicity, we suppose  $m_z$  intersects each of  $m_x, m_{xy\bar{x}}, \dots, m_{\bar{y}xy}, m_y$  in a point of  $\mathbf{H}_{\mathbb{C}}^2$ , denoted by  $p_{xz}, p_{xy\bar{x}z},$  and so on. The  $q$  points  $p_{xz}, p_{xy\bar{x}z}, \dots, p_{yz}$  form the vertices of a  $q$ -gon in the line  $m_z$ . Together with the point  $p_{xy}$ , they form the vertices of a pyramid with apex  $p_{xz}$  and base the  $q$ -gon in  $m_z$ . The combinatorial model for the side is obtained by adding edges as follows. We include each of the  $q$  edges of the  $q$ -gon in the base, together with an edge from each of the base vertices to  $p_{xy}$  (see Figure 3).

In order for our polyhedron to have a well-defined side pairing, given a pyramid as above, it is natural to construct an opposite isometric pyramid. Note that the reflection  $R_z$  fixes the base of the above pyramid pointwise. We find a second pyramid by applying  $R_z$  to the first one. In this case  $x$  is replaced with  $zx\bar{z}$  and  $y$  is replaced with  $zy\bar{z}$  and so on.

The above procedure is illustrated in Figure 3. Part (a) shows a square pyramid with  $x = 2, y = 3, z = 1$ , and part (b) shows its opposite pyramid. Part (c) shows a triangular pyramid with  $x = 1, y = \bar{3}23$  and  $z = 23\bar{2}$ , and part (d) shows (the image under  $P^{-2}$  of) its opposite pyramid; here  $P^{-2}z^{-1}xzP^2P^{-2}(\bar{3}23)1(\bar{3}23)P^2 = 1$ , and similarly  $P^{-2}z^{-1}yzP^2 = 23\bar{2}$  and  $P^{-2}zP^2 = 1\bar{3}23\bar{1}$ .

The number of sides in these examples come from the fact that  $R_2$  and  $R_3$  braid with order 4, and  $R_1$  and  $R_{\bar{3}23}$  braid with order 3 (see section 4.3). Note also that we use relations in the group to write  $\bar{y}xyz = \bar{3}\bar{2}31\bar{3}2323\bar{2} = \bar{3}\bar{2}3123$  and  $yz = \bar{3}2323\bar{2} = 23$ .

Schwartz uses a similar procedure in [Sch03]. Since his generating reflections have order  $p = 2$ , in his case  $x = \bar{x}$  and  $y = \bar{y}$ . Consider Fig 4.2 of [Sch03] which depicts what Schwartz calls an odd  $B$  piece. This is made up of two square pyramids. In the front one,  $x = 1$ ,  $y = 3$  and  $z = 2$ . The apex is  $p_{xy} = [13]$  and the vertices around the base are  $p_{xz} = [12]$ ,  $p_{xy\bar{x}z} = [1312]$ ,  $p_{\bar{y}xyz} = [3132]$  and  $p_{yz} = p_{zy} = [23]$ . The rear pyramid is the image of the front one under  $R_z = I_2$  and has  $x = 212$ ,  $y = 232$  and  $z = 2$ .

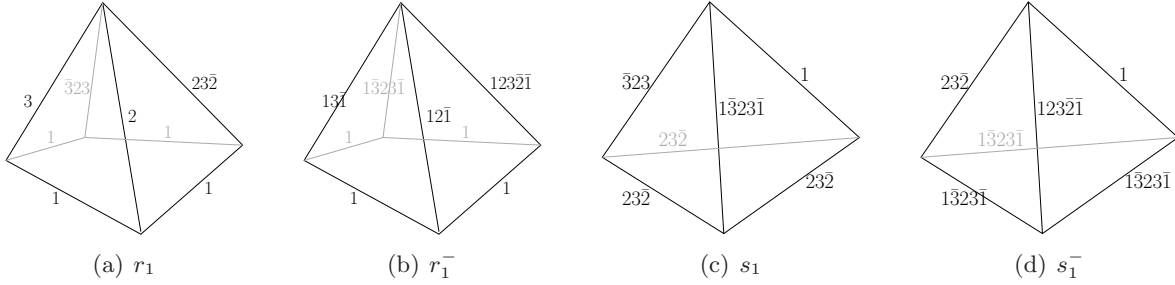


Figure 3: Combinatorial structure of the faces, in the case  $p = 3$  or  $4$ . Since all vertices are inside  $\mathbf{H}_{\mathbb{C}}^2$ , no truncation is needed.

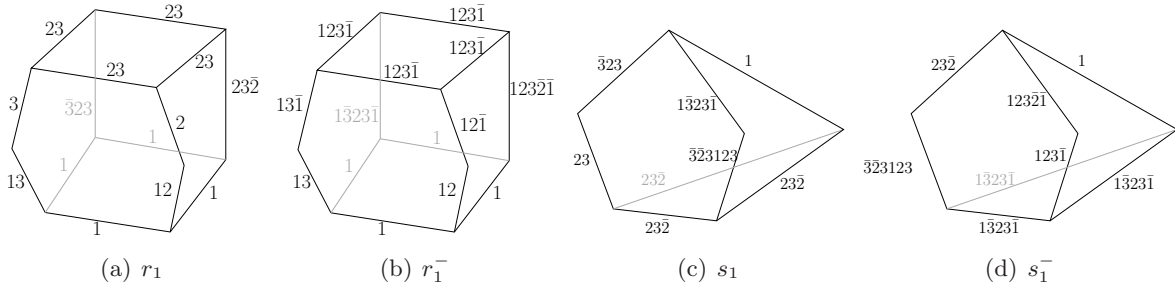


Figure 4: Combinatorial structure of the faces, in the case  $p = 5$  or  $6$ . A first truncation has occurred since the mirrors of  $R_1$ ,  $R_2$  and  $R_3$  are ultraparallel.

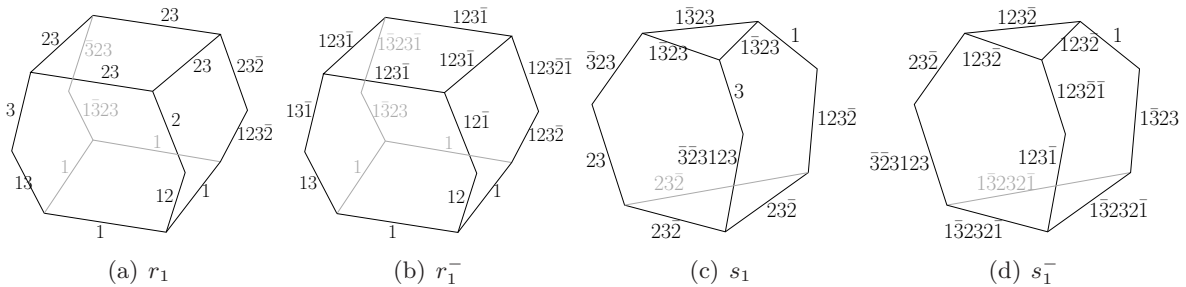


Figure 5: Combinatorial structure of the faces, in the case  $p = 8$  or  $12$ . Further truncation has occurred since the mirrors of  $R_1$  and  $R_3^{-1}R_2R_3$  are ultraparallel.

Given one pyramid as above, the ridges containing the apex are all triangles, for example the ridge determined by the three complex lines  $m_x$ ,  $m_y$ ,  $m_z$  with vertices  $p_{xy}$ ,  $p_{xz}$ ,  $p_{yz}$ . We can repeat the whole of the above construction starting with a different pair of these

complex lines, for example  $m_z$  and  $m_y$ . This will yield a new pyramid, whose base lies in  $m_x$  and which shares a common triangular side with our initial pyramid. In order to construct a combinatorial model for our polyhedron, we repeat this process. For each side of each pyramid, there should be exactly one other pyramid with the same triangular side, and the whole collection should close up and be invariant under powers of  $P$ . This game should be compared with [Sch03] or [Tho10] where a similar game is played. The main difference is that Schwartz is not interested in triangles if all three vertices lie outside complex hyperbolic space.

#### 4.4.2 Truncation

It may be that some, or all, of the vertices of the pyramid lie outside complex hyperbolic space. In this case, it turns out the intersection point is the polar vector of a mirror of a complex reflection in the group (provided  $p \geq 3$ ). With the notation above, suppose  $m_x$  and  $m_y$  are ultraparallel. As we have seen,  $(R_x R_y)^{q/2}$  or  $(R_x R_y)^q$ , for  $q$  even or odd respectively, is a complex reflection and commutes with  $R_x$  and  $R_y$ . Therefore the common orthogonal to  $m_x$  and  $m_y$  is the mirror  $m_{xy}$  of this power of  $R_x R_y$ .

The simplest case of this are the even  $A$  piece of Schwartz depicted in Figure 4.3 of [Sch03]. In this case  $q = 7$  (and he still has  $p = 2$ ) and he has two pyramids with a heptagonal base. For the front pyramid  $x = 131$ ,  $y = 2$  and  $z = 1$ . Thus the apex of the pyramid is  $p_{xy} = [1312]$ . Of the base vertices, four are points of complex hyperbolic space, namely:  $p_{xz} = [1311] = [13]$ ,  $p_{xy\bar{x}z} = [13121311] = [131213]$ ,  $p_{\bar{y}xyz} p_{z\bar{y}xy} = [121312]$  and  $p_{yz} = p_{zy} = [12]$ . The other three base vertices lie outside complex hyperbolic space. The rear pyramid is the image of the first under  $R_z = I_1$ , and so has  $x = 3$ ,  $y = 121$  and  $z = 1$ . Schwartz's picture does not illustrate the truncation arising from vertices lying outside complex hyperbolic space.

We now explain the implications of this truncation process for our polyhedra. The simplest feature is when  $m_x$  and  $m_y$  are ultraparallel. We denote their common orthogonal by  $m_{xy}$ . The  $q$  lines  $m_x, m_{xy\bar{x}}, m_{xyx\bar{y}\bar{x}}, \dots, m_{\bar{y}xy}, m_y$  are all orthogonal to  $m_{xy}$  and their intersection points with  $m_{xy}$  (denoted  $p_{xy}^x = m_x \cap m_{xy}$  etc.) now form the vertices of a  $q$ -gon in  $m_{xy}$ ; compare Figure 3(a) with Figure 4(a) and Figure 5(a), where the apex  $p_{23}$  has been replaced with a quadrilateral.

Next, we explain how the truncation affects base vertices. Suppose the mirrors  $m_x$  and  $m_z$  of  $R_x$  and  $R_z$  are ultraparallel. Then consider their common perpendicular line  $m_{xz}$ . The mirrors  $m_x$  and  $m_z$  intersect  $m_{xz}$  in distinct points, which we label  $p_{xz}^x$  and  $p_{xz}^z$  respectively. The point  $p_{xz}$  is then replaced with a line in  $m_{xz}$  between these two points. Compare Figure 3(c) with Figure 4(c). In particular, the vertex  $p_{23}$  has been replaced with an arc from  $p_{23}^{\bar{3}23}$  to  $p_{23}^{23\bar{2}}$ . We can still build up a polyhedron from these truncated polyhedra, the main difference being that the sides that were formerly triangles may be quadrilaterals, pentagons or hexagons.

#### 4.5 Definition of the polyhedron $E$

In this section we define the fundamental polyhedron  $E$ . We will show that  $E$  is a piecewise smooth polyhedron (as defined in Section 3.2), and in parallel we determine its precise combinatorics. This allows us to show that  $E$  is a fundamental domain for the action of the cosets of  $\Upsilon = \text{Stab}_\Gamma(E)$  in  $\Gamma$ .

### 4.5.1 Bounding bisectors

The basic fact we will use is that the pyramids constructed in section 4.4 have a natural geometric realization inside a suitable bisector. Indeed, for a given pyramid, there is a unique bisector that contains the base of the pyramid in a complex slice, and whose extended real spine contains its apex. We call this bisector the *supporting bisector* of the pyramid. Concretely, if the base is given by  $\mathbf{m}^\perp$  and the apex by  $\mathbf{a}$ , the real spine of the supporting bisector is given by the real span of  $\mathbf{a}$  and  $\mathbf{a} - \langle \mathbf{a}, \mathbf{m} \rangle \mathbf{m} / \langle \mathbf{m}, \mathbf{m} \rangle$  (a lift of the orthogonal projection of  $\mathbf{a}$  onto the base). The following gives a geometric justification for considering such bisectors:

**Proposition 4.7** *The supporting bisector of a pyramid contains all real geodesic segments between its vertices.*

This is obvious for edges in the base, as the base is contained in a complex slice of the supporting bisector. For edges through the apex, it follows from the fact that a bisector contains all geodesics intersecting the real spine. For edges in truncation faces, it follows from the fact that the complex line containing the truncation face is a complex slice of the supporting bisector.

The basic building blocks of  $E$  will be the following four bisectors, which are the supporting bisectors of the four faces described in section 4.4.

- Definition 4.8**
1.  $\mathcal{R}_1$  is the bisector whose extended real spine contains  $\mathbf{n}_1$  and  $\mathbf{n}_{23}$ ;
  2.  $\mathcal{R}_1^-$  is the image of  $\mathcal{R}_1$  under  $R_1$ ;
  3.  $\mathcal{S}_1$  is the bisector whose extended real spine contains  $\mathbf{n}_{23\bar{2}}$  and  $\mathbf{n}_{1\bar{3}23}$ ;
  4.  $\mathcal{S}_1^-$  is the image of  $\mathcal{S}_1$  under  $S_1$ .

Recall from section 4.1 that we denote by  $\mathbf{p}$  the isolated fixed point of  $P$ .

**Definition 4.9** *Let  $F$  be the intersection of the 28 half-spaces containing  $\mathbf{p}$  bounded by the bisectors  $P^k \mathcal{R}_1^\pm$  and  $P^k \mathcal{S}_1^\pm$  ( $k = 0, \pm 1, \pm 2, \pm 3$ ). The region  $E$  is the connected component of  $F$  containing  $\mathbf{p}$ .*

We will refer to the 28 bisectors of the form  $P^k \mathcal{R}_1^\pm$  and  $P^k \mathcal{S}_1^\pm$  as the **bounding bisectors**.

**Remark 4.10** (1) The domain  $E$  has much simpler combinatorics than the Dirichlet domains that were used in [DPP11] (when  $p \geq 4$ ). As a slight drawback of not using Dirichlet domains, it is unclear whether  $E$  is star-shaped with respect to  $\mathbf{p}$ , and hence it is not convenient to use geodesic cone arguments; rather we use fundamental domains for coset decompositions.

(2) It turns out to be complicated to determine the precise combinatorics of the polyhedron  $F$  bounded by the bounding bisectors; in fact it is not even obvious that  $F$  is connected. This is why we define  $E$  as a component of  $F$ . In fact one could prove that  $E = F$  (which would then give a description of the combinatorial structure of  $F$ ) but this is not needed in order to prove our main theorem. The main reason for working with  $E$  rather than  $F$  is that it significantly reduces the number of computer calculations.

It will be useful to distinguish between sides of  $E$  and the bisector that contains them, so we will use the following notation:

**Definition 4.11** *The intersection of  $E$  with a given bounding bisector is called a **bounding side**. The 28 bounding sides will be denoted by*

$$P^k r_1^\pm = E \cap P^k \mathcal{R}_1^\pm; \quad P^k s_1^\pm = E \cap P^k \mathcal{S}_1^\pm,$$

for  $k = 0, \pm 1, \pm 2, \pm 3$ .

The combinatorial structure of the bounding sides  $P^k r_1^\pm$  and  $P^k s_1^\pm$  is described in detail in Section 4.6.2. Note that for a polyhedron  $E$  bounded by bisectors in  $\mathbf{H}_{\mathbb{C}}^2$ , it is by no means obvious how to determine the combinatorics of  $E$  from the knowledge of its vertices, which explains the length of the sections stating and proving the combinatorics.

#### 4.5.2 Symmetry

The polyhedron  $E$  is by definition  $P$ -invariant. Our notation for bisectors is set up so that the  $P$ -orbits can be conveniently read off their labels. For vertices (and mirrors of reflections), it is a bit more tedious but completely straightforward to study these orbits. For concreteness we treat a couple of examples in detail.

The basic point is that  $P = R_1 J$ , and  $J R_k J^{-1} = R_{k+1}$ , i.e. conjugation by  $J$  raises indices by one (mod 3). The  $P$ -image of the mirror of  $R_1$ , which corresponds to the complex line polar to  $m_1$ , is polar to  $P m_1 = m_{12\bar{1}}$ , since

$$P1P^{-1} = 1J1J^{-1}\bar{1} = 12\bar{1}.$$

The  $P$ -image of  $p_{23}$  is simply  $p_{13}$ , since it is fixed by  $P23P^{-1} = 1J23J^{-1}\bar{1} = 131\bar{1} = 13$ . Similarly,  $Pp_{13} = p_{12}$ . Applying  $P$  often yields slightly more complicated results, for instance the  $P$ -image of  $p_{12}$  is given by  $p_{P12P^{-1}} = p_{123\bar{1}}$ , since

$$P12P^{-1} = 1J12J^{-1}\bar{1} = 123\bar{1}.$$

It will be important in the sequel to observe that  $E$  also has an antiholomorphic involutive symmetry, which we now explain. The antiholomorphic map

$$\iota_{23} : \begin{bmatrix} z_1 \\ z_2 \\ z_3 \end{bmatrix} \mapsto \begin{bmatrix} \bar{z}_1 \\ \bar{z}_3 \\ \bar{z}_2 \end{bmatrix}. \quad (17)$$

clearly induces an isometry of  $\mathbf{H}_{\mathbb{C}}^2$ , since  $\langle \iota_{23} \mathbf{v}, \iota_{23} \mathbf{w} \rangle = \overline{\langle \mathbf{v}, \mathbf{w} \rangle}$ . It is easy to see that  $\iota_{23}$  conjugates  $J$  into  $J^{-1}$ ,  $R_1$  into  $R_1^{-1}$ ,  $R_2$  into  $R_3^{-1}$  and  $R_3$  into  $R_2^{-1}$ . From this it follows that the antiholomorphic map  $\iota$  given by

$$\iota = R_1 \iota_{23} \quad (18)$$

is an involution as well, and this will be useful several times throughout the paper.

**Proposition 4.12** *The involution  $\iota$  preserves  $E$ , sending  $r_1$  to  $r_1^-$  and  $s_1$  to  $s_1^-$ .*

PROOF. Since  $P = R_1 J$ , it follows easily that  $\iota$  conjugates  $R_1$  into  $R_1^{-1}$ , and  $P$  into  $P^{-1}$  (beware that  $\iota_{23}$  does not conjugate  $P$  into  $P^{-1}$ ). In particular,  $\iota$  fixes  $\mathbf{p}$ .

The fact that  $\iota$  conjugates  $S_1$  into  $S_1^{-1}$  follows from the fact that  $S_1$  can be expressed as a palindromic word in  $R_1$  and  $P$ , namely  $S_1 = P^2 R_1 P^{-2} R_1 P^2$ .

Hence  $\iota$  sends the half-space containing  $\mathbf{p}$  bounded by  $P^k \mathcal{R}_1^\pm$  (respectively  $P^k \mathcal{S}_1^\pm$ ) to the half-space containing  $\mathbf{p}$  bounded by  $P^{-k} \mathcal{R}_1^\mp$  (respectively  $P^{-k} \mathcal{S}_1^\mp$ ). This shows that  $\iota$  preserves  $F$ , and this implies that it preserves  $E$  (which is the connected component of  $F$  containing  $\mathbf{p}$ ).  $\square$

Note that  $\iota$  conjugates an isometry given by a word  $w$  (see Section 4.2) into the isometry given by the word  $1w'\bar{1}$ , where  $w'$  is obtained from  $w$  by replacing each occurrence of  $1, 2, 3$  by  $\bar{1}, \bar{3}, \bar{2}$  respectively. One can then read the action of  $\iota$  on the vertices  $p_w, q_w$  by applying this rule to the label  $w$ . For instance, we have

$$\begin{aligned}\iota(p_{12}) &= p_{1\bar{1}\bar{3}\bar{1}} = p_{\bar{3}\bar{1}} = p_{13} \\ \iota(p_{23}) &= p_{1\bar{3}\bar{2}\bar{1}} = p_{123\bar{1}},\end{aligned}\tag{19}$$

and

$$\iota(q_{123\bar{2}}) = q_{\bar{3}\bar{2}\bar{3}\bar{1}} = q_{1\bar{3}23}\tag{20}$$

Observe that  $Pp_{13} = p_{12}$  implies  $P^3p_{12} = P^{-3}p_{13}$ . Since  $p_{\bar{3}\bar{2}\bar{3}123} = R_3^{-1}R_2^{-1}R_1^{-1}p_{13} = P^{-3}p_{13}$  and  $\iota(p_{\bar{3}\bar{2}\bar{3}123}) = R_1(p_{23\bar{2}\bar{1}\bar{3}\bar{2}}) = R_1R_2R_3p_{12} = P^3p_{12}$ , we get

$$\iota(p_{\bar{3}\bar{2}\bar{3}123}) = p_{\bar{3}\bar{2}\bar{3}123}.\tag{21}$$

### 4.5.3 Alternative descriptions

Since the bounding bisectors  $\mathcal{R}_1^\pm, \mathcal{S}_1^\pm$  are central to the construction of the fundamental domain, it will be useful to have alternative descriptions. In Table 1 we write the bounding bisectors as equidistant from a pair of points and we also give some information that is useful for computational purposes; see also Section 4.8.3). We label vectors that appear in the table following the conventions from Section 4.2;  $y_0$  denotes the intersection point of the complex spines of  $\mathcal{R}_1$  and  $\mathcal{S}_1$  (see below for explicit computation).

Bisector	Equidistant	$\mathbb{R}$ -spine	Polar	Reflections
$\mathcal{R}_1$	$\mathcal{B}(y_0, R_1^{-1}y_0)$	$\text{Span}_{\mathbb{R}}(\mathbf{n}_1, \mathbf{n}_{23})$	$\mathbf{f}_1 = [0, \bar{\tau}, \bar{a}\tau]$	$1, (23)^2$
$\mathcal{R}_1^-$	$\mathcal{B}(y_0, R_1y_0)$	$\text{Span}_{\mathbb{R}}(a^2\mathbf{n}_1, \bar{a}\mathbf{n}_{123\bar{1}})$	$\mathbf{f}_2 = \mathbf{f}_1$	$1, 1(23)^2\bar{1}$
$\mathcal{S}_1$	$\mathcal{B}(y_0, S_1^{-1}y_0)$	$\text{Span}_{\mathbb{R}}(a\mathbf{n}_{23\bar{2}}, \mathbf{n}_{1\bar{3}23})$	$\mathbf{f}_3 = [a^2\bar{\tau}, -a, -\bar{\tau}]$	$23\bar{2}, (1\bar{3}23)^3$
$\mathcal{S}_1^-$	$\mathcal{B}(y_0, S_1y_0)$	$\text{Span}_{\mathbb{R}}(\bar{a}\mathbf{n}_{1\bar{3}23\bar{1}}, \mathbf{n}_{123\bar{2}})$	$\mathbf{f}_4 = [a^2\bar{\tau}, a\tau, 1]$	$1\bar{3}23\bar{1}, (123\bar{2})^3$

Table 1: Descriptions of the bisectors  $\mathcal{R}_1^\pm$  and  $\mathcal{S}_1^\pm$  as equidistant hypersurfaces, and in terms of vectors spanning their extended real spines. We also give polar vectors for their complex spines and reflections whose mirrors are contained in each bisector (the mirror is either a complex line or a point, depending on the value of  $p$ ).

In the table, we list two vectors  $\mathbf{w}, \mathbf{v}$  with real inner products, so that the extended real spine is obtained by taking real linear combinations of these two vectors (the real spine corresponds to such vectors with negative square norm). For convenience, we also give a polar vector to the complex spine, i.e. a nonzero vector  $\mathbf{f}$  with  $\langle \mathbf{w}, \mathbf{f} \rangle = \langle \mathbf{v}, \mathbf{f} \rangle = 0$ , as well as specific reflections whose mirrors are slices of these bisectors.

**Proposition 4.13** *The bisectors  $\mathcal{R}_1, \mathcal{R}_1^-, \mathcal{S}_1$  and  $\mathcal{S}_1^-$  are all coequidistant from a point in  $\mathbf{H}_{\mathbb{C}}^2$ , which we denote by  $y_0$ . More specifically,  $\mathcal{R}_1^{\pm} = \mathcal{B}(y_0, R_1^{\mp 1} y_0)$  and  $\mathcal{S}_1^{\pm} = \mathcal{B}(y_0, S_1^{\mp 1} y_0)$ .*

PROOF. From a pair of vectors  $\mathbf{w}, \mathbf{v}$  spanning the real spine of a bisector, one easily finds a vector orthogonal to both of them, since this amounts to finding a vector  $\mathbf{f}$  that satisfies

$$\mathbf{w}^* H \mathbf{f} = \mathbf{v}^* H \mathbf{f} = 0$$

which is a linear system in  $\mathbf{f}$ . This allows us to get formulae for the four vectors  $\mathbf{f}_j$ . Note that  $\mathcal{R}_1$  and  $\mathcal{R}_1^-$  are cospinal, i.e. they have the same complex spine.

From the  $\mathbf{f}_j$ , one can easily find the intersection between two of the complex spines, again by solving a linear system. The vector  $\mathbf{y}_0$  can be obtained in this way, being the unique intersection point of the complex spines of  $\mathcal{R}_1$  and  $\mathcal{S}_1$ . For future reference, we give explicit coordinates:

$$\mathbf{y}_0 = \begin{bmatrix} -a^3(\bar{a}^2\bar{\tau} + a)^2 \\ (a^2\bar{\tau} + \bar{a}\tau)(a^2\bar{\tau} - \bar{a}) \\ (a^2\bar{\tau} + \bar{a}\tau)(\bar{a}^2\tau - a) \end{bmatrix}, \quad (22)$$

One easily checks that  $\langle \mathbf{y}_0, \mathbf{f}_j \rangle = 0$  for all  $j = 1, 2, 3, 4$ , so that all four bisectors  $\mathcal{R}_1^{\pm}, \mathcal{S}_1^{\pm}$  are equidistant from  $\mathbf{y}_0$ . A further simple check shows that  $\langle \mathbf{y}_0, \mathbf{y}_0 \rangle < 0$  and so  $\mathbf{y}_0$  corresponds to a point  $y_0 \in \mathbf{H}_{\mathbb{C}}^2$ .

We now show that  $\mathcal{R}_1 = \mathcal{B}(y_0, R_1^{-1} y_0)$ . From Table 1 we see that the spine of  $\mathcal{R}_1$  is the real span of  $\mathbf{n}_1$  and  $\mathbf{n}_{23}$ . These vectors are both fixed by the involution  $\iota_{23}$  defined in (17), and so it also fixes any vector on the real spine of  $\mathcal{R}_1$ . Applying  $\iota_{23}$  to  $\mathbf{y}_0$  and simplifying, we see that  $\iota_{23} \mathbf{y}_0 = \bar{a}^2 R_1^{-1} \mathbf{y}_0$ . Therefore, if  $\mathbf{s}$  is any vector in the real spine of  $\mathcal{R}_1$  we have:

$$\langle \mathbf{y}_0, \mathbf{s} \rangle = \overline{\langle \iota_{23} \mathbf{y}_0, \iota_{23} \mathbf{s} \rangle} = a^2 \overline{\langle R_1^{-1} \mathbf{y}_0, \mathbf{s} \rangle}.$$

Therefore, any point of  $\mathcal{R}_1$  is equidistant from  $y_0$  and  $R_1^{-1} y_0$ . Applying  $R_1$  we see that  $\mathcal{R}_1^-$  is equidistant from  $R_1 y_0$  and  $y_0$ .

Similarly, the involution  $\bar{3}\bar{2}\bar{3}\bar{1}\bar{3}\iota_{12}$  fixes  $a\mathbf{n}_{23\bar{2}}$  and  $\mathbf{n}_{1\bar{3}23}$  and so fixes the spine of  $\mathcal{S}_1$  pointwise. We calculate that  $\bar{3}\bar{2}\bar{3}\bar{1}\bar{3}\iota_{12} \mathbf{y}_0 = \bar{a}^2 S_1^{-1} \mathbf{y}_0$ . Hence  $\mathcal{S}_1 = \mathcal{B}(y_0, S_1^{-1} y_0)$ . Applying  $S_1$ , we find that  $\mathcal{S}_1^- = \mathcal{B}(S_1 y_0, y_0)$ .  $\square$

Later, in Table 3 we describe  $\mathcal{R}_1^{\pm}, \mathcal{S}_1^{\pm}$  and their images under powers of  $P$  as equidistant hypersurfaces with respect to some other points.

## 4.6 Combinatorics of $E$

In this section we describe the combinatorics of  $E$  and show that it is a topological ball with piecewise smooth boundary, each piece being contained in one of the bounding bisectors. The proof of the precise combinatorics of  $E$  is difficult, but necessary to apply the Poincaré polyhedron theorem. In fact it is delicate even to give a detailed description of the combinatorics (this will be done in Section 4.6.1). Indeed, for a general polyhedron bounded by bisectors in  $\mathbf{H}_{\mathbb{C}}^2$ , it is not sufficient to give the vertices, as there can be for instance distinct 1-cells joining two given vertices (see [DFP05]).

In order to prove the combinatorics, we first construct a combinatorial model  $\widehat{E}$  for  $E$ . We then describe its geometric realization, which is a map  $\phi$  from  $\widehat{E}$  into  $\overline{\mathbf{H}_{\mathbb{C}}^2}$ , sending each 3-cell into one of the bounding bisectors (see Definition 4.8), and we prove that  $\phi(\widehat{E}) = E$ .



This simultaneously proves the statement of the combinatorics of  $E$ , and shows that  $E$  is a polyhedron in the sense of Section 3.2.

Our combinatorial model is somewhat similar to the one used by Schwartz in Section 6 of [Sch03]. However, our geometric realization of  $\widehat{E}$  uses bisectors whereas Schwartz uses affine cells.

#### 4.6.1 Statement of the combinatorics of $E$

We state the combinatorics in the form of pictures of the 3-cells, with incidence information along each piece of the skeleton. Recall from Section 4 that  $E$  only has two isometry classes of faces (applying  $\iota$  and powers of  $P$ ), so we need only draw pictures for  $r_1 = \mathcal{R}_1 \cap E$  and  $s_1 = \mathcal{S}_1 \cap E$ .

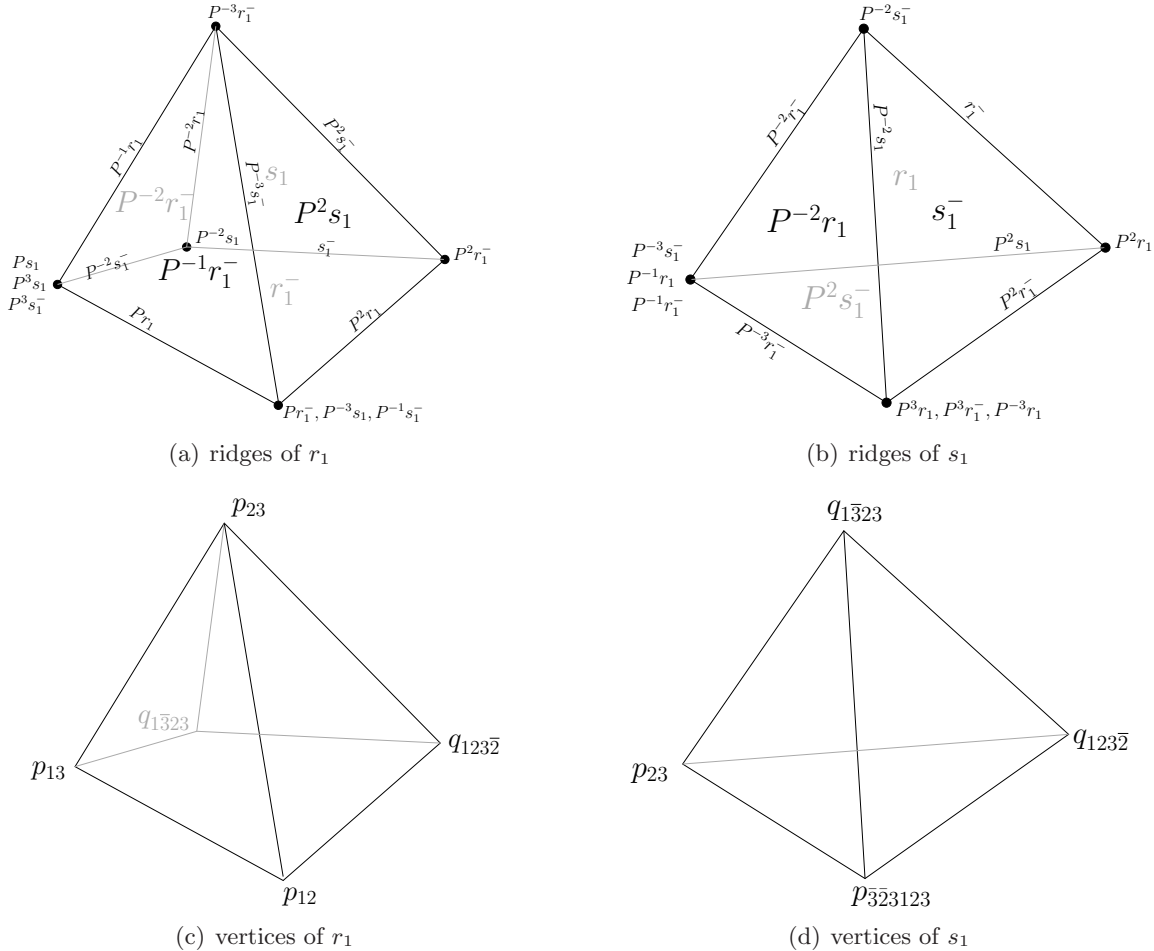


Figure 6: Adjacency relations of  $r_1$  and  $s_1$  with other faces of  $\widehat{E}$ , for  $p = 3, 4$ . Larger font is used to label ridges, and smaller fonts to label lower-dimensional facets.

Figures 6 to 8 give a concise, efficient description of the combinatorics. For each 3-face, we give two different pictures (top and bottom), one listing bisectors containing each facet, one listing vertices. At first glance, the pictures may seem a little cryptic, so we briefly explain how the incidence relations can be read off.

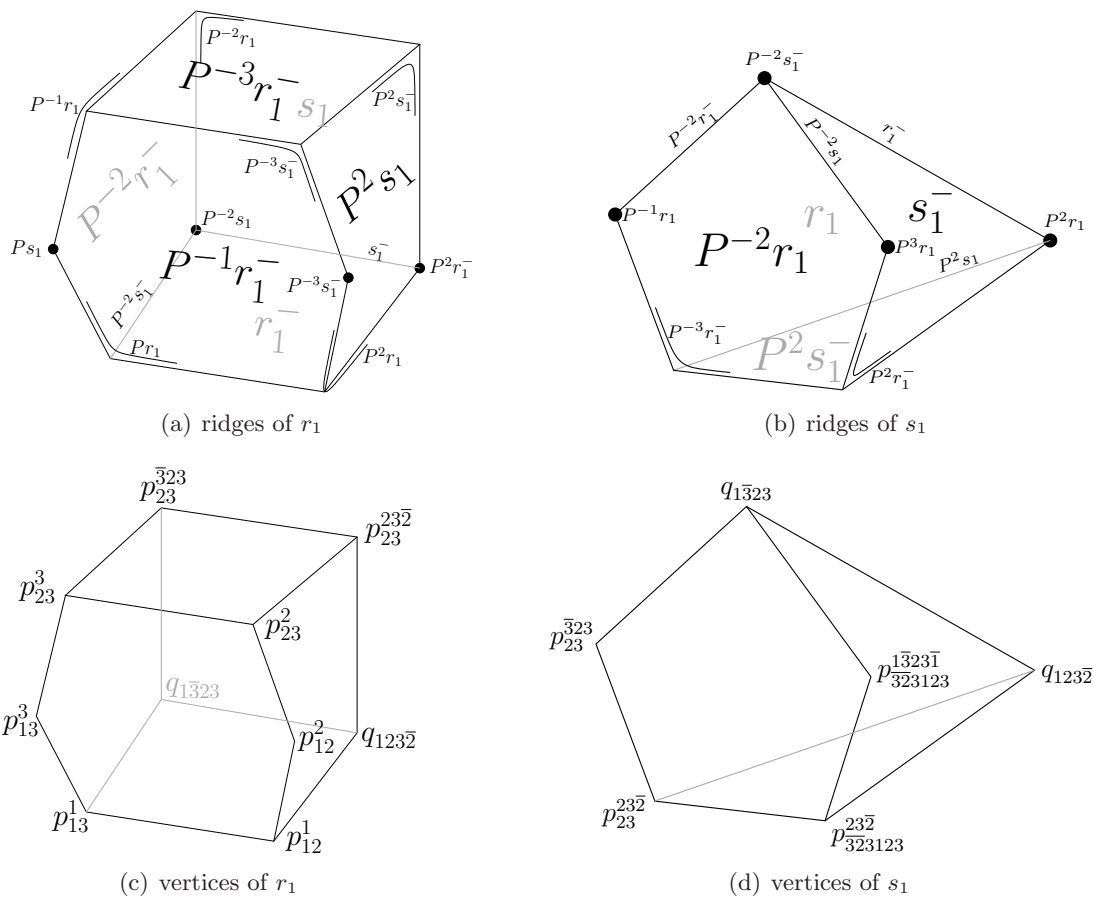


Figure 7: Adjacency relations of  $r_1$  and  $s_1$  with other faces of  $\widehat{E}$ , for  $p = 5, 6$ . We draw curved lines when two neighboring edges lie on the same intersection of three bisectors.

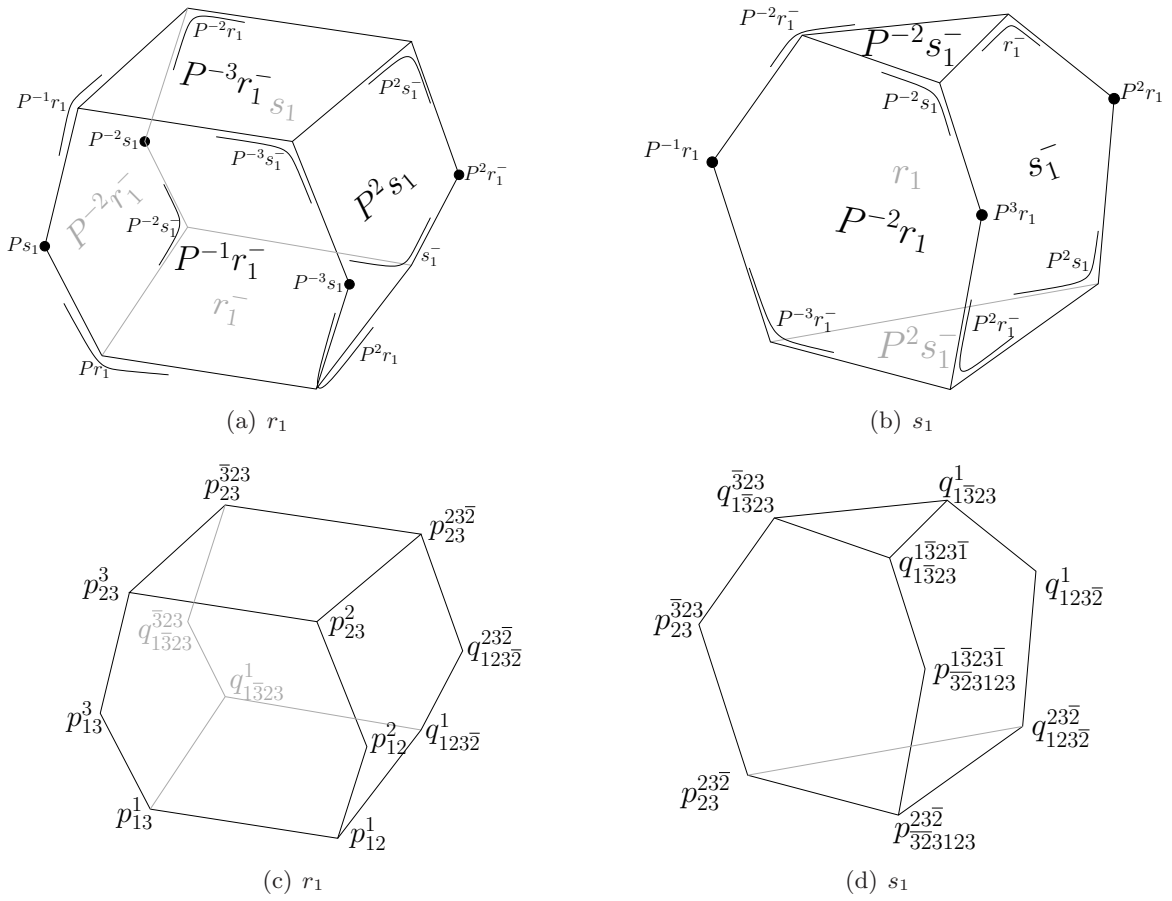


Figure 8: Adjacency relations of  $r_1$  and  $s_1$  with other faces of  $\widehat{E}$ , for  $p = 8, 12$ .

Each cell in the picture is contained in the union of the cells whose names are on facets incident to that cell. As an example, we obtain the list of all bounding sides containing the vertex labelled  $p_{12}$  on part (c) of Figure 6. Obviously it is contained in  $r_1$ . The picture in (a) suggests that it is on three 2-cells of  $r_1$ , whose labels indicate that  $p_{12}$  is also on  $r_1^-$ ,  $P^{-1}r_1^-$ , and  $P^2s_1$ . Similarly, from the 1-cells of  $r_1$  containing  $p_{12}$ , we see that it is also on  $Pr_1$ ,  $P^{-3}s_1^-$  and  $P^2r_1$ . Finally, the labels near that vertex in part (a) of the Figure indicate that it is on  $Pr_1^-$ ,  $P^{-3}s_1$  and  $P^{-1}s_1^-$ . (See Remark 6.1 below for the vertex notation  $p_u^v$ ,  $q_u^v$ ).

Note that the pictures for  $P^k r_1$  and  $P^k s_1$  are obtained simply by applying  $P^k$ , whereas those for  $P^k r_1^-$  and  $P^k s_1^-$  one also needs to apply the antiholomorphic involution  $\iota$  from Section 4.5.2. Recall that  $\iota$  conjugates  $R_1$  into  $R_1^{-1}$ ,  $S_1$  into  $S_1^{-1}$ , and  $P$  into  $P^{-1}$ , so the image of the figures in part (a) and (b) under  $\iota$  are obtained simply by changing signs. For the figures in parts (c) and (d), one needs to use the description of the action of  $\iota$  on vertices according to their labels (see Section 4.5.2).

**Remark 4.14** • The vector  $\mathbf{n}_{23}$  is a negative vector when  $p = 3$  and a null vector when  $p = 4$ . The corresponding point  $p_{23}$  is therefore in  $\mathbf{H}_{\mathbb{C}}^2$  and on  $\partial\mathbf{H}_{\mathbb{C}}^2$  respectively. Hence, for  $p = 3$  and  $p = 4$ , the combinatorics of the polyhedra  $E$  are only the same when viewed in  $\mathbf{H}_{\mathbb{C}}^2 \cup \partial\mathbf{H}_{\mathbb{C}}^2$ , some vertices being on the ideal boundary for  $p = 4$  (see also the discussion around Figure 2). A similar remark is in order for  $p = 5$  and  $p = 6$ , since for  $p = 6$  the polyhedron  $E$  has vertices on the ideal boundary  $\partial\mathbf{H}_{\mathbb{C}}^2$ .

- The vector  $\mathbf{n}_{23}$  is a positive vector when  $p \geq 5$ . Therefore the vertex  $p_{23}$  of  $r_1$  is replaced with a ridge in  $m_{23}$ , the complex line polar to  $\mathbf{n}_{23}$ . We refer to this process as **truncation**. In  $s_1$ , the vertex  $p_{23}$  is only replaced with an edge in  $m_{23}$  since it only intersects two complex lines orthogonal to  $m_{23}$ , namely  $m_{23\bar{2}}$  and  $m_{\bar{3}23}$ . Similarly, the vertices  $p_{12}$ ,  $p_{13}$  of  $r_1$  and the vertex  $p_{\bar{3}\bar{2}3123}$  of  $s_1$  are replaced with edges in the corresponding complex lines. A second truncation process occurs for the  $q_*$  vertices for  $p \geq 8$ . We use notation of the form  $p_u^v$ ,  $q_u^v$  for the new vertices appearing after truncation:  $p_u^v$  or  $q_u^v$  denotes the intersection of the complex lines polar to  $\mathbf{n}_u$  and  $\mathbf{n}_v$ .

#### 4.6.2 Outline of the geometrization of the combinatorial model $\widehat{E}$

In this section, we build a combinatorial model  $\widehat{E}$  for  $E$ . To keep the notation reasonable, we do not introduce new symbols for the facets of  $\widehat{E}$ , and simply label them the same as the corresponding facets of  $E$ .

In order to define  $\widehat{E}$ , we first define its 3-skeleton  $\widehat{E}_3$ . This is made up of 28 cells, attached according to the adjacency relations indicated in Figures 6 to 8.

Note that each 2-cell is on precisely two 3-cells, which makes it obvious which combinatorial 2-cells get identified. The gluing is then uniquely determined by matching labels of the vertices. The identifications for 0 and 1-cells are most conveniently read off parts (c), (d) of the figures. Indeed the action of  $\iota$  and  $P$  on the vertices can easily be read off the labels; see Section 4.6.1 and also Tables 16 to 19 in the appendix (Section 7).

It is easy to see that all  $k$ -cells of the 3-skeleton  $\widehat{E}_3$  are homeomorphic to embedded closed balls, and in particular for each  $k$ -cell  $f$  of  $\widehat{E}_3$ ,  $\partial f$  is an embedded  $(k-1)$ -sphere (see Figures 6 through 8).

We will also prove the following, which is much less obvious (see Section 4.7).

**Theorem 4.15**  $\widehat{E}_3$  is homeomorphic to  $S^3$ .

This allows us to define  $\widehat{E}$ , which is obtained by attaching a single 4-cell to  $\widehat{E}_3$  in the obvious manner.

We now describe a piecewise smooth geometric realization  $\phi : \widehat{E} \rightarrow \overline{\mathbf{H}}_{\mathbb{C}}^2$ , i.e. we describe a specific  $k$ -ball in  $\overline{\mathbf{H}}_{\mathbb{C}}^2$  for each  $k$ -cell of  $\widehat{E}$ . Naturally, the realization is uniquely determined by the requirement that each 3-cell be mapped into the appropriate bisector (or rather its closure in  $\overline{\mathbf{H}}_{\mathbb{C}}^2$ , since for  $p = 4$  or  $6$  some vertices of  $E$  lie on the ideal boundary).

We define  $\phi$  inductively on dimension, starting from vertices, then extending it successively to the 1-skeleton, then to the 2-skeleton, and so forth. When realizing the  $k$ -faces, we will check the following conditions on the restriction of  $\phi$  to the  $k$ -skeleton  $\widehat{E}_k$ :

- (Consistency) For each  $k$ -face  $f$ ,  $\phi(f)$  is contained in all the bisectors indicated by the labels in Figures 6 through 8;
- (Correct side)  $\phi(\widehat{E}_k)$  is entirely contained in  $F$ ;
- (Embeddedness)  $\phi$  gives an embedding of  $\widehat{E}_k$ .

The consistency condition is obvious for 2 and 3-faces, but it requires some calculations for vertices and edges (note that these lie on more bisectors than their codimension).

The fact that  $\phi(\widehat{E}_k)$  lies inside  $F$  amounts to showing that for each bounding bisector  $\mathcal{B}$ ,  $\phi(\widehat{E}_k)$  is on the same side of  $\mathcal{B}$  as  $\mathbf{p}$ . We will do this by analyzing, for each  $k$ -face  $f$ , the intersection  $f \cap \mathcal{B}$  with every bounding bisector  $\mathcal{B}$ . Because the intersection patterns of  $F$  are governed by the intersection of bisectors, the “correct side” condition actually implies the embeddedness.

Note that  $\phi(\widehat{E})$  is connected, so  $\phi(\widehat{E}) \subset F$  actually implies  $\phi(\widehat{E}) \subset E$  (recall that  $E$  is the connected component of  $F$  containing  $\mathbf{p}$ ), provided we can connect  $\mathbf{p}$  to a single point in  $\phi(\widehat{E})$  within  $F$ . This is contained in the following result, which is easily proved by giving explicit parametrizations for the relevant geodesic segments (see Section 4.8.2), and checking that  $\mathbf{p}$  is on the correct side of the 28 bounding bisectors.

**Lemma 4.16** *For  $p = 3, 4$  (respectively  $p = 5, 6, 8, 12$ ) the geodesic segment  $[\mathbf{p}, p_{12}]$  (resp.  $[\mathbf{p}, p_{12}^1]$ ) intersects the 28 bounding bisectors at most at the endpoint  $p_{12}$  (resp.  $p_{12}^1$ ). It is contained in  $F$ , whereas the complementary geodesic ray, from  $p_{12}$  (resp. from  $p_{12}^1$ ) to  $\partial\mathbf{H}_{\mathbb{C}}^2$  is entirely outside  $F$ .*

We now sketch the general scheme that allows us to construct the geometric realization  $\phi$ . For vertices, the labels in the bottom part of Figures 6 through 8 determine an embedding of the 0-skeleton of  $\widehat{E}$  (each vertex is the fixed point of a specific isometry in the group). The embedding part of this statement corresponds simply to the fact that all vertices in the list are distinct. The consistency condition will be checked in Section 4.8.1, and the correct side condition then amounts to checking a small set of (strict) inequalities, which can easily be done with a computer.

Now let  $k \geq 1$ , and suppose  $\phi$  is already known to give an embedding of the  $(k-1)$ -skeleton. In order to extend  $\phi$  across a  $k$ -cell  $f$  of  $\widehat{E}$ , we exhibit a specific closed  $k$ -dimensional ball  $D^k$  in  $\overline{\mathbf{H}}_{\mathbb{C}}^2$  containing the  $(k-1)$ -skeleton of  $f$ , which is in fact forced by the consistency condition. More specifically, for  $k = 1$ , each ball is simply the (unique) real geodesic segment between the two vertices realizing the 0-skeleton of  $f$ . For  $k = 2$  or  $3$ , the  $k$ -ball is given by the intersection of  $4 - k$  (closures of) bisectors. The specific set of bisectors is obtained from the labels in Figures 6 to 8. Finally, for  $k = 4$ , the ball is of course the whole of  $\overline{\mathbf{H}}_{\mathbb{C}}^2$ .

Since we assume  $\phi$  induces an embedding of the  $(k - 1)$  skeleton,  $\phi(\partial f)$  is a piecewise smoothly embedded  $(k - 1)$ -sphere in  $D^k$  (with finitely many points on  $\partial \mathbf{H}_{\mathbb{C}}^2$ ). This gives a well-defined  $k$ -ball that realizes  $f$ . Implicit in the above description is the assumption that the relevant pairs of bisectors intersect in disks, which will be proved in Section 4.8.3. We postpone the proof of consistency and embeddedness of the 0, 1, 2 and 3-skeletons, which will be discussed in Sections 4.8.1 through 4.8.5 (for clarity, we collect all results about each dimension in a separate section). Among all the consistency, correct side and embeddedness conditions, the most difficult one is correct side condition for the 2-skeleton. This relies on difficult computations, explained in detail in Section 4.8.4.

Assuming these results, we obtain a realization of all  $\widehat{E}$ , by mapping the single 4-cell to the 4-ball bounded by  $\phi(\widehat{E}_3)$  (this is a piecewise smoothly embedded copy of  $S^3$  so it bounds a well-defined closed ball). Note that this ball component contains the fixed point  $\mathbf{p}$  of  $P$ , by Lemma 4.16. As a summary, we get the following:

**Theorem 4.17**  $\phi$  defines an embedding of  $\widehat{E}$ , with image contained in  $F$ .

The following result then follows from elementary topology.

**Corollary 4.18** The realization of  $\widehat{E}$  is equal to  $E$ . In particular,  $E$  is a polyhedron in the sense of Section 3.2.

PROOF. (of Corollary 4.18) By Theorem 4.17,  $\phi(\widehat{E}) \subset E$ . We now show  $E \subset \phi(\widehat{E})$ . No point of  $E^\circ$  is contained in any of the 28 bounding bisectors, hence  $E^\circ$  has empty intersection with  $\phi(\widehat{E}_3)$ . Since  $E^\circ$  is connected and contains  $\mathbf{p}$ , which is contained in  $\phi(\widehat{E})$ , we get that  $E \subset \phi(\widehat{E})$  as required.  $\square$

#### 4.7 $\widehat{E}_3$ is homeomorphic to $S^3$

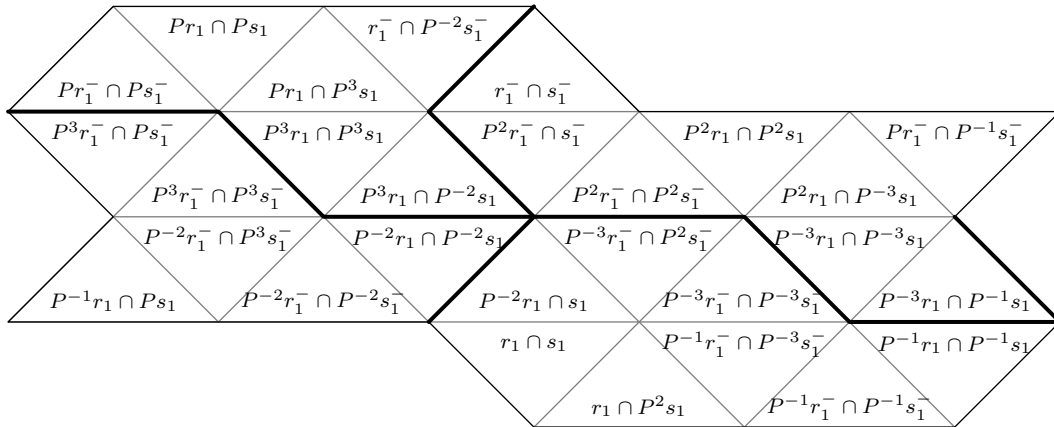


Figure 9: The combinatorics of the intersection  $T^r \cap T^s$ , for  $p = 3, 4$ . This intersection is a torus, and accordingly the top and bottom sides (resp. left and right sides) are identified by translation. The bold lines describe 2 splittings of the torus into annuli, corresponding to splittings of the solid tori into pairs of solid cylinders.

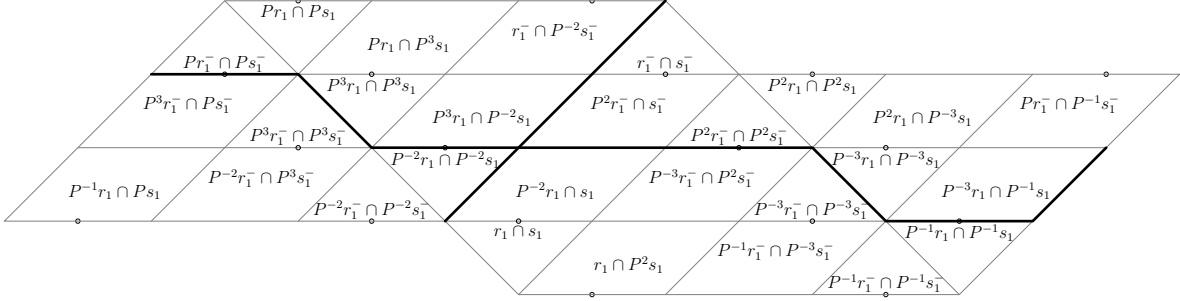


Figure 10: The combinatorics of the intersection  $T^r \cap T^s$ , for  $p = 5, 6$ .

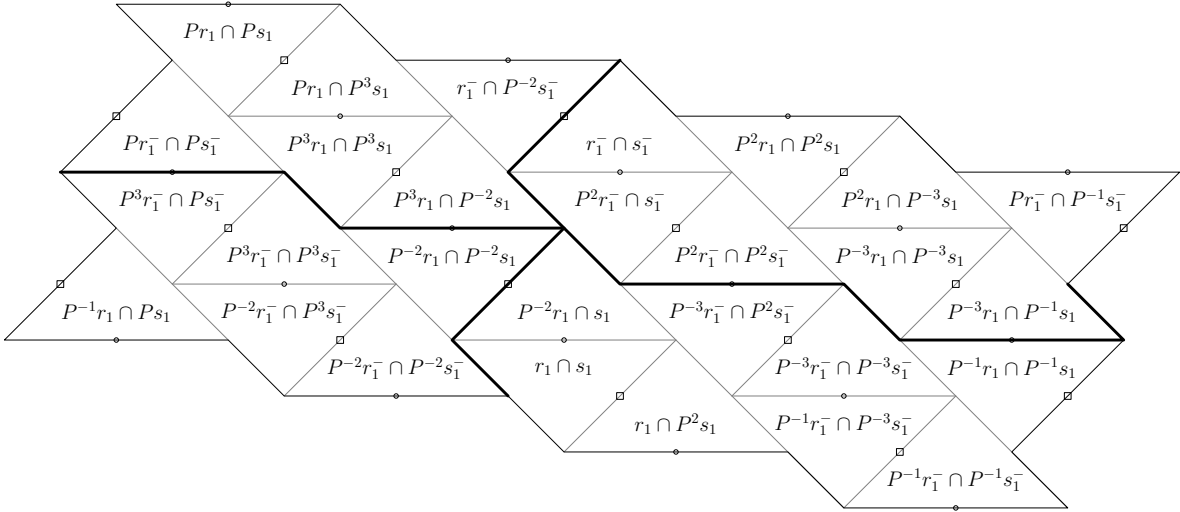


Figure 11: The combinatorics of the intersection  $T^r \cap T^s$ , for  $p = 8, 12$ . The torus is now not embedded, the white squares correspond to pinch points, i.e. they come in pairs that get identified in  $\mathbf{H}_{\mathbb{C}}^2$ .

This section contains a proof of Theorem 4.15. We will exhibit  $\widehat{E}_3$  as the union of two solid tori with common boundary, and check that the boundary circles of a meridian in each intersect at a single point.

In order to do this, consider the following two unions of 3-cells:

$$T^r = \bigcup_{k=-3}^3 P^k(r_1 \cup r_1^-) \quad \text{and} \quad T^s = \bigcup_{k=-3}^3 P^k(s_1 \cup s_1^-).$$

Note that these are clearly  $P$ -invariant (hence their intersection is  $P$ -invariant as well).

For  $p \leq 6$ , these will turn out to give a solid torus decomposition. For  $p = 8, 12$ , the solid tori are obtained from these by an adequate local surgery, to be discussed later in the proof (see Lemma 4.22).

The combinatorial pattern of the intersection of  $T^r$  and  $T^s$  is depicted in Figures 9, 10 and 11 for various values of  $p$  (compare this to Figure 6.2 of [Sch03]). These pictures can be obtained by somewhat painful bookkeeping from Figures 6 through 8 and their obvious variations, i.e. images under powers of  $P$  and/or the antiholomorphic symmetry  $\iota$ .

A few remarks are in order for the pictures to be read properly. First note that we cannot draw a Euclidean plane figure, since hexagonal faces of  $T^r \cap T^s$  are often glued along two consecutive sides. For instance, we represent hexagons by triangles, thinking of the midpoint of the edge of the triangle as a vertex of the hexagon (see Figure 11).

Secondly, the pictures are embedded in  $\widehat{E}_3$  only for  $p = 3, 4, 5$  and 6; for  $p = 8$  or 12, the intersection  $T^r \cap T^s$  is obtained from the torus in Figure 11 by identifying 7 pairs of points, indicated in the figure by square vertices. We will refer to these 7 points as **pinch points**.

We first treat the case  $p \leq 6$ .

**Lemma 4.19** *If  $p \leq 6$  then  $T^r$  and  $T^s$  are both solid tori, with union homeomorphic to  $S^3$ .*

Note that it would suffice to prove that  $\pi_1(T^r) = \pi_1(T^s) = \mathbb{Z}$ . It would then follow from Seifert-Van Kampen that  $\pi_1(\widehat{E}_3) = \pi_1(T^r \cup T^s) = 1$ , which implies that  $\widehat{E}_3$  is homeomorphic to  $S^3$  (this argument requires checking that  $\widehat{E}_3$  is a manifold, which follows from the detailed study of the links of its vertices). Using the solution of the Poincaré conjecture seems like overkill, so we now give a bare hands proof.

We prove Lemma 4.19 by constructing disjoint closed disks  $D_1^r$  and  $D_2^r$  in  $T^r$  whose complements are balls (and similarly  $D_1^s$  and  $D_2^s$  in  $T^s$ ), and check that  $D_1^r$  and  $D_1^s$  intersect in a single point. The boundary of each of these disks is depicted in Figures 9 and 10; the bold horizontal line is  $\partial D_1^r$ , the top (or bottom) horizontal line is  $\partial D_2^r$ , and similarly for vertical lines and  $\partial D_j^s$ .

Specifically,

$$\begin{aligned} D_1^s &= P^{-2}s_1 \cap s_1^-, \\ D_2^s &= P^{-1}s_1 \cap Ps_1^-, \\ D_1^r &= (P^3r_1 \cap P^3r_1^-) \cup (P^{-2}r_1 \cap P^2r_1^-) \cup (P^{-3}r_1 \cap P^{-3}r_1^-) \cup (P^{-3}r_1 \cap P^3r_1^-), \\ D_2^r &= (Pr_1 \cap P^{-1}r_1^-) \cup (Pr_1 \cap P^{-2}r_1^-) \cup (r_1 \cap r_1^-) \cup (P^2r_1 \cap P^{-1}r_1^-). \end{aligned} \tag{23}$$

The fact that these are indeed disks is readily checked by using the description of the combinatorics and adjacency relations between the 3-cells given in Figures 6 to 7. The following is clear from those pictures:



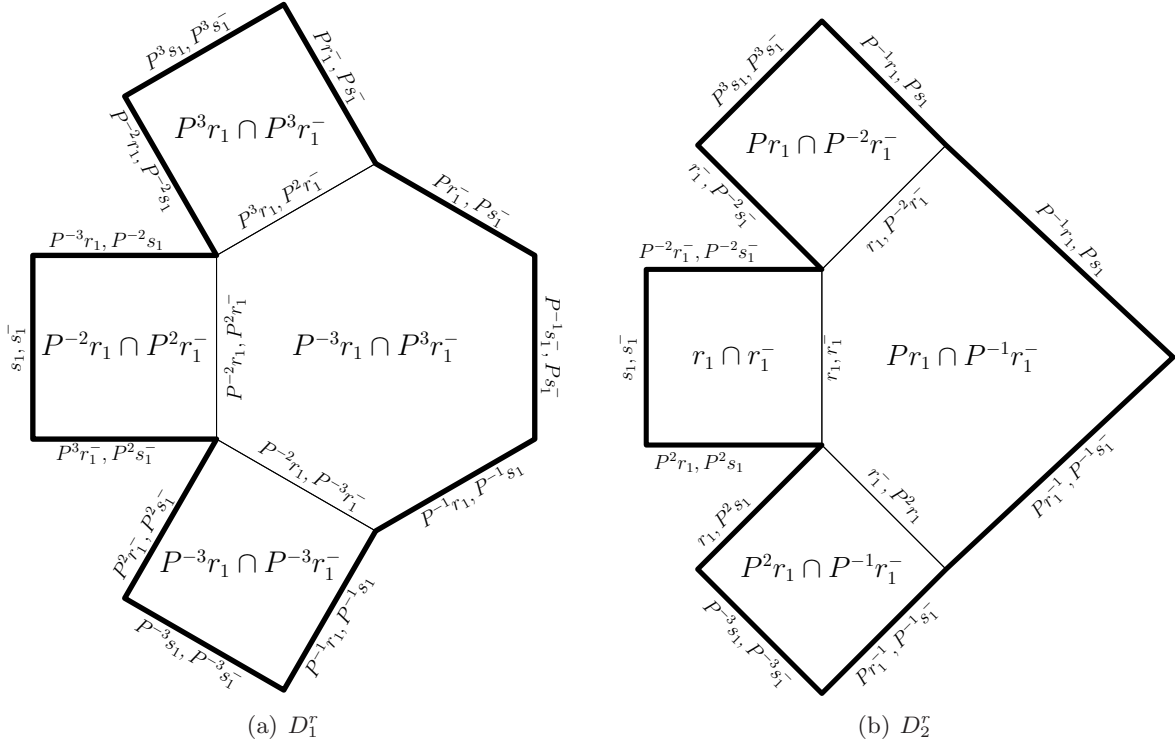


Figure 12: The combinatorics of the disks  $D_1^r$  and  $D_2^r$ , for  $p = 5, 6$ .

**Proposition 4.20** *The circles  $\partial D_1^r$  and  $\partial D_1^s$  intersect in a single point.*

For completeness, we give the combinatorial structure of the disks  $D_1^r$  and  $D_2^r$  in Figure 12.

We write  $T^r = U^r \cup V^r$  (resp.  $T^s = U^s \cup V^s$ ) for the decompositions corresponding to splitting along these disks, which are given in terms of 3-cells of  $\widehat{E}_3$  by the following:

$$\begin{aligned}
U^s &= P s_1 \cup P s_1^- \cup P^3 s_1 \cup P^3 s_1^- \cup P^{-2} s_1 \cup P^{-2} s_1^-, \\
V^s &= s_1 \cup s_1^- \cup P^2 s_1 \cup P^2 s_1^- \cup P^{-3} s_1 \cup P^{-3} s_1^- \cup P^{-1} s_1 \cup P^{-1} s_1^-, \\
U^r &= r_1 \cup P^{-1} r_1 \cup P^{-1} r_1^- \cup P^{-2} r_1 \cup P^{-2} r_1^- \cup P^3 r_1^- \cup P^{-3} r_1^-, \\
V^r &= r_1^- \cup P r_1 \cup P r_1^- \cup P^2 r_1 \cup P^2 r_1^- \cup P^3 r_1 \cup P^{-3} r_1.
\end{aligned} \tag{24}$$

In order to prove Lemma 4.19, it is enough to prove the following.

**Lemma 4.21**  *$U^s$  and  $V^s$  are homeomorphic to balls, and intersect precisely in the two disks  $D_1^s, D_2^s$ . Likewise,  $U^r$  and  $V^r$  are homeomorphic to balls, and intersect precisely in the two disks  $D_1^r, D_2^r$ .*

PROOF. This follows from a careful study of the gluings, using the fact that each 3-cell of  $\widehat{E}_3$  is a 3-ball. This is easiest for  $U^s$  and  $V^s$ , since  $F = s_1 \cup s_1^-$  is a ball,  $F \cap P^{\pm 2} F$  are both disks and  $F \cap P^4 F$  is empty; note that

$$V^s = F \cup P^2 F \cup P^4 F \cup P^6 F \quad \text{and} \quad U^s = P F \cup P^3 F \cup P^5 F.$$

For the  $r$ -splitting, we write each of  $U^r$  and  $V^r$  as an increasing union, gluing a ball along a single closed disk at each stage. More specifically, given a subcomplex  $Z$  (which is either

$U^r$  or  $V^r$ ), we give an explicit sequence  $C_n$  of subcomplexes with  $C_0 = F_0$  a 3-cell,

$$C_n = C_{n-1} \cup F_n$$

for a single 3-cell  $F_n$  of  $\widehat{E}_3$ , and which terminates with  $C_N = Z$ . The point is to choose the 3-cells  $F_n$  so that  $F_n \cap C_{n-1}$  is homeomorphic to a disk.

To be specific, we give an explicit such sequence for  $V^r$  that works for all values of  $p$ :

$$P^{-3}r_1, P^2r_1^-, P^3r_1, Pr_1^-, P^2r_1, r_1^-, Pr_1.$$

At each stage, we check that  $C_{n-1} \cap F_n$  is indeed a disk by using the description of the combinatorics given in Figures 6 to 8 (and obvious variations, obtained by applying the suitable power of  $P$  and/or the symmetry  $\iota$ ).

The corresponding sequence for  $U^r$  is easily deduced from the one for  $V^r$  by applying the antiholomorphic involution  $\iota$ . This finishes the proof of Lemma 4.21, hence also the proof of Lemma 4.19.  $\square$

We now consider the case  $p \geq 8$ . What remains true from the statement of Lemma 4.19 is the following:

**Lemma 4.22** *For  $p = 8$  and  $12$ ,  $T^r \cup T^s$  is homeomorphic to  $S^3$ .*

However,  $T^r$  and  $T^s$  are now singular handlebodies, with complementary singularities as we now explain.

A lot of the description of  $T^r$  and  $T^s$  for  $p \leq 6$  goes through. In particular, we use the same definition for  $D_1^r, D_2^r, D_1^s, D_2^s$ , see equation (23), and for  $U^r, V^r, U^s, V^s$ , see equation (24). The picture in Figure 11 makes it clear that  $U^r$  and  $V^r$  are cylinders, whereas  $U^s$  and  $V^s$  are both singular. We state this more precisely in Lemmas 4.23 and 4.24.

**Lemma 4.23** *Let  $p = 8$  or  $12$ . Then  $D_1^r$  and  $D_2^r$  are disjoint embedded closed disks,  $U^r$  and  $V^r$  are both homeomorphic to 3-balls. The intersection  $U^r \cap V^r$  is given by the disjoint union of  $D_1^r, D_2^r$  and seven isolated points. The interior of  $T^r$  is an open solid torus.*

The seven isolated points are given by  $q_{1232}^{23\bar{2}}$  (which is the single intersection point of the 3-cells  $r_1$  and  $P^2r_1^-$ ), and the six other points in its  $P$ -orbit. These are indicated by square vertices in Figure 11. As mentioned earlier, we refer to these as pinch points.

The corresponding result for  $T^s$  is the following. By a **bowtie**, we mean the result of gluing two triangles along a single vertex, which we call the **apex** of the bowtie.

**Lemma 4.24** *Let  $p = 8$  or  $12$ . Then  $D_1^s, D_2^s$  are disjoint bowties, with apex at a pinch point.  $U^s$  contains 3 pinch points,  $V^s$  contains 4 pinch points, and the interior of  $T^s$  is an open handlebody of genus 8.*

We now analyze the local structure around any of the seven pinch points, say  $q_{1232}^{23\bar{2}}$ . It lies on precisely six 3-cells of  $\widehat{E}_3$  (see Figure 8), namely  $r_1, P^2r_1^-, s_1, P^2s_1, s_1^-, P^2s_1^-$ , and appears as the intersection of two different pairs of hexagons on the boundary torus,

$$r_1 \cap s_1, r_1 \cap P^2s_1$$

on the one hand, and

$$P^2 r_1^- \cap s_1^-, P^2 r_1^- \cap P^2 s_1,$$

see Figure 11.

The link of that vertex is shown in Figure 13. Note that it is homeomorphic to a sphere, so even though both pieces  $T^r$  and  $T^s$  are singular, the union  $T^r \cup T^s$  is a 3-manifold.

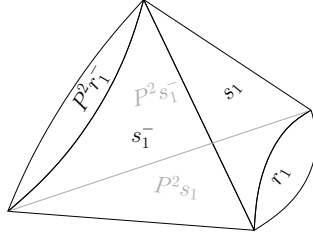


Figure 13: Link of  $q_{1232}^{232}$ , for  $p = 8$  or  $12$ .

We construct a non-singular solid torus  $\tilde{T}^r$  (resp.  $\tilde{T}^s$ ) from  $T^r$  (resp.  $T^s$ ) by performing an obvious surgery in a small ball near each pinch point, using the picture of the link given in Figure 13 as a guide.



Figure 14: We draw vertical sections of a rotationally symmetric local model (think of  $T^r$  near the pinch point as a circular cone). After surgery near the pinch points, the white bowties become disks.

After surgery, the two bowties (shown in white in Figure 14) become disjoint disks,  $\tilde{D}_1^s$  and  $\tilde{D}_2^s$ , which exhibits  $\tilde{T}^s$  as a solid torus (union of two cylinders). The disk  $D_1^r$  is unaffected by the surgery, and it clearly intersects  $\tilde{D}_1^s$  in a single point, since the intersection point of the bold lines in Figure 11 occurs away from the pinch points.  $\square$

## 4.8 Geometric realization

### 4.8.1 Realization of the vertices of $\hat{E}$

In this section, we describe in detail the 0-skeleton of  $\hat{E}$ , depending on the parameter  $p$ . We describe the geometric realization  $\phi$  on the level of the 0-skeleton, check the consistency of this realization with the labels in Figures 6 through 8, as well as the embeddedness of the realization (see Section 4.6.2 for the explanation of this terminology).

Consistency is checked by finding the complete list of bounding bisectors (see Section 4) that contain the realization of each vertex. This will be done case by case in Propositions 4.26, 4.28 and 4.30. Checking embeddedness then requires no further verifications,

since the vertices turn out to be uniquely determined by the set of bounding bisectors that contain them. The correct side condition for vertices amounts to proving a small number of strict inequalities, which is easily done with a computer (the point is that the relevant vertices and bisectors are  $k$ -rational, where  $k = \mathbb{Q}(a, \tau)$ , see the discussion in Section 2.7).

As mentioned in Section 4.6.2, the realization of the vertices of  $\widehat{E}$  is determined by Figures 6 through 8, where vertices are described as fixed point sets of the isometry given in word notation by their labels (see Section 4.2). The figures only list the vertices of  $r_1$  and  $s_1$ , but the other ones are obtained from those by applying  $\iota$  and/or a power of  $P$ . For completeness, we list the  $P$ -orbits of these vertices, depending on the value of  $p$ . There are two types of vertices, which we call  $p_*$ -vertices and  $q_*$ -vertices (see Section 4.2).

**Case  $p = 3$  or 4:** In this case there are two  $P$ -orbits of vertices, so that  $\widehat{E}$  has 14 vertices. There is one  $P$ -orbit of  $p_*$ -vertices and one  $P$ -orbit of  $q_*$ -vertices.

1. The realization of the vertex  $p_w$  is the unique fixed point in  $\overline{\mathbf{H}}_{\mathbb{C}}^2$  of the element of  $\Gamma$  represented by the word  $w$ . The seven  $p_*$ -vertices are realized by ideal vertices when  $p = 4$ .
2. The realization of the vertex  $q_w$  is the unique fixed point in  $\mathbf{H}_{\mathbb{C}}^2$  of the map  $w \in \Gamma$ .

A representative of the  $P$ -orbit of  $p_*$ -vertices is  $p_{12}$ , realized as the unique fixed point of  $R_1 R_2$ . A representative of the  $q_*$ -vertices is  $q_{123\bar{2}}$ , realized by the unique fixed point of  $R_1 R_2 R_3 R_2^{-1}$ . The  $P$ -orbits are easy to compute from the fact that  $P = R_1 J$  (and  $P^7 = \text{Id}$ ), for instance

$$\begin{aligned} P1\bar{P} &= 1J1\bar{J}\bar{1} = 12\bar{1}, \\ P23\bar{2}\bar{P} &= 1J23\bar{2}\bar{J}\bar{1} = 131\bar{3}\bar{1} = \bar{3}13, \end{aligned}$$

where the last equality follows from the higher braid relation  $(31)^2 = (13)^2$ . These two equalities give  $Pq_{123\bar{2}} = q_{12\bar{1}\bar{3}\bar{1}3}$ . The vertices are given in Tables 16 and 18 in the appendix (Section 7). From the preceding discussion, we obtain a realization of the 0-skeleton of  $\widehat{E}$  into  $\overline{\mathbf{H}}_{\mathbb{C}}^2$ , i.e. a definition of  $\phi$  on the level of the 0-skeleton; we now check the consistency of this embedding with the labels of Figures 6 to 8.

First, let us show that  $\phi$  sends the vertices of  $r_1$  and  $s_1$  to points in the bisectors  $\mathcal{R}_1$  and  $\mathcal{S}_1$  respectively.

**Lemma 4.25** 1. *The bisector  $\mathcal{R}_1$  contains  $p_{12}$ ,  $p_{13}$ ,  $p_{23}$ ,  $q_{123\bar{2}}$  and  $q_{1\bar{3}23}$ .*

2. *The bisector  $\mathcal{S}_1$  contains  $p_{23}$ ,  $p_{\bar{3}\bar{2}3123}$ ,  $q_{123\bar{2}}$  and  $q_{1\bar{3}23}$ .*

PROOF. By construction,  $\mathbf{n}_{23}$  lies on the real spine of  $\mathcal{R}_1$ . This vector projects to  $p_{23}$ , the unique fixed point in  $\overline{\mathbf{H}}_{\mathbb{C}}^2$  of 23. Likewise, the complex line  $m_1$  fixed by  $R_1$  is a slice of  $\mathcal{R}_1$ . The fixed points of 12, 13,  $123\bar{2}$  and  $1\bar{3}23$  all lie on  $m_1$  and so are contained in  $\mathcal{R}_1$  (see notation from section 4.3). This proves part (1). For part (2), begin by observing that the braid relation (see Proposition 4.5) implies  $\bar{3}\bar{2}3123 = 1323\bar{1}23\bar{2}$  and so its fixed point lies on  $m_{23\bar{2}}$  and  $m_{1\bar{3}23\bar{1}}$ . The rest of the proof follows as in part (1).  $\square$

To finish the consistency verification, we list the bounding bisectors containing  $p_{12}$  and  $q_{123\bar{2}}$  (the list of bisectors containing *any* vertex is then obtained by applying suitable powers of  $P$ ).

**Proposition 4.26** *Let  $p = 3$  or  $4$ . Then among the 28 bounding bisectors:*

1. *The vertex  $p_{12}$  is on  $\mathcal{R}_1, \mathcal{R}_1^-, P\mathcal{R}_1, P^{-1}\mathcal{R}_1^-, P^2\mathcal{R}_1, P^2\mathcal{S}_1, P^{-3}\mathcal{S}_1, P^{-3}\mathcal{S}_1^-, P\mathcal{R}_1^-, P^{-1}\mathcal{S}_1^-$ ;*
2. *The vertex  $q_{123\bar{2}}$  is on  $\mathcal{R}_1, \mathcal{R}_1^-, \mathcal{S}_1, \mathcal{S}_1^-, P^2\mathcal{R}_1, P^2\mathcal{R}_1^-, P^2\mathcal{S}_1, P^2\mathcal{S}_1^-$ .*

PROOF. This follows from Lemma 4.25 and Tables 16, 18 in Section 7 (see also the action of  $\iota$  on the vertices described in Section 4.6.1). We only treat a couple of cases. For instance,  $p_{12} \in P^{-1}\mathcal{R}_1^-$  is equivalent to  $Pp_{12} = p_{123\bar{1}} \in \mathcal{R}_1^-$ . Applying  $\iota$ , this is equivalent to  $p_{23} \in \mathcal{R}_1$ , which was proved in Lemma 4.25.

The fact that  $p_{12}$  is on  $P^{-3}\mathcal{S}_1^-$  translates into  $P^3p_{12} = p_{\bar{3}\bar{2}3123} \in \mathcal{S}_1^-$ , or equivalently by applying  $\iota$ ,  $P^{-3}p_{13} \in \mathcal{S}_1$ . Since  $Pp_{13} = p_{12}$  and  $P^7 = id$ , we have  $P^{-3}p_{13} = P^3p_{12}$ .  $\square$

**Case  $p = 5$  or  $6$ :** For  $p \geq 5$  the word  $(R_1R_2)^2$  is a complex reflection fixing the complex line  $m_{12}$ . In that case, we replace the vertex  $p_{12}$  with four vertices  $p_{12}^1, p_{12}^2, p_{12}^{\bar{2}12}$  and  $p_{12}^{1\bar{2}}$ , that are given by the intersections of  $m_{12}$  with  $m_1, m_2, m_{\bar{2}12}$ , and  $m_{12\bar{1}}$  respectively. The  $q_*$ -vertices are unchanged. Thus, there are five  $P$ -orbits of vertices, so that  $\hat{E}$  has 35 vertices.

1. The realization of the vertex  $p_w^v$  is the intersection of the complex lines  $m_v$  and  $m_w$ , fixed by  $v$  and  $w^2$  respectively.
2. The realization of the vertex  $q_w$  is the unique fixed point of  $w$ . The seven  $q_*$  vertices map to ideal points when  $p = 6$ .

The cycles of  $q_*$ -vertices are the same as for  $p = 3, 4$  (see the second row of Table 18). The four orbits of  $p_*$ -vertices are listed in Table 17.

**Lemma 4.27** 1. *The bisector  $\mathcal{R}_1$  contains the vertices  $p_{12}^2, p_{12}^1, p_{13}^1, p_{13}^3, p_{23}^3, p_{23}^2, p_{23}^{\bar{2}\bar{3}}, p_{23}^{\bar{3}\bar{2}}, q_{123\bar{2}}$  and  $q_{1\bar{3}23}$ .*

2. *The bisector  $\mathcal{S}_1$  contains the vertices  $p_{23}^{\bar{3}\bar{2}}, p_{23}^{\bar{2}\bar{3}}, p_{323123}^{\bar{2}\bar{3}}, p_{323123}^{\bar{1}\bar{3}\bar{2}\bar{3}}, q_{123\bar{2}}$  and  $q_{1\bar{3}23}$ .*

PROOF. For  $\mathcal{R}_1$ , the statement is obvious for eight of the ten vertices, since vertices of the form  $p_*^1$  and  $p_{23}^*$  lie on  $m_1$  and  $m_{23}$  respectively, and these are complex slices of  $\mathcal{R}_1$ . The last two are handled using Lemma 2.3. We treat the case of  $p_{12}^2$  in detail,  $p_{13}^3$  is entirely similar.

Note that  $m_{12}$  is orthogonal to  $m_1$ , since  $R_1$  and  $(R_1R_2)^2$  commute. Similarly,  $m_2$  is orthogonal to  $m_{23}$ . Lemma 2.3 implies that  $\mathcal{R}_1$  intersects each of the complex lines  $m_2$  and  $m_{12}$  in a real geodesic, and by definition  $p_{12}^2$  is the intersection point of these two geodesics. This proves part (1). Part (2) is proved similarly.  $\square$

The analogue of Proposition 4.26 is the following:

**Proposition 4.28** *Let  $p = 5$  or  $6$ . Then among the 28 bounding bisectors:*

1. *the vertex  $p_{12}^1$  is on  $\mathcal{R}_1, \mathcal{R}_1^-, P\mathcal{R}_1, P^2\mathcal{R}_1, P^2\mathcal{S}_1, P^{-1}\mathcal{R}_1^-$ ;*
2. *the vertex  $p_{12}^2$  is on  $\mathcal{R}_1, P^2\mathcal{R}_1, P^2\mathcal{S}_1, P^{-3}\mathcal{S}_1, P^{-3}\mathcal{S}_1^-, P^{-1}\mathcal{R}_1^-$ ;*
3. *the vertex  $p_{23}^2$  is on  $\mathcal{R}_1, P^2\mathcal{S}_1, P^2\mathcal{S}_1^-, P^{-3}\mathcal{R}_1^-, P^{-3}\mathcal{S}_1^-, P^{-1}\mathcal{R}_1^-$ ;*

4. the vertex  $p_{23}^3$  is on  $\mathcal{R}_1, P^{-3}\mathcal{R}_1^-, P^{-3}\mathcal{S}_1^-, P^{-2}\mathcal{R}_1^-, P^{-1}\mathcal{R}_1, P^{-1}\mathcal{R}_1^-$ ;
5. the vertex  $q_{123\bar{2}}$  is on  $\mathcal{R}_1, \mathcal{R}_1^-, \mathcal{S}_1, \mathcal{S}_1^-, P^2\mathcal{R}_1, P^2\mathcal{R}_1^-, P^2\mathcal{S}_1$  and  $P^2\mathcal{S}_1^-$ .

**Case  $p = 8$  or  $12$ :** In this case there are seven  $P$ -orbits of vertices (so that  $\widehat{E}$  has 49 vertices). The cycles of  $p_*$ -vertices are the same as for  $p = 5, 6$  (there are four of them, see Table 17), and there are three orbits of  $q_*$ -vertices, listed in Table 19. Since  $(R_1R_2R_3R_2^{-1})^3$  is a complex reflection fixing the complex line  $m_{123\bar{2}}$ , we replace the vertex  $q_{123\bar{2}}$  with three vertices lying in this complex line.

1. The realization of the vertex  $p_w^v$  is the intersection of the complex lines  $m_v$  and  $m_w$ , fixed by  $v$  and  $w^2$  respectively.
2. The realization of the vertex  $q_w^v$  is the intersection of the complex lines  $m_v$  and  $m_w$ , fixed by  $v$  and  $w^3$  respectively.

The following lemma is proved as before.

- Lemma 4.29**
1. The bisector  $\mathcal{R}_1$  contains the vertices  $p_{12}^2, p_{12}^1, p_{13}^1, p_{13}^3, p_{23}^3, p_{23}^2, p_{23}^{2\bar{3}}, p_{23}^{\bar{3}23}, q_{123\bar{2}}^{2\bar{3}}, q_{123\bar{2}}^1, q_{323}^1$  and  $q_{1323}^{\bar{3}23}$ .
  2. The bisector  $\mathcal{S}_1$  contains the vertices  $p_{23}^{\bar{3}23}, p_{23}^{2\bar{3}}, p_{\bar{3}23123}^{2\bar{3}}, p_{\bar{3}23123}^{\bar{3}23}, q_{123\bar{2}}^{2\bar{3}}, q_{123\bar{2}}^1, q_{1323}^1, q_{1323}^{\bar{3}23}$  and  $q_{1323}^{\bar{3}23\bar{1}}$ .

**Proposition 4.30** *Let  $p = 8$  or  $12$ . The  $p_*$ -vertices are on the same bounding bisectors as in the case  $p = 5, 6$ , and the  $q_*$ -vertices are on the following bounding bisectors:*

1. the vertex  $q_{1323}^1$  is on  $\mathcal{R}_1, \mathcal{R}_1^-, \mathcal{S}_1, \mathcal{S}_1^-, P^{-2}\mathcal{R}_1^-$  and  $P^{-2}\mathcal{S}_1^-$ ;
2. the vertex  $q_{1323}^{\bar{3}23}$  is on  $\mathcal{R}_1, \mathcal{S}_1, P^{-2}\mathcal{R}_1, P^{-2}\mathcal{R}_1^-, P^{-2}\mathcal{S}_1$  and  $P^{-2}\mathcal{S}_1^-$ ;
3. the vertex  $q_{123\bar{2}}^{2\bar{3}}$  is on  $\mathcal{R}_1, \mathcal{S}_1, \mathcal{S}_1^-, P^2\mathcal{R}_1^-, P^2\mathcal{S}_1$  and  $P^2\mathcal{S}_1^-$ .

#### 4.8.2 Realizing edges of $\widehat{E}$

In this section, we check the consistency and the embeddedness condition for the realization of the 1-skeleton. Each 1-cell is realized as a geodesic segment joining the realization of its two endpoints. According to the description of  $\widehat{E}$ , each 1-cell is on four 3-cells, so we need to check that the geodesic segment realizing each 1-cell is contained in the appropriate set of four bisectors (the set of bisectors is indicated by the labels of Figures 6 to 8). Recall from Section 2.4 that in order to check that a geodesic segment  $[v_0, v_1]$  is on a bisector  $\mathcal{B}$ , it is not enough to check that its endpoints  $v_0$  and  $v_1$  are on  $\mathcal{B}$ .

**Proposition 4.31** *The realization of the 1-skeleton of  $\widehat{E}$  is consistent.*

**PROOF.** This follows from repeated use of Lemmas 2.2 or 2.3. We illustrate this in a couple of specific cases. First, suppose  $p = 3$  or  $4$ , and consider the geodesic through  $p_{12}$  and  $p_{13}$ . According to Proposition 4.26, it should be contained in

$$\mathcal{R}_1, \mathcal{R}_1^-, P\mathcal{R}_1, P^{-1}\mathcal{R}_1^-.$$

By definition of the points  $p_{12}$  and  $p_{13}$ , they are both in the mirror of  $R_1$ , which is a common complex slice of  $\mathcal{R}_1$  and  $\mathcal{R}_1^-$ . Moreover,  $p_{13}$  (resp.  $p_{12}$ ) is on the real spine of  $P\mathcal{R}_1$  (resp.  $P^{-1}\mathcal{R}_1^-$ ), so the geodesic is contained in  $P\mathcal{R}_1$  (resp.  $P^{-1}\mathcal{R}_1^-$ ).

Now suppose  $p \geq 5$ , and consider the geodesic  $\alpha$  through  $p_{13}^1$  and  $p_{12}^1$ . These two points are on  $m_1$ , which is a common slice of  $\mathcal{R}_1$  and  $\mathcal{R}_1^-$ . Moreover,  $m_1$  is by construction orthogonal to the complex line  $m_{12}$ , which is a complex slice of  $P^{-1}\mathcal{R}_1^-$ , so Lemma 2.3 implies that  $\alpha$  is contained in  $P^{-1}\mathcal{R}_1^-$ . Similarly,  $m_1$  is orthogonal to the slice of  $P\mathcal{R}_1$  given by  $\mathbf{n}_{13}^\perp$ , so  $\alpha$  is contained in  $P\mathcal{R}_1$ .

In some cases, one needs to use both Lemmas 2.2 and 2.3. For instance, for  $p = 5$  or  $6$ ,  $p_{12}^1$  and  $q_{123\bar{2}}$  are contained in  $m_1$ , so clearly the geodesic joining them is in  $\mathcal{R}_1$  and  $\mathcal{R}_1^-$ . The fact that it is contained in  $P^2\mathcal{R}_1$  follows from Lemma 2.3 (and the fact that  $\langle \mathbf{n}_1, \mathbf{n}_{12} \rangle = 0$ ), whereas the fact that it is contained in  $P^2\mathcal{S}_1$  follows from Lemma 2.2 (and the fact that  $q_{123\bar{2}}$  is on the real spine of  $P^2\mathcal{S}_1$ ).

In some cases, the application of Lemma 2.3 is not completely obvious, since the orthogonality check can be a bit more involved. For instance, consider the geodesic through  $p_{\bar{3}\bar{2}3123}^{\bar{1}\bar{3}231}$  and  $q_{1\bar{3}23}$ . Clearly these two points are on  $m_{1\bar{3}23\bar{1}}$ , so the geodesic is contained in  $\mathcal{S}_1^-$  and  $P^{-2}\mathcal{S}_1$ . It is contained in  $\mathcal{S}_1$  simply because  $q_{1\bar{3}23}$  is a point of its real spine, but in order to check that it is contained in  $P^{-2}\mathcal{R}_1$ , one needs to check that  $\langle \mathbf{n}_{1\bar{3}23\bar{1}}, \mathbf{n}_{\bar{3}\bar{2}3123} \rangle = 0$ . Since  $\mathbf{n}_{1\bar{3}23\bar{1}} = P^3\mathbf{n}_2$  and  $\mathbf{n}_{\bar{3}\bar{2}3123} = P^3\mathbf{n}_{12}$  the result follows from  $\langle \mathbf{n}_2, \mathbf{n}_{12} \rangle = 0$ .  $\square$

**Remark 4.32** Lemma 2.3 shows a bit more than the relevant inclusions of geodesics in bisectors. It also implies that the geodesic is in a real slice of certain bisectors - when two adjacent edges are contained in real slices of the same bisector (and their intersection is not on the real spine of that bisector), the two real slices must actually coincide.

**Proposition 4.33** *The realization of the 1-skeleton of  $\widehat{E}$  is embedded and contained in  $F$ .*

PROOF. Let  $f$  be a 1-cell of  $\widehat{E}$ . We have just proved that its realization  $\phi(f)$  is on (at least) four bounding bisectors. For each other bounding bisector  $\mathcal{B}$ , we check that  $\phi(f)$  is on the correct half-space bounded by  $\mathcal{B}$ . Since the endpoints of  $\phi(f)$  are  $k$ -rational (with  $k = \mathbb{Q}(a, \tau)$ ), this can be done using arithmetic in  $k$ , see Section 2.7.

Note that the situation where some 1-cells are tangent to some of the bounding bisectors, alluded to in Section 2.7, really does occur. Specifically, it occurs when an endpoint of the 1-face is a cusp, which happens at certain specific vertices when  $p = 4$  and  $p = 6$ .

Note that because of the symmetry given by  $P$  and  $\iota$ , it is enough to study the tangencies that appear in (the intersection of  $\phi(\widehat{E})$  with)

$$\mathcal{R}_1 \cap \mathcal{R}_1^-, \mathcal{R}_1 \cap \mathcal{S}_1, \mathcal{R}_1 \cap P^{-3}\mathcal{R}_1^-, \mathcal{R}_1 \cap P^{-2}\mathcal{R}_1^-, \mathcal{R}_1 \cap P^{-1} \cap \mathcal{R}_1^-, \mathcal{S}_1 \cap P^2\mathcal{S}_1^-, \mathcal{S}_1 \cap P^{-2}\mathcal{S}_1^-. \quad (25)$$

Although not technically needed for the proof, it can be instructive to draw figures of these Giraud disks and their intersection with all bounding bisectors. This is done in Figure 16 for  $\mathcal{R}_1 \cap \mathcal{S}_1$ , where it should be apparent that tangencies only occur for  $p = 4$  and  $p = 6$  (see parts (b) and (d) of the figure). In order for the figure to be read properly, notice that the labels on curves in the graph correspond to the index of the bisectors given in Table 2.

We treat these two tangencies in Proposition 4.34. The other ones are similar.

Bisector	$P^k \mathcal{R}_1$	$P^k \mathcal{R}_1^-$	$P^k \mathcal{S}_1$	$P^k \mathcal{S}_1^-$
Index notation	$\mathcal{B}_{1+4k}$	$\mathcal{B}_{2+4k}$	$\mathcal{B}_{3+4k}$	$\mathcal{B}_{4+4k}$

Table 2: Numbering of the bounding bisectors according to  $P$ -symmetry, for  $k = 0, \dots, 6$ .

**Proposition 4.34** 1. For  $p = 4$ , the real geodesic through  $p_{23}$  and  $q_{1\bar{3}23}$  intersects  $P^{-1}\mathcal{R}_1$  only at the ideal vertex  $p_{23}$ .

2. For  $p = 6$ , the real geodesic through  $p_{23}^{\bar{2}3\bar{2}}$  and  $q_{123\bar{2}}$  intersects  $P^2\mathcal{R}_1^-$  only at the ideal vertex  $q_{123\bar{2}}$ .

3. For  $p = 6$ , the real geodesic through  $p_{23}^{\bar{3}2\bar{3}}$  and  $q_{1\bar{3}23}$  intersects  $P^{-2}\mathcal{S}_1$  only at the ideal vertex  $q_{1\bar{3}23}$ .

4. For  $p = 6$ , the real geodesic through  $q_{123\bar{2}}$  and  $q_{1\bar{3}23}$  intersects  $P^2\mathcal{R}_1$  only at the ideal vertex  $q_{123\bar{2}}$ .

PROOF. First let  $p = 4$ . The geodesic arc from  $p_{23}$  to  $q_{1\bar{3}23}$  is a side of  $r_1 \cap s_1$ . We check that it only intersects  $P^{-1}\mathcal{R}_1$  at  $p_{23}$ . Apart from  $q_{1\bar{3}23}$ , the extended real geodesic is parametrized by vectors of the form  $\mathbf{a} + t\mathbf{b}$  with

$$\mathbf{a} = \mathbf{n}_{23}, \quad \mathbf{b} = \langle \mathbf{n}_{23}, \mathbf{n}_{1\bar{3}23} \rangle \mathbf{n}_{1\bar{3}23},$$

and  $t \in \mathbb{R}$  (there are further restrictions on  $t$ , but this will be irrelevant in what follows). The corresponding point is on  $P^{-1}\mathcal{R}_1$  (or rather its extension to projective space) if and only if

$$|\langle \mathbf{a} + t\mathbf{b}, P^{-1}\mathbf{y}_0 \rangle|^2 = |\langle \mathbf{a} + t\mathbf{b}, P^{-1}R_1^{-1}\mathbf{y}_0 \rangle|^2.$$

Using  $\tau = -(1 + i\sqrt{7})/2$ , then  $a = e^{2\pi i/12} = (\sqrt{3} + i)/2$ , we compute

$$|\langle \mathbf{a} + t\mathbf{b}, P^{-1}\mathbf{y}_0 \rangle|^2 - |\langle \mathbf{a} + t\mathbf{b}, P^{-1}R_1^{-1}\mathbf{y}_0 \rangle|^2 = -(196156 + 74140\sqrt{7}) t^2,$$

the latter vanishing precisely at  $t = 0$ .

For  $p = 6$  and  $\mathbf{a} = q_{123\bar{2}}$ ,  $\mathbf{b} = p_{23}^{\bar{2}3\bar{2}}$ , one gets

$$|\langle \mathbf{a} + t\mathbf{b}, P^2\mathbf{y}_0 \rangle|^2 - |\langle \mathbf{a} + t\mathbf{b}, P^2R_1\mathbf{y}_0 \rangle|^2 = -(2525 + 551\sqrt{7}\sqrt{3}) t^2.$$

For  $p = 6$  and  $\mathbf{a} = q_{1\bar{3}23}$ ,  $\mathbf{b} = q_{1\bar{3}23}$ , one gets

$$|\langle \mathbf{a} + t\mathbf{b}, P^2\mathbf{y}_0 \rangle|^2 - |\langle \mathbf{a} + t\mathbf{b}, P^2R_1^{-1}\mathbf{y}_0 \rangle|^2 = -(161797 + 35307\sqrt{7}\sqrt{3})t^2/2.$$

For  $p = 6$  and  $\mathbf{a} = q_{1\bar{3}23}$ ,  $\mathbf{b} = p_{23}^{\bar{3}2\bar{3}}$ , one gets

$$|\langle \mathbf{a} + t\mathbf{b}, P^{-2}\mathbf{y}_0 \rangle|^2 - |\langle \mathbf{a} + t\mathbf{b}, P^{-2}S_1^{-1}\mathbf{y}_0 \rangle|^2 = -(3524 + 769\sqrt{7}\sqrt{3}) t^2.$$

□



### 4.8.3 Realizing ridges of $\widehat{E}$ - consistency

The goal of this section is to show the consistency result for the 2-skeleton of  $\widehat{E}$ . Recall that we want to realize each 2-face  $f$  by using the realization of  $\partial f$ , which is a piecewise smooth circle (possibly with some ideal vertices) in the intersection of two of the bounding bisectors. We now need to show that the intersection of these two bisectors is a disk. We split the discussion in two cases, depending on the geometry of the intersection (see Section 2.3).

#### Complex ridges

We first list the ridges of  $\widehat{E}$  that get realized in complex lines, calling them simply “complex ridges”. The detailed list is given in the appendix (see Table 15).

For  $p = 3, 4$  there are 14 complex lines containing complex ridges, namely the  $P$ -orbits of  $m_1$  and  $m_2$ . For  $p \geq 5$  the point  $p_{12}$  is replaced with a ridge in the complex line  $m_{12}$  and so there are 21 complex ridges. The  $P$ -orbits of  $m_{12}$  may be found from Table 16 by replacing  $p_w$  with  $m_w$  (these are closely related, in fact they are polar to each other). For  $p = 8, 12$  we similarly replace  $q_{123\bar{2}}$  with a ridge in  $m_{123\bar{2}}$ , and its  $P$ -orbit may be read of from the same table by replacing  $q_w$  with  $m_w$  in Table 18; this gives a total of 28 complex ridges.

We only analyze the ridges that appear on  $r_1$  and  $s_1$ , see the bottom and top 2-cells of Figures 6 to 8 (the top 2-cell reduces to a point for small values of  $p$ ). We have already shown that, for each such 2-face  $f$ , the vertices and edges in  $\phi(\partial f)$  are contained in a complex line, which is the mirror of a certain complex reflection in the group (see Section 4.8.2). Moreover, the adjacency pictures suggest that we should realize the 2-face in the intersection of two specific bisectors.

The consistency verification amounts to the verification that these two specific bisectors intersect precisely along the complex line mentioned above. We state this in the following.

**Proposition 4.35**    1.  $\mathcal{R}_1 \cap \mathcal{R}_1^-$  is a complex line, which is  $m_1$ .

2. For  $p \geq 5$ ,  $\mathcal{R}_1 \cap P^{-3}\mathcal{R}_1^-$  is a complex line, which is  $m_{23}$ .

3.  $\mathcal{S}_1 \cap P^2\mathcal{S}_1^-$  is a complex line, which is  $m_{23\bar{2}}$ .

4. For  $p \geq 8$ ,  $\mathcal{S}_1 \cap P^{-2}\mathcal{S}_1^-$  is a complex line, which is  $m_{1\bar{3}23}$ .

PROOF. Parts 1 and 3 are relatively easy, since the corresponding pairs of bisectors are not only cotranchal, they are in fact cospinal. This is obvious for  $\mathcal{R}_1 \cap \mathcal{R}_1^-$ , since the complex spine of  $\mathcal{R}_1$  is by construction orthogonal to the mirror of  $R_1$ , so  $\mathcal{R}_1$  and  $\mathcal{R}_1^- = R_1(\mathcal{R}_1)$  have the same complex spine.

The case of  $\mathcal{S}_1 \cap P^2\mathcal{S}_1^-$  is just a little bit more complicated. By construction  $P^2S_1$  maps  $\mathcal{S}_1$  to  $P^2\mathcal{S}_1^-$ , and Proposition 4.4 implies that  $P^2S_1$  is a complex reflection fixing  $\mathbf{n}_{23\bar{2}}$ , hence it preserves the complex spine of  $\mathcal{S}_1$ .

For parts 2 and 4, we first prove that the corresponding pair of bisectors is cotranchal, i.e. that the mirror of the relevant complex reflection is indeed contained in the bisector intersection. Then we prove that the intersection really consists only of that common complex slice, by using Proposition 2.7.

**Part 2:** In this case we need to verify the criterion from Proposition 2.7. That is, we must find the intersection of the real spine  $\sigma(\mathcal{R}_1)$  of  $\mathcal{R}_1$  with  $m_{23}$  and lift it to a point  $\mathbf{v}_1$  so that  $\sigma(\mathcal{R}_1)$  is given by real linear combinations of  $\mathbf{n}_{23}$  and  $\mathbf{v}_1$ . We know that  $\sigma(\mathcal{R}_1)$  is the real

span of  $\mathbf{n}_1$  and  $\mathbf{n}_{23}$  and that  $\langle \mathbf{n}_1, \mathbf{n}_{23} \rangle$  is real. Hence we take

$$\mathbf{v}_1 = \mathbf{n}_1 - \frac{\langle \mathbf{n}_1, \mathbf{n}_{23} \rangle}{\langle \mathbf{n}_{23}, \mathbf{n}_{23} \rangle} \mathbf{n}_{23} = \frac{1}{a^3 + \bar{a}^3} \begin{bmatrix} 0 \\ -a^2\bar{\tau} + \bar{a} \\ -\bar{a}^2\tau + a \end{bmatrix}.$$

Now  $P^{-3}\mathcal{R}_1^- = (R_2R_3)^{-1}\mathcal{R}_1$  and  $\bar{a}^2(R_2R_3)^{-1}$  fixes  $\mathbf{n}_{23}$  and so we take

$$\mathbf{v}_2 = \bar{a}^2(R_2R_3)^{-1}\mathbf{v}_1 = \frac{1}{a^3 + \bar{a}^3} \begin{bmatrix} 0 \\ \bar{a}^4\bar{\tau} + \bar{a} \\ -\bar{a}^2\tau - \bar{a}^5 \end{bmatrix}.$$

Then

$$\begin{aligned} \langle \mathbf{v}_1, \mathbf{v}_1 \rangle &= \langle \mathbf{v}_2, \mathbf{v}_2 \rangle = (a^3 - 1)((1 - \tau) - \bar{a}^3(1 - \bar{\tau})) / (a^3 + \bar{a}^3), \\ \langle \mathbf{v}_2, \mathbf{v}_1 \rangle &= -(a^3 - 1)((1 - \bar{\tau})\bar{a}^3 + (1 - \tau)\bar{a}^6) / (a^3 + \bar{a}^3). \end{aligned}$$

Thus

$$\begin{aligned} &\frac{(a^3 + \bar{a})^2}{(2 - a^3 - \bar{a}^3)} \left( 4\langle \mathbf{v}_1, \mathbf{v}_1 \rangle \langle \mathbf{v}_2, \mathbf{v}_2 \rangle - (\langle \mathbf{v}_1, \mathbf{v}_2 \rangle + \langle \mathbf{v}_2, \mathbf{v}_1 \rangle)^2 \right) \\ &= (a^3 + \bar{a}^3)(2|1 - \tau|^2 - a^3(1 - \bar{\tau})^2 - \bar{a}^3(1 - \tau)^2) + 2(a^3 - \bar{a}^3)(a^3(1 - \bar{\tau})^2 - \bar{a}^3(1 - \tau)^2). \end{aligned}$$

Both terms are positive for all  $p > 4$ .

**Part 4:** We argue as in Part 2. The real spine  $\sigma(\mathcal{S}_1)$  of  $\mathcal{S}_1$  is the real span of  $a\mathbf{n}_{23\bar{2}}$  and  $\mathbf{n}_{1\bar{3}23}$ . Its image under  $a^21\bar{3}23$  is the real span of  $-a\mathbf{n}_{13\bar{1}}$  and  $\mathbf{n}_{1\bar{3}23}$ . Therefore we construct:

$$\begin{aligned} \mathbf{v}_1 &= a\mathbf{n}_{23\bar{2}} - \frac{\langle a\mathbf{n}_{23\bar{2}}, \mathbf{n}_{1\bar{3}23} \rangle}{\langle \mathbf{n}_{1\bar{3}23}, \mathbf{n}_{1\bar{3}23} \rangle} \mathbf{n}_{1\bar{3}23} = \frac{1}{a^3 + \bar{a}^3 - 1} \begin{bmatrix} -a^2 - \bar{a}\bar{\tau} \\ a\bar{\tau} + \bar{a}^2\tau \\ -1 + \tau + 2\bar{a}^3 \end{bmatrix}, \\ \mathbf{v}_2 &= -a\mathbf{n}_{13\bar{1}} - \frac{\langle -a\mathbf{n}_{13\bar{1}}, \mathbf{n}_{1\bar{3}23} \rangle}{\langle \mathbf{n}_{1\bar{3}23}, \mathbf{n}_{1\bar{3}23} \rangle} \mathbf{n}_{1\bar{3}23} = \frac{1}{a^3 + \bar{a}^3 - 1} \begin{bmatrix} a^5\bar{\tau} + a^2\bar{\tau} \\ -a^4\tau - a \\ -2a^3 - \bar{\tau} \end{bmatrix}. \end{aligned}$$

We have

$$\begin{aligned} \langle \mathbf{v}_1, \mathbf{v}_1 \rangle &= \langle \mathbf{v}_2, \mathbf{v}_2 \rangle = (a^3 - 1)((2 - \tau) - \bar{a}^3(2 - \bar{\tau})) / (a^3 + \bar{a}^3 - 1), \\ \langle \mathbf{v}_2, \mathbf{v}_1 \rangle &= (a^3 - 1)(2 - \bar{\tau})a^3 / (a^3 + \bar{a}^3 - 1). \end{aligned}$$

Then

$$\begin{aligned} &\frac{(a^3 + \bar{a}^3 - 1)^2}{(2 - a^3 - \bar{a}^3)} \left( 4\langle \mathbf{v}_1, \mathbf{v}_1 \rangle \langle \mathbf{v}_2, \mathbf{v}_2 \rangle - (\langle \mathbf{v}_1, \mathbf{v}_2 \rangle + \langle \mathbf{v}_2, \mathbf{v}_1 \rangle)^2 \right) \\ &= 6|2 - \tau|^2 - (4a^3 + \bar{a}^6)(2 - \tau)^2 - (4\bar{a}^3 + a^6)(2 - \bar{\tau})^2. \end{aligned}$$

This is positive for all  $p > 6$ .

This completes the proof of Proposition 4.35.  $\square$

**Generic ridges**

Bisector	Equidistant	Bisector	Equidistant
$\mathcal{R}_1$	$\mathcal{B}(y_0, R_1^{-1}y_0)$	$\mathcal{R}_1^-$	$\mathcal{B}(y_0, R_1y_0)$
$\mathcal{S}_1$	$\mathcal{B}(y_0, S_1^{-1}y_0)$	$\mathcal{S}_1^-$	$\mathcal{B}(y_0, S_1y_0)$
$\mathcal{R}_1$	$\mathcal{B}(y_1, R_1^{-1}Py_1)$	$P^{-1}\mathcal{R}_1^-$	$\mathcal{B}(y_1, P^{-1}R_1y_1)$
$\mathcal{R}_1$	$\mathcal{B}(y_2, R_1^{-1}P^2y_2)$	$P^{-2}\mathcal{R}_1^-$	$\mathcal{B}(y_2, P^{-2}R_1y_2)$
$P^2\mathcal{S}_1$	$\mathcal{B}(y_2, P^2S_1^{-1}P^{-3}y_2)$	$P^3\mathcal{S}_1^-$	$\mathcal{B}(y_2, P^3S_1P^{-2}y_2)$

Table 3: Description of bounding bisectors in terms of  $y_0$ ,  $y_1$  and  $y_2$

In the first part of this section, we checked the consistency of the embedding of complex ridges. We now prove the analogous statement for all the other ridges, which will be realized inside Giraud disks. Recall that given a 2-cell  $f$  of  $\widehat{E}$ , Figures 6 to 8 suggest a pair  $\mathcal{B}, \mathcal{B}'$  of bounding bisectors that should contain the realization  $\phi(f)$ . We have already defined the realization on the level of the 1-skeleton, and shown that  $\phi(\partial f)$  lies inside  $\mathcal{B} \cap \mathcal{B}'$  (or possibly its union with finitely many ideal vertices).

The corresponding consistency verification is almost automatic, we simply verify that all the corresponding intersections  $\mathcal{B} \cap \mathcal{B}'$  are indeed disks, hence  $\phi(\partial f)$  bounds a well defined disk, which we use as the realization  $\phi(f)$ . In order to get these disks, we simply prove that the corresponding pairs of bisectors are coequidistant (see Section 2.3).

Let  $\mathbf{y}_0, \mathbf{y}_1, \mathbf{y}_2$  be given by the following formulae:

$$\mathbf{y}_0 = \begin{bmatrix} -a^3(\bar{a}^2\bar{\tau} + a)^2 \\ (a^2\bar{\tau} + \bar{a}\tau)(a^2\bar{\tau} - \bar{a}) \\ (a^2\bar{\tau} + \bar{a}\tau)(\bar{a}^2\tau - a) \end{bmatrix}, \quad \mathbf{y}_1 = \begin{bmatrix} a(1 - a^3\bar{\tau})^2 \\ (1 - a^3\bar{\tau})(a^3 - \tau) \\ \bar{a}(a^3 - \tau)^2 \end{bmatrix}, \quad \mathbf{y}_2 = \begin{bmatrix} (a^3 - \tau)(\bar{a}^3 + \tau) \\ \bar{a}(1 - a^3\bar{\tau})(1 + \bar{a}^3\bar{\tau}) \\ a(1 - \bar{a}^3\tau)(1 + \bar{a}^3\bar{\tau}) \end{bmatrix}. \quad (26)$$

Note that  $\langle \mathbf{y}_j, \mathbf{y}_j \rangle < 0$  and so  $\mathbf{y}_j$  corresponds to a point  $y_j$  of  $\mathbf{H}_{\mathbb{C}}^2$ . Indeed, the following lemma, which is verified by direct computation, implies that all three points are in  $E$ .

**Lemma 4.36** *Let  $y_0, y_1, y_2$  be the points in  $\mathbf{H}_{\mathbb{C}}^2$  corresponding to the vectors given in (26). If  $\mathcal{B}$  is any of the 28 bounding bisectors, then the half-space determined by  $\mathcal{B}$  that contains the fixed point of  $P$  also contains  $y_0, y_1$  and  $y_2$ .*

We have already seen in Proposition 4.13 that  $\mathcal{R}_1, \mathcal{R}_1^-, \mathcal{S}_1$  and  $\mathcal{S}_1^-$  are coequidistant from  $\mathbf{y}_0$ . Since  $y_0$  does not lie on any of their real spines, their pairwise intersections are Giraud disks (apart from  $\mathcal{R}_1 \cap \mathcal{R}_1^-$ , since these two bisectors have the same complex spine). Using the points  $y_1$  and  $y_2$  we can describe some of the other intersections between bounding bisectors in a similar way.

**Proposition 4.37** *Let  $y_0, y_1$  and  $y_2$  be the points in  $\mathbf{H}_{\mathbb{C}}^2$  corresponding to the vectors  $\mathbf{y}_0, \mathbf{y}_1, \mathbf{y}_2$  given in (26). The intersections among bounding bisectors listed in Table 4 are contained in Giraud disks defined by  $y_0, y_1$  and  $y_2$ .*

PROOF. We must first prove that certain bounding bisectors are coequidistant from  $y_0, y_1$  and  $y_2$  listed in Table 3. This was proved for  $y_0$  in Proposition 4.13. We use a similar method to show equidistance from  $y_1$  and  $y_2$ . Namely, consider two of the bisectors  $\mathcal{B}$  and  $\mathcal{B}'$ . We first show that the complex spines of  $\mathcal{B}$  and  $\mathcal{B}'$  intersect in  $\mathbf{y}_j$ , for  $j = 1$  or  $2$ . We can find vectors spanning the real spine of  $\mathcal{B}$  by applying a suitable power of  $P$  to the vectors listed

Intersection	Giraud disk
$\mathcal{R}_1 \cap \mathcal{S}_1$	$\mathcal{G}(y_0, R_1^{-1}y_0, S_1^{-1}y_0)$
$\mathcal{R}_1^- \cap \mathcal{S}_1^-$	$\mathcal{G}(y_0, R_1 y_0, S_1 y_0)$
$\mathcal{S}_1 \cap \mathcal{S}_1^-$	$\mathcal{G}(y_0, S_1^{-1}y_0, S_1 y_0)$
$\mathcal{R}_1 \cap P^{-1}\mathcal{R}_1^-$	$\mathcal{G}(y_1, R_1^{-1}P y_1, P^{-1}R_1 y_1)$
$\mathcal{R}_1 \cap P^2\mathcal{S}_1$	$\mathcal{G}(y_2, R_1^{-1}P^2 y_2, P^2 S_1^{-1}P^{-3}y_2)$
$\mathcal{R}_1 \cap P^{-2}\mathcal{R}_1^-$	$\mathcal{G}(y_2, R_1^{-1}P^2 y_2, P^{-2}R_1 y_2)$
$P^{-2}\mathcal{R}_1^- \cap P^3\mathcal{S}_1^-$	$\mathcal{G}(y_2, P^{-2}R_1 y_2, P^3 S_1 P^{-2}y_2)$

Table 4: Giraud intersections among bounding bisectors.

in Table 1. Using  $\iota$ , we find an antiholomorphic isometry fixing the spines of  $\mathcal{B}$ . From this we can then find an image of  $y_j$  so that  $\mathcal{B}$  is coequidistant from  $y_j$  and this second point.

To be specific, the real spine of  $\mathcal{R}_1$  is invariant under the involution  $\iota_{23}$  defined in (17). We see that  $\iota_{23} \mathbf{y}_1 = \bar{a}^6 J \mathbf{y}_1$  and  $\iota_{23} \mathbf{y}_2 = a^2 R_1^{-1} P^2 \mathbf{y}_2$ . Therefore, using  $J = R_1^{-1} P$  we see that  $\mathcal{R}_1 = \mathcal{B}(y_1, R_1^{-1} P y_1) = \mathcal{B}(y_2, R_1^{-1} P^2 y_2)$ . Similarly, the spine of  $P^2 \mathcal{S}_1$  is the real span of  $\mathbf{n}_2 = -P^2 \mathbf{n}_{23\bar{2}}$  and  $\mathbf{n}_{123\bar{2}} = P^2 \bar{a} \mathbf{n}_{1\bar{3}23}$ . These two vectors are fixed by  $\bar{a}^2 R_2 \iota_{13}$ , where  $\iota_{13}$  is defined analogously to  $\iota_{23}$ . We find that  $\bar{a}^2 R_2 \iota_{13} \mathbf{y}_2 = a^2 P^2 S_1^{-1} P^{-3} \mathbf{y}_2$ . Therefore  $P^2 \mathcal{S}_1 = \mathcal{B}(y_2, P^2 S_1^{-1} P^{-3} y_2)$ .

The claims in Table 4 follow at once from those in Table 3.  $\square$

#### 4.8.4 Realizing ridges of $\widehat{E}$ - embedding

From the results in Section 4.8.3, we get that  $\phi$  gives a well defined realization of each 2-face  $f$  of  $\widehat{E}$ , inside the intersection of two specific bounding bisectors.

For every other bounding bisector  $\mathcal{B}$ , we now prove that  $\phi(f)$  is on the correct side of  $\mathcal{B}$ . In particular, we will show that  $\phi(f^\circ)$  does not intersect  $\mathcal{B}$ , and  $\mathcal{B}$  intersects  $\phi(f)$  precisely as predicted from the labels in Figures 6 to 8. From this, it follows that  $\phi$  is an embedding on the level of  $\widehat{E}_2$ .

First, observe that when  $\phi(f)$  is in a complex line, no further verifications are needed, due to the following.

**Lemma 4.38** *Let  $Q$  be a polygon contained in a complex line  $C$ , and let  $\mathcal{B}$  be a bisector. If  $\partial Q$  is entirely on one side of  $\mathcal{B}$ , then so is  $Q$ .*

PROOF. The restriction to  $C$  of the orthogonal projection onto the complex spine of  $\mathcal{B}$  is an open map (because it is holomorphic). Recall that a set is entirely on one side of  $\mathcal{B}$  if and only if its orthogonal projection onto the complex spine is in the corresponding half disk bounded by the real spine.  $\square$

Orthogonal projections restricted to Giraud disks are, in general, not open. Hence the cases where  $\phi(f)$  lies in a Giraud disk are considerably more complicated. They will occupy us for the remainder of this section.

Let us start with a Giraud polygon  $T$  in a Giraud disk  $\mathcal{G}$  (i.e. a disk bounded by a piecewise geodesic simple closed curve) and a bisector  $\mathcal{B}$  not containing  $\mathcal{G}$ . We describe a general method to prove that  $T$  is entirely on one side of  $\mathcal{B}$ .

Let  $\mathcal{B} = \mathcal{B}(x_0, x_1)$ , and assume that  $\mathbf{x}_0, \mathbf{x}_1$  are lifts of  $x_0, x_1$  with  $\langle \mathbf{x}_0, \mathbf{x}_0 \rangle = \langle \mathbf{x}_1, \mathbf{x}_1 \rangle$ . Using the parametrization given in Section 2.5 (4), we may write an equation for the trace of  $\mathcal{B}$  on  $\mathcal{G}$  as

$$g(t_1, t_2) = 0, \text{ where } g(t_1, t_2) = |\langle V(t_1, t_2), \mathbf{x}_0 \rangle|^2 - |\langle V(t_1, t_2), \mathbf{x}_1 \rangle|^2. \quad (27)$$

Since  $V(t_1, t_2)$  is affine in each variable, equation (27) is quadratic in each variable.

If we claim that  $\mathcal{B} \cap T$  is empty, we need to prove that  $g$  does not vanish on  $T$ , for instance that  $g > 0$  (switch  $x_0$  and  $x_1$  if needed). In order to do this, we

1. check that  $g > 0$  on the boundary of  $T$  (see Section 2.7).
2. find the critical points of  $g$ . If they are in  $T$ , check the sign of the corresponding values of  $g$ .

This strategy works well in most cases, because of the following.

**Proposition 4.39** *The coefficients of  $g$  lie in the field  $\mathbb{Q}(a, \tau)$ . The fact that  $g$  only has non-degenerate critical points can be proved using computations in that number field, and the critical points can then be computed with arbitrary precision.*

Since the key to these computations is to be able to compute critical points of  $g$ , we expand a little on how this can be done in practice. We write  $g$  as

$$g(t_1, t_2) = a_0 + a_1 t_1 + a_2 t_2 + a_{11} t_1^2 + a_{12} t_1 t_2 + a_{22} t_2^2 + a_{112} t_1^2 t_2 + a_{122} t_1 t_2^2 + a_{1122} t_1^2 t_2^2,$$

where all coefficients are real, and depend explicitly on the vectors  $\mathbf{v}_j, \mathbf{w}_j$  (and are known in exact form, see Proposition 4.39). The partial derivatives of this function are given by

$$\begin{cases} \frac{\partial g}{\partial t_1}(t_1, t_2) = (a_1 + a_{12} t_2 + a_{1122} t_2^2) + 2t_1(a_{11} + a_{112} t_2 + a_{1122} t_2^2) = P_2(t_2) + t_1 Q_2(t_2) \\ \frac{\partial g}{\partial t_2}(t_1, t_2) = (a_2 + a_{12} t_1 + a_{112} t_1^2) + 2t_2(a_{22} + a_{122} t_1 + a_{1122} t_1^2) = P_1(t_1) + t_2 Q_1(t_1) \end{cases}$$

where the polynomials  $P_j, Q_j$  have degree at most two. Coordinates of the critical points must be solutions of a polynomial of degree five, obtained as the resultant of  $\frac{\partial g}{\partial t_1}$  and  $\frac{\partial g}{\partial t_2}$  (with respect to, say  $t_1$ ).

Explicitly, if  $(t_1, t_2)$  is a critical point, then  $t_2$  is a root of  $\sum_{k=0}^5 b_k x^k$  where

$$\begin{aligned} b_0 &= a_1^2 a_{112} + 4a_2 a_{11}^2 - 2a_{12} a_{11} a_1 \\ b_1 &= -4a_{122} a_{11} a_1 + 2a_1^2 a_{1122} + 8a_{22} a_{11}^2 - 2a_{12}^2 a_{11} + 8a_2 a_{11} a_{112} \\ b_2 &= 8a_2 a_{11} a_{1122} + 2a_1 a_{1122} a_{12} - 2a_1 a_{112} a_{122} - 6a_{12} a_{11} a_{122} \\ &\quad + 4a_2 a_{112}^2 - a_{12}^2 a_{112} + 16a_{22} a_{11} a_{112} \\ b_3 &= 8a_2 a_{112} a_{1122} + 8a_{22} a_{112}^2 - 4a_{12} a_{112} a_{122} - 4a_{122}^2 a_{11} + 16a_{22} a_{11} a_{1122} \\ b_4 &= -3a_{122}^2 a_{112} - 2a_{122} a_{1122} a_{12} + 4a_2 a_{1122}^2 + 16a_{22} a_{112} a_{1122} \\ b_5 &= -2a_{122}^2 a_{1122} + 8a_{22} a_{1122}^2 \end{aligned}$$

The real roots of this polynomial can be computed with arbitrary precision, most easily when it only has simple roots (in that case the Sturm algorithm suffices). In particular, we can count critical points and locate them.

There are situations where the resultant has multiple roots, but there is an easy way to work around these, which turns out to work for all verifications needed in our paper. The point is that there is a simple reason why the resultant can have multiple roots, namely that the intersection  $\mathcal{G} \cap \mathcal{B}$  contains a horizontal or a vertical segment.

Each time this happens, we can factor out a linear expression in one of the two variables (or in some cases one factor for each variable), and in fact we will be able to do this exactly (i.e. no numerical approximation is involved).

More specifically, suppose the line  $t_1 = \alpha$  is contained in the graph (the situation is obviously entirely similar for horizontal lines). Then we write the function in the form

$$g(t_1, t_2) = p_0(t_1) + p_1(t_1)t_2 + p_2(t_1)t_2^2,$$

where the  $p_j$  are polynomials of degree at most two. Then the coefficients  $p_0$ ,  $p_1$  and  $p_2$  must have  $\alpha$  as a common root, and these roots are easily computed.

**Lemma 4.40** *The vertical lines in the graph of  $g(t_1, t_2) = 0$  are given by the equations  $t_1 = \alpha$  where  $\alpha$  is a common root of the polynomials  $p_j$ ,  $j = 0, 1, 2$ .*

It can easily be guessed using numerical computations whether or not these three polynomials have a common root; when they do not, these numerical computations constitute a proof (possibly after adjusting the precision). When they seem to have a common root, we need to verify this by exact calculations. We will work out the details of these verifications for some explicit examples below.

Note that when  $\{t_1 = \alpha\}$  is indeed contained in the graph, it is of course easy to extract a factor  $(t_1 - \alpha)$  from  $g(t_1, t_2)$ . Explicitly, we write

$$g(t_1, t_2) = q_0(t_2) + q_1(t_2)t_1 + q_2(t_2)t_1^2 = (t_1 - \alpha)h(t_1, t_2) \tag{28}$$

and equate the coefficients of degree 0 and 2 in  $t_1$ , to get

$$h(t_1, t_2) = q_2(t_2)t_1 + q_1(t_2) + \alpha q_2(t_2).$$

**Remark 4.41** When we do this factorization, it is convenient to adjust the sign of  $h$  so that it has the same sign as  $g$  on the open ridge we are studying. Depending on whether the side lies to the left or right of the line  $t_1 = \alpha$ , we factor either  $(t_1 - \alpha)$  or  $(\alpha - t_1)$ .

The point of this remark is that in order to verify  $g \geq 0$  on a Giraud polygon  $T$ , it is enough to verify that  $h \geq 0$  on  $T$ , and we will do this by computing the critical points of  $h$ . Note that the critical points of  $h$  are of course not the same as those of  $g$ , but they are easier to handle computationally (the relevant resultants will have simple roots, see the above discussion).

We now work out the details of the above computations in some specific cases. In order to allow for the reader to verify the numerical figures given below, we specify explicit coordinates for the relevant Giraud disks, giving specific choices of vectors  $\mathbf{v}_j$  and  $\mathbf{w}_j$  defining spinal coordinates as in (4).

It is convenient to adjust the Giraud disk to be bounded in these coordinates, hence we choose the  $\mathbf{w}_j$  to be negative vectors. For instance, for  $\mathcal{R}_1$  one can choose  $\mathbf{v} = \mathbf{n}_1$  and

$$\mathbf{w} = \langle \mathbf{n}_1, \mathbf{n}_1 \rangle \mathbf{n}_{23} - \langle \mathbf{n}_{23}, \mathbf{n}_1 \rangle \mathbf{n}_1,$$

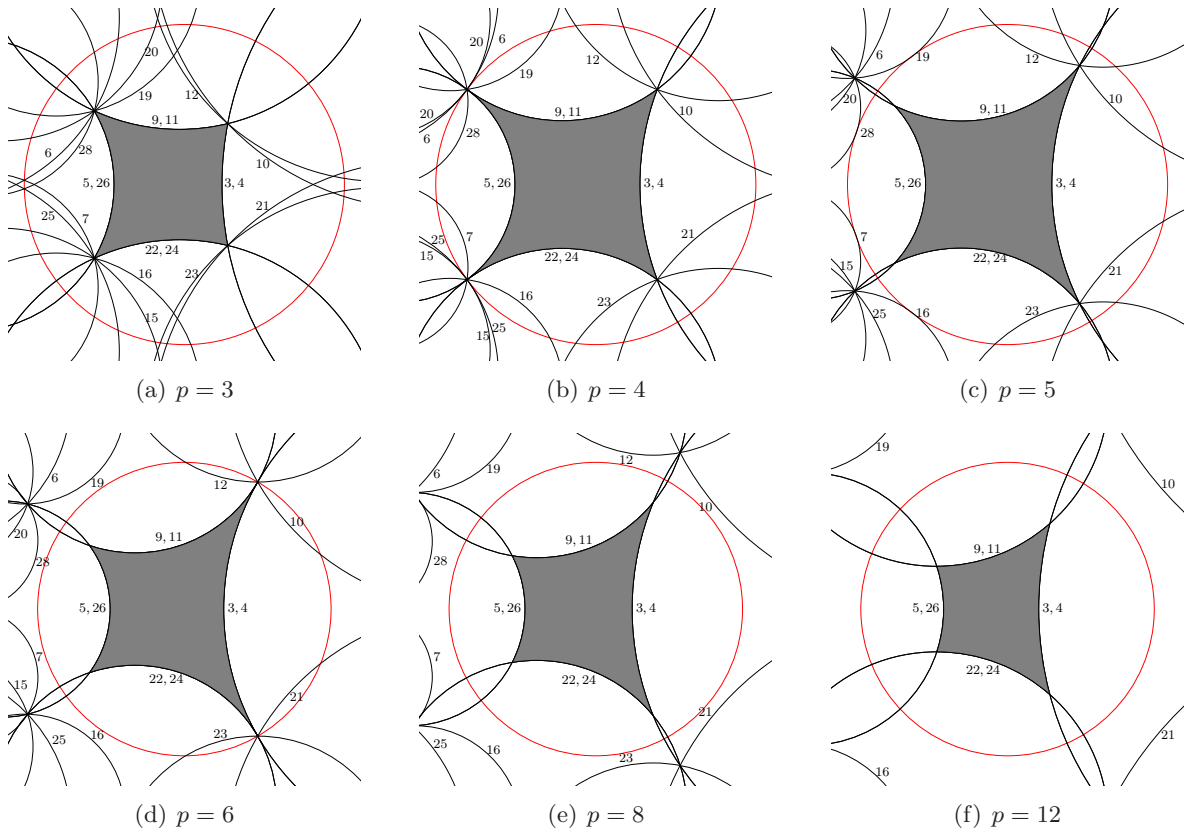


Figure 15: Intersection pattern of all the bounding sides with the complex line  $\mathcal{R}_1 \cap \mathcal{R}_1^-$ , according to the values of  $p$ .

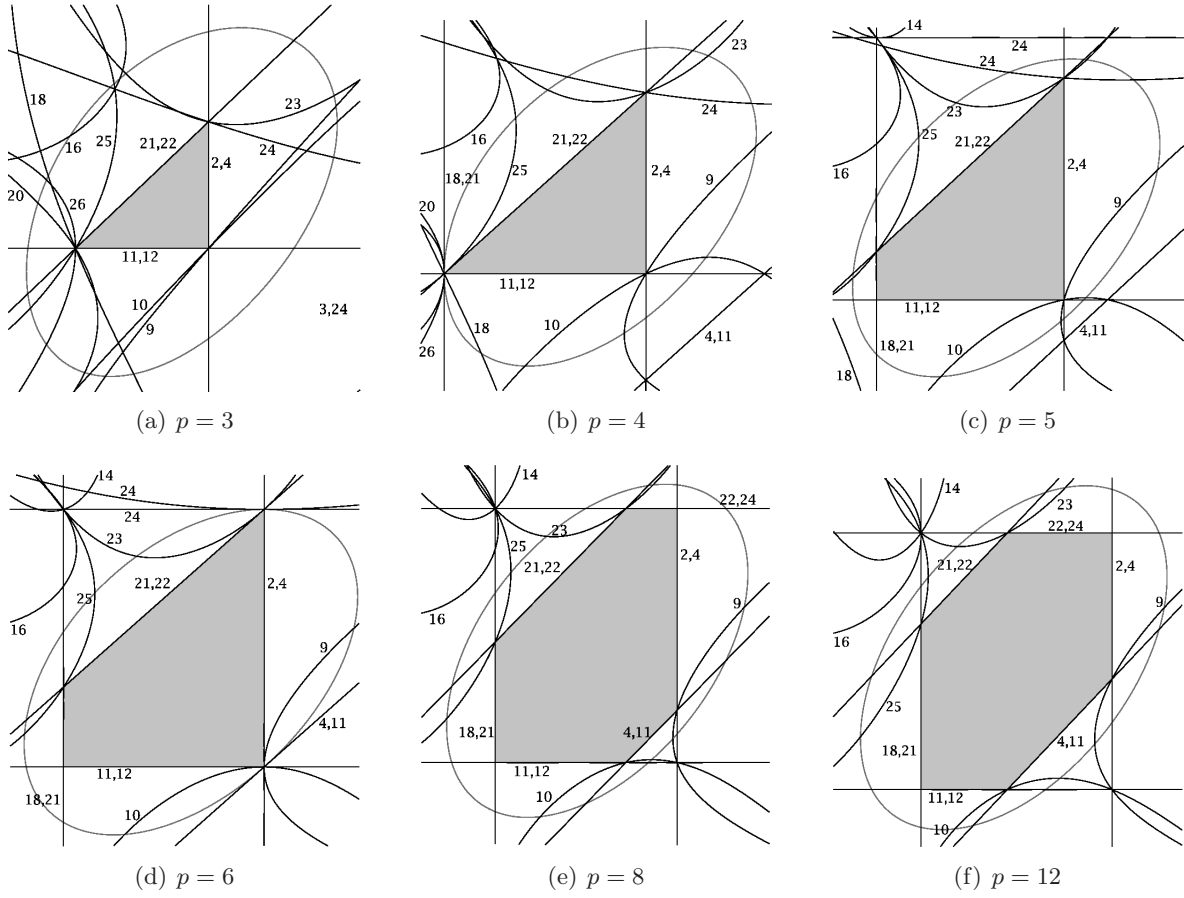


Figure 16: Intersection pattern of all the bounding sides with the Giraud disk  $\mathcal{R}_1 \cap \mathcal{S}_1$ , according to the values of  $p$ .



which corresponds to the intersection of the real spine of  $\mathcal{R}_1$  with the mirror of  $R_1$ . For  $\mathcal{S}_1$ , one can choose  $\mathbf{v} = \mathbf{n}_{23\bar{2}}$  and

$$\mathbf{w} = \langle \mathbf{n}_{23\bar{2}}, \mathbf{n}_{1\bar{3}23} \rangle \{ \langle \mathbf{n}_{23\bar{2}}, \mathbf{n}_{23\bar{2}} \rangle \mathbf{n}_{1\bar{3}23} - \langle \mathbf{n}_{1\bar{3}23}, \mathbf{n}_{23\bar{2}} \rangle \mathbf{n}_{23\bar{2}} \}.$$

There is then a well-defined parametrization for every Giraud intersection of bounding bisectors, obtained from the above vectors by applying  $R_1$ ,  $S_1$  and/or powers of  $P$ .

We give the verifications for one situation, namely  $\mathcal{G} = \mathcal{R}_1 \cap \mathcal{S}_1 = \mathcal{B}_1 \cap \mathcal{B}_3$  (see Table 2 on page 48 for an explanation of the labelling of the sides). For concreteness, we start by assuming  $p = 3$  (for other values of  $p$  and other ridges, the computations are only longer, but not more complicated). In this case  $T$  is a triangle.

The intersection  $\mathcal{G} \cap \mathcal{B}_2$  is particularly easy, since  $\mathcal{R}_1 \cap \mathcal{R}_1^-$  is a complex line, namely the mirror of  $R_1$  (see Section 4.8.3). If we take  $\mathbf{x}_0 = \mathbf{y}_0$ ,  $\mathbf{x}_1 = R_1 \mathbf{y}_0$  and write an equation for  $\mathcal{G} \cap \mathcal{B}_2$ , we get

$$g(t_1, t_2) = 81(582 + 127\sqrt{21})(-14 + 3\sqrt{21} + 3t_2 - 18t_2^2)t_1,$$

where the degree 2 polynomial in  $t_2$  never vanishes, so the intersection is given by the  $t_2$ -axis.

When  $\mathcal{B} = \mathcal{S}_1^- = \mathcal{B}_4$ , we take  $\mathbf{x}_0 = \mathbf{y}_0$ ,  $\mathbf{x}_1 = S_1 \mathbf{x}$ . In that case, we already know that the  $t_2$ -axis is part of  $\mathcal{G} \cap \mathcal{S}_1^-$  (see Section 4.8.2), so we must have  $a_0 = a_2 = a_{22} = 0$ , but in fact no other coefficient vanishes. The reduced equation  $g = f/t_1$  is given by

$$h(t_1, t_2) = 81(6741 + 1471\sqrt{21})(36 - 8\sqrt{21} - 15t_1 + 3t_1\sqrt{21} - 3t_2\sqrt{21} + 9t_2 + 18t_1t_2)/4.$$

Here the partial derivatives are both functions of one variable only, which immediately gives a critical point with coordinates

$$\left( (-3 + \sqrt{21})/6, (5 - \sqrt{21})/6 \right) \approx (0.26376261\dots, 0.06957071\dots).$$

It is easy to verify that this is outside  $T$ .

The case  $\mathcal{B} = P\mathcal{R}_1 = \mathcal{B}_5$  is in a sense generic; there are no horizontal or vertical lines, and the resultant of  $\partial f/\partial t_1$  and  $\partial f/\partial t_2$  with respect to  $t_2$  is given by

$$\begin{aligned} & -223205130784873566 - 48707352729720306\sqrt{21} \\ & + (1289075326223152230 + 281299298043708180\sqrt{21})t_1 \\ & - (1960742086219144494 + 427869001351675404\sqrt{21})t_1^2 \\ & + (2269952366448531240 + 495344216342598840\sqrt{21})t_1^3 \\ & - (1166845194031834926 + 254626496473636566\sqrt{21})t_1^4 \\ & + (259717950970322292 + 56675103317162172\sqrt{21})t_1^5. \end{aligned}$$

This polynomial has precisely one real root, which is a simple root, given approximately by  $t_1 = 0.23860554\dots$ . Substituting this value into the partial derivatives yields a polynomial of degree 1 and a polynomial of degree 2; solving the degree one equation gives one value for  $t_2$ , and we get precisely one critical point with coordinates  $(0.23860554\dots, 0.01603880\dots)$ . This point is outside  $T$ .

From now on, we do not write down all the calculations, but simply mention some of the possible phenomena.

$p$	$\mathcal{B}_2$	$\mathcal{B}_4$	$\mathcal{B}_{11}$	$\mathcal{B}_{12}$	$\mathcal{B}_{18}$
3	$t_1 = 0$	$t_1 = 0$ $t_2 = (7 - \sqrt{21})/21$	$t_1 = (21 + \sqrt{21})/42$ $t_2 = 0$	$t_2 = 0$	$t_1 = (-3 + \sqrt{21})/6$
4	$t_1 = 0$	$t_1 = 0$ $t_2 = 1 - 5\sqrt{7}/14$	$t_1 = (-7 + 5\sqrt{7})/14$ $t_2 = 0$	$t_2 = 0$	$t_1 = (3 - \sqrt{7})/2$
5	$t_1 = 0$	$t_1 = 0$ $t_2 = 0.05801393\dots$	$t_1 = 0.44786394\dots$ $t_2 = 0$	$t_2 = 0$	$t_1 = 0.18371174\dots$
6	$t_1 = 0$	$t_1 = 0$ $t_2 = 4 - 6\sqrt{21}/7$	$t_1 = (-7 + 3\sqrt{21})/14$ $t_2 = 0$	$t_2 = 0$	$t_1 = (5 - \sqrt{21})/2$
8	$t_1 = 0$	$t_1 = 0$ $t_2 = 0.11986937\dots$	$t_1 = 0.57827900\dots$ $t_2 = 0$	$t_2 = 0$	$t_1 = 0.27949078\dots$
12	$t_1 = 0$	$t_1 = 0$ $t_2 = 0.28759793\dots$	$t_1 = 0.80219658\dots$ $t_2 = 0$	$t_2 = 0$	$t_1 = (\sqrt{3} - \sqrt{7})/2$

$p$	$\mathcal{B}_{21}$	$\mathcal{B}_{22}$	$\mathcal{B}_{24}$	$\mathcal{B}_{26}$
3	$t_1 = (-3 + \sqrt{21})/6$ $t_2 = (7 - \sqrt{21})/21$	$t_1 = 1/2 + \sqrt{21}/42$ $t_2 = (5 - \sqrt{21})/6$	$t_2 = (5 - \sqrt{21})/6$	$t_1 = 1/2 + \sqrt{21}/42$
4	$t_1 = (3 - \sqrt{7})/2$ $t_2 = 1 - 5\sqrt{7}/14$	$t_1 = -1/2 + 5\sqrt{7}/14$ $t_2 = 4 - 3\sqrt{7}/2$	$t_2 = 4 - 3\sqrt{7}/2$	$t_1 = -1/2 + 5\sqrt{7}/14$
5	$t_1 = 0.18371174\dots$ $t_2 = 0.05801393\dots$	$t_1 = 0.44786394\dots$ $t_2 = 0.03375000\dots$	$t_2 = 0.03375000\dots$	$t_1 = 0.44786394\dots$
6	$t_1 = (5 - \sqrt{21})/2$ $t_2 = 4 - 6\sqrt{21}/7$	$t_1 = -1/2 + 3\sqrt{21}/14$ $t_2 = (23 - 5\sqrt{21})/2$	$t_2 = (23 - 5\sqrt{21})/2$	$t_1 = -1/2 + 3\sqrt{21}/14$
8	$t_1 = 0.27949078\dots$ $t_2 = 0.11986937\dots$	$t_1 = 0.57827900\dots$ $t_2 = 0.07811509\dots$	$t_2 = 0.07811509\dots$	$t_1 = 0.57827900\dots$
12	$t_1 = 0.45685025\dots$ $t_2 = 0.28759793\dots$	$t_1 = 0.80219658\dots$ $t_2 = 0.20871215\dots$	$t_2 = (5 - \sqrt{21})/2$	$t_1 = 0.80219658\dots$

Table 5: Lines parallel to coordinate axes contained in the graphs, for  $\mathcal{B}_1 \cap \mathcal{B}_3$ .

$p$	Side	Coordinates	Function value
8	$\mathcal{B}_9$	(0.22347669... , 0.06214532...)	11.44128654...
12	$\mathcal{B}_9$	(0.38008133... , 0.18112900...)	0.23597323...
	$\mathcal{B}_{10}$	(0.38823985... , 0.13852442...)	0.18097266...

Table 6: Critical points inside the ridge for  $\mathcal{B}_1 \cap \mathcal{B}_3$ .

Consider the intersection of  $\mathcal{G}$  with  $P\mathcal{S}_1^- = \mathcal{B}_{11}$ , for instance. In that case  $g$  is given by  $27(6741 + 1471\sqrt{21})(-15t_1 + 3t_1\sqrt{21} + 36 - 8\sqrt{21} + 18t_1t_2 - 3t_2\sqrt{21} + 9t_2)(21 - 42t_1 + \sqrt{21})t_2/56$ .

Clearly there are both a horizontal and a vertical line in this intersection, in which case we factor out two linear factors, one linear in  $t_1$  and the other linear in  $t_2$ . The reduced equation is given by the function

$$81(6741 + 1471\sqrt{21})(-15t_1 + 3t_1\sqrt{21} + 36 - 8\sqrt{21} + 18t_1t_2 - 3t_2\sqrt{21} + 9t_2)/4.$$

The latter has one critical point given by

$$\left( (-3 + \sqrt{21})/6, (5 - \sqrt{21})/6 \right) \approx (0.26376261 \dots, 0.06957071 \dots)$$

and this point is outside  $T$ .

In fact for  $p \leq 6$ , all critical points turn out to be outside the Giraud polygon, whereas this is not quite true for  $p = 8$  or  $12$  (see Table 6). For higher values of  $p$ , the computations are a bit longer and more tedious than for  $p = 3$ , since the coefficients of the equations live in slightly larger number fields, but they are not more difficult in any essential way.

For the convenience of the skeptic reader (who may be willing to check our claims), we list all horizontal and vertical lines for curves on  $\mathcal{B}_1 \cap \mathcal{B}_3$ , see Table 5. These are needed to reduce to the case of resultants with only simple root. The numbers given as decimal expansions are written in this manner simply to avoid writing huge formulae, one can easily get explicit algebraic expressions instead.

In Table 6, we list the critical points that lie inside the ridge  $\mathcal{B}_1 \cap \mathcal{B}_3$  (there are critical points inside only for  $p = 8$  and  $p = 12$ ). For each of them, we need to check that the corresponding value of the function  $h$  is strictly positive (recall that  $h$  is equal to the equation of the intersection in most cases, it is obtained by dividing by appropriate linear factors in one variable).

For future reference we mention the following consequence of the above arguments.

**Proposition 4.42** *Let  $\rho$  be a ridge of  $\widehat{E}$ , and let  $D$  be the (Giraud or complex) disk containing  $\phi(\rho)$ . Then there is an open neighborhood  $U$  of  $\phi(\rho)$  in  $D$  such that  $U \cap E = \phi(\rho)$ .*

In particular, even though we did not prove that  $\phi(\rho) = D \cap F$ , we know that  $\phi(\rho)$  is a connected component of  $D \cap F$ .

#### 4.8.5 Realizing sides of $\widehat{E}$

As mentioned early in Section 4.6, no consistency verifications are needed for 3-cells. We do need to check embeddedness. More specifically, we check the following.

**Proposition 4.43** *For each 3-cell  $f$  of  $\widehat{E}$  and every bounding bisector  $\mathcal{B}$ ,  $\phi(f)$  is on the correct side of  $\mathcal{B}$ . In particular,  $\phi(f)$  is contained in  $F$ .*

This will follow from the following result, which is of general independent interest.

**Lemma 4.44** *Let  $f$  be one of the bounding sides and let  $\mathcal{B}$  be any bisector. If  $\mathcal{B}$  intersects the interior  $f^\circ$ , then it intersects its boundary  $\partial f$  as well.*

PROOF. (of Lemma 4.44) We may assume that  $\mathcal{B}$  does not contain  $f$ , and we denote by  $\mathcal{B}_f$  the bisector containing  $f$ . By Lemma 9.1.5 in [Gol99],  $\mathcal{B} \cap \mathcal{B}_f$  is either empty or a union of properly embedded disks. If  $\mathcal{B}$  intersects the interior of  $f$ , then by properness it must also intersect its boundary (in  $\overline{\mathbf{H}}_{\mathbb{C}}^2$ ).  $\square$

PROOF. (of Proposition 4.43) Recall that for each 3-cell  $f$  of  $\widehat{E}$ ,  $\partial f$  is a 2-sphere, and we have checked in Section 4.8.4 that  $\phi$  embeds that 2-sphere inside one of the bounding bisectors  $\mathcal{B}_f$  (as well as inside  $E$ ). Now if  $\mathcal{B}$  is any other bounding bisector,  $\mathcal{B}$  cannot intersect  $\phi(f^\circ)$ . For this we argue by contradiction; if it did, then by Lemma 4.44, it would also intersect  $\phi(\partial f)$ . But this cannot happen, since the closed set  $\phi(f) \cap \mathcal{B} \cap \mathcal{B}_f$  has a neighborhood in  $\mathcal{B} \cap \mathcal{B}_f$  which does not intersect  $\phi(f^\circ)$  (see Proposition 4.42).  $\square$

For completeness, we mention the following consequence of Proposition 4.43.

**Proposition 4.45** *Let  $\mathcal{B}$  be one of the bounding bisectors, and  $f$  the side of  $\widehat{E}$  such that  $\phi(f) \subset \mathcal{B}$ . Then  $\mathcal{B} \cap E = \phi(f)$ .*

Note that we have not proved that  $\phi(f)$  can also be described as  $\mathcal{B} \cap F$ , but once again this is not needed in order to apply the Poincaré polyhedron theorem (see the discussion at the beginning of Section 4).

## 5 Applying the Poincaré polyhedron theorem

We proved in Section 4.6 that  $E$  is a polyhedron. In this section we verify the remaining hypotheses of the Poincaré polyhedron theorem (Sections 5.2 and 5.3). Using the theorem, we obtain a presentation for  $\Gamma$  and we calculate the orbifold Euler characteristic of the quotient orbifold.

Along with the verification of the hypotheses, we will determine local stabilizers of every facet  $f$  of  $E$ . By local stabilizer, we mean the group obtained from the side-pairing maps by following all possible cycles involving  $f$ . The description of local stabilizers for cusps will imply the existence of a consistent system of horoballs.

Note that the local stabilizer of a facet  $f$  is always a subgroup of the full stabilizer of  $f$  in  $\Gamma$ . It will follow from the Poincaré polyhedron that local stabilizers are actually equal to the corresponding full stabilizer. We will determine local stabilizers of ridges in Section 5.2, then for vertices and edges in Section 5.3.

### 5.1 Hypotheses - side pairing

In this section, we describe a side pairing for  $E$  (in the sense of Section 3.2). For each side  $s$ , we define an isometry  $S = \sigma(s)$  that pairs two sides  $s$  and  $s^-$  of  $E$ . We also show that  $E \cap S(E)$  is given precisely by  $s^-$ .

**Lemma 5.1** *The map  $R_1$  sends  $r_1 = \mathcal{R}_1 \cap E$  to  $r_1^- = \mathcal{R}_1^- \cap E$  preserving the cell structure. The map  $S_1$  sends  $s_1 = \mathcal{S}_1 \cap E$  to  $s_1^- = \mathcal{S}_1^- \cap E$  preserving the cell structure.*

PROOF. Using the description of the bisectors given in Table 1 it is clear that  $R_1$  maps  $\mathcal{R}_1$  to  $\mathcal{R}_1^-$ . Moreover,  $R_1$  maps the complex lines containing ridges of  $r_1$  to the complex

lines containing ridges of  $r_1^-$ . Specifically,  $R_1$  sends  $m_1 = \mathcal{R}_1 \cap \mathcal{R}_1^-$  to itself and maps  $m_{23} = \mathcal{R}_1 \cap P^{-3}\mathcal{R}_1^-$  to  $m_{123\bar{1}} = \mathcal{R}_1^- \cap P^3\mathcal{R}_1$ .

We claim that the Giraud disks containing ridges of  $\mathcal{R}_1$  are mapped to Giraud disks containing ridges of  $\mathcal{R}_1^-$ . For a list of these Giraud disks, see Table 4. We give the details for one such Giraud disk, namely  $\mathcal{R}_1 \cap P^2\mathcal{S}_1$ , the other arguments are entirely similar. Recall that the two corresponding bisectors have the following description in terms of the point  $y_2$ :

$$\mathcal{R}_1 = \mathcal{B}(y_2, R_1^{-1}P^2y_2), \quad P^2\mathcal{S}_1 = \mathcal{B}(y_2, P^2S_1^{-1}P^{-3}y_2).$$

Applying  $R_1$  to these bisectors, we obtain

$$\mathcal{R}_1^- = R_1\mathcal{R}_1 = \mathcal{B}(R_1y_2, P^2y_2), \quad R_1P^2\mathcal{S}_1 = \mathcal{B}(R_1y_2, P^2R_1^{-1}P^2y_2).$$

Here we have used  $S_1 = P^2R_1P^{-2}R_1P^2$  and  $P^{-5} = P^2$  to write  $R_1P^2S_1^{-1}P^{-3} = P^2R_1^{-1}P^2$ . The third bisector containing this Giraud disk is

$$\mathcal{B}(P^2y_2, P^2R_1^{-1}P^2y_2) = P^2\mathcal{B}(y_2, R_1^{-1}P^2y_2) = P^2\mathcal{R}_1.$$

Therefore the Giraud disk  $\mathcal{R}_1 \cap P^2\mathcal{S}_1$  is sent by  $R_1$  to the Giraud disk  $\mathcal{R}_1^- \cap P^2\mathcal{R}_1$ .

This shows that the complex lines and Giraud disks containing the ridges of  $r_1$  are sent to complex lines and Giraud disks containing ridges of  $r_1^-$ . The corresponding statement about vertices (resp. edges) follows from the one about ridges, since the vertices (resp. edges) can be described as intersections of ridges. This shows that  $R_1$  maps  $r_1 = \mathcal{R}_1 \cap E$  to  $r_1^- = \mathcal{R}_1^- \cap E$ , preserving the cell structure.  $\square$

We now define the side pairing used in our application of the Poincaré polyhedron theorem.

**Proposition 5.2** *The following map  $\sigma$  defines a side pairing on the sides of  $E$ :*

$$\sigma(P^k r_1^\pm) = P^k R_1^{\pm 1} P^{-k}, \quad \sigma(P^k s_1^\pm) = P^k S_1^{\pm 1} P^{-k},$$

where  $k = -3, \dots, 3$ . Moreover, this side pairing is compatible with  $\Upsilon = \langle P \rangle$ .

PROOF. We only give the argument for  $r_1 = \mathcal{R}_1 \cap E$ . Applying powers of  $P$  and the symmetry  $\iota$  gives the result for the other faces  $P^k r_1^\pm$ , and the faces  $P^k s_1^\pm$  are similar.

In Lemma 5.1 we showed that  $R_1$  sends  $r_1$  to  $r_1^-$  preserving the cell structure. Moreover, the interior of  $E$  is contained in the half-space closer to  $y_0$  than to  $R_1 y_0$ , where  $y_0$  is given in Lemma (4.36). Hence, the interior of  $R_1^{-1}E$  is contained in the half-space closer to  $R_1^{-1}y_0$  than to  $y_0$ . Thus  $E$  and  $R_1^{-1}E$  intersect in  $\mathcal{R}_1 \cap E = r_1$  (see Proposition 4.45) and their interiors are disjoint. Furthermore, any point in the interior of  $r_1$  has an open neighborhood contained in  $E \cup R_1^{-1}E$ .  $\square$

## 5.2 Hypotheses - local tessellation

We now study the ridge cycles of  $E$ , as explained in Section 3.2.

For  $p = 3$  and  $p = 4$  we obtain the ridge cycles given in Table 7. The second column lists the successive ridges in the cycle, given as the intersection of two sides, whereas in the third column we list the corresponding vertices (with ordering coherent with the successive

$R_1$	$r_1 \cap r_1^-$	$p_{12}$	$p_{13}$	$q_{1\bar{3}23}$	$q_{123\bar{2}}$
	$r_1 \cap r_1^-$	$p_{12}$	$p_{13}$	$q_{1\bar{3}23}$	$q_{123\bar{2}}$
$R_1$	$r_1 \cap P^{-1}r_1^-$	$p_{12}$	$p_{13}$	$p_{23}$	
$P^{-1}$	$Pr_1 \cap r_1^-$	$p_{12}$	$p_{13}$	$p_{123\bar{1}}$	
	$r_1 \cap P^{-1}r_1$	$p_{13}$	$p_{23}$	$p_{12}$	
$R_1$	$r_1 \cap P^2s_1$	$p_{23}$	$p_{12}$	$q_{123\bar{2}}$	
$P^2R_1P^{-2}$	$P^2r_1 \cap r_1^-$	$p_{123\bar{1}}$	$p_{12}$	$q_{123\bar{2}}$	
$S_1^{-1}$	$s_1^- \cap P^2r_1^-$	$p_{123\bar{1}}$	$p_{\bar{3}\bar{2}3123}$	$q_{123\bar{2}}$	
$P^2$	$P^{-2}r_1 \cap s_1$	$p_{\bar{3}\bar{2}3123}$	$p_{23}$	$q_{1\bar{3}23}$	
	$r_1 \cap P^2s_1$	$p_{23}$	$p_{12}$	$q_{123\bar{2}}$	
$R_1$	$r_1 \cap s_1$	$p_{23}$	$q_{1\bar{3}23}$	$q_{123\bar{2}}$	
$S_1^{-1}$	$s_1^- \cap r_1^-$	$p_{123\bar{1}}$	$q_{1\bar{3}23}$	$q_{123\bar{2}}$	
$S_1^{-1}$	$s_1^- \cap s_1$	$p_{\bar{3}\bar{2}3123}$	$q_{123\bar{2}}$	$q_{1\bar{3}23}$	
	$r_1 \cap s_1$	$p_{23}$	$q_{1\bar{3}23}$	$q_{123\bar{2}}$	
$S_1$	$s_1 \cap P^2s_1^-$	$p_{23}$	$p_{\bar{3}\bar{2}3123}$	$q_{123\bar{2}}$	
$P^2$	$P^{-2}s_1 \cap s_1^-$	$p_{\bar{3}\bar{2}123}$	$p_{123\bar{1}}$	$q_{1\bar{3}23}$	
	$s_1 \cap P^2s_1^-$	$p_{23}$	$p_{\bar{3}\bar{2}3123}$	$q_{123\bar{2}}$	

Table 7: The ridge cycles for  $p = 3, 4$ . For higher values of  $p$  the cycles are the same, but additional vertices appear in the right and column.

side pairing maps). Applying the side pairing map in the first column (which corresponds to the first side in the second column) gives the line below. The product of these side pairing maps gives the cycle transformation.

This cycle transformation may not be the identity on  $\mathbf{H}_{\mathbb{C}}^2$ , or even on the ridge. However, we can find a power that is the identity, which gives the cycle relation. For example,  $R_1$  maps  $r_1 \cap r_1^-$  to itself and acts as the identity on this ridge (which can be seen from the vertices in the third column). The cycle relation is  $R_1^p = id$ . On the other hand, for  $r_1 \cap P^{-1}r_1^-$  we obtain the cycle transformation  $P^{-1}R_1$ . This maps  $r_1 \cap P^{-1}r_1^-$  to itself but cyclically permutes the vertices. Therefore the cycle relation is  $(P^{-1}R_1)^3 = id$ .

As a last example, we work out the cycle for the ridge  $r_1 \cap P^2s_1$ . It is mapped by  $R_1$  to  $P^2r_1 \cap r_1^-$  (see the proof of Proposition 5.2), which is then mapped by  $P^2R_1P^{-2}$  to  $s_1^- \cap P^2r_1^-$ , which is then mapped by  $S_1^{-1}$  to  $P^{-2}r_1 \cap s_1$ . This is clearly in the image of the original ridge under a power of  $P$ , and the corresponding cycle transformation is

$$P^2 \cdot S_1^{-1} \cdot P^2R_1P^{-2} \cdot R_1.$$

This isometry is in fact the identity (see its expression in terms of the vertices in the last column of Table 7), which corresponds to our definition of  $S_1$  (see Section 4.1).

For  $p = 5, 6, 8$  and  $12$ , the ridge cycles from  $p = 3, 4$  persist, even though the corresponding polygons have extra vertices corresponding to the truncations. We also have an extra ridge cycle associated to  $r_1 \cap P^{-3}r_1^-$  given in Table 8. Note that  $P^{-3}R_1$  maps  $r_1 \cap P^{-3}r_1^-$  to itself but does not act as the identity on this ridge;  $(P^{-3}R_1)^2$  acts as the identity on  $r_1 \cap P^{-3}r_1^-$  but not on  $\mathbf{H}_{\mathbb{C}}^2$  and  $(P^{-3}R_1)^{4p/(p-4)} = id$ . When  $p = 8$  and  $p = 12$  we also have the ridge cycle associated to  $s_1 \cap P^{-2}s_1^-$  given in Table 8.

As a summary, thanks to the action of powers of  $P$  and the freedom to choose the initial ridge inside a given ridge cycle (which does not affect the cycle relation, see Section 3.2), it is

$p \geq 5$	$R_1$	$r_1 \cap P^{-3}r_1^-$	$p_{23}^2$	$p_{23}^{232}$	$p_{23}^{323}$	$p_{23}^3$
	$P^{-3}$	$P^3r_1 \cap r_1^-$	$p_{123\bar{1}}^{12\bar{1}}$	$p_{123\bar{1}}^{1232\bar{1}}$	$p_{123\bar{1}}^{1323\bar{1}}$	$p_{23}^{13\bar{1}}$
		$r_1 \cap P^{-3}r_1^-$	$p_{23}^{323}$	$p_{23}^3$	$p_{23}^2$	$p_{23}^{232}$
$p \geq 8$	$S_1$	$s_1 \cap P^{-2}s_1^-$	$q_{1323}^1$	$q_{1323}^{323}$	$q_{1323}^{13231}$	
	$P^{-2}$	$P^2 \cap s_1^-$	$q_{123\bar{2}}^1$	$q_{123\bar{2}}^{232}$	$q_{123\bar{2}}^{1232\bar{1}}$	
		$s_1 \cap P^{-2}s_1^-$	$q_{1323}^{323}$	$q_{1323}^{1323\bar{1}}$	$q_{1323}^1$	$q_{1323}^{232}$

Table 8: Additional ridge cycles for higher values of  $p$ .

enough to consider the ridges  $r_1 \cap r_1^-$ ,  $r_1 \cap P^{-1}r_1^-$ ,  $r_1 \cap P^2s_1$ ,  $r_1 \cap s_1$ ,  $s_1 \cap P^2s_1^-$ ,  $r_1 \cap P^{-3}r_1^-$  and  $s_1 \cap P^{-2}s_1^-$ . In the penultimate case we only need consider  $p = 5, 6, 8$  and  $12$  and for the last case, we only need consider  $p = 8$  and  $12$ . We now show local tiling around each of these ridges.

Recall that the ridges of  $E$  are of two very different types, depending on whether they are contained in complex lines or in Giraud disks (see Section 4.8.3).

We first consider the complex ridges (see Proposition 4.35 and Section 4.8.4), and show that the local images of  $E$  tessellate around those.

**Lemma 5.3** *The images of  $E$  tessellate a neighborhood of  $r_1 \cap r_1^-$ ,  $r_1 \cap P^{-3}r_1^-$ ,  $s_1 \cap P^2s_1^-$  and  $s_1 \cap P^{-2}s_1^-$  for the appropriate values of  $p$ . Specifically:*

1.  $R_1^k E$  for  $k = 0, 1, \dots, p-1$  cover a neighborhood of the interior of  $r_1 \cap r_1^-$ ;
2. if  $p = 5, 6, 8, 12$  then  $(R_2R_3)^k E$  for  $k = 0, 1, \dots, 2c-1 = 4p/(p-4) - 1$  cover a neighborhood of the interior of  $r_1 \cap P^{-3}r_1^-$ ;
3.  $(R_2R_3R_2^{-1})^k E$  for  $k = 0, 1, \dots, p-1$  cover a neighborhood of the interior of  $s_1 \cap P^2s_1^-$ ;
4. if  $p = 8, 12$  then  $(R_1R_3^{-1}R_2R_3)^k E$  for  $k = 0, 1, \dots, 3d-1 = 6p/(p-6) - 1$  cover a neighborhood of the interior of  $s_1 \cap P^{-2}s_1^-$ .

PROOF. Using Lemma 3.4 it suffices to consider a fixed point  $o$  in each of these ridges and to show that on the orthogonal complex line  $C_o^\perp$  the cycle transformation acts as a rotation through angle  $2\pi/\ell$ .

For Parts 1 and 3 this is straightforward since  $R_1$  and  $R_2R_3R_2^{-1}$  are complex reflections with angle  $2\pi/p$  fixing  $r_1 \cap r_1^-$  and  $s_1 \cap P^2s_1^-$  respectively. For Parts 2 and 4 we find the rotation angle by finding eigenvalues associated to the complex line and the fixed point.

For  $p \geq 5$ , the complex line  $m_{23}$  and the fixed point  $o_{23}$  of  $R_2R_3$  contained in  $m_{23}$  correspond to the eigenvectors  $\mathbf{n}_{23}$  and  $\mathbf{o}_{23}$  of  $R_2R_3$  given by:

$$\mathbf{n}_{23} = \begin{bmatrix} a^3 + \bar{a}^3 \\ a^2\bar{\tau} - \bar{a} \\ \bar{a}^2\tau - a \end{bmatrix}, \quad \mathbf{o}_{23} = \begin{bmatrix} 0 \\ a\tau \\ 1 - i \end{bmatrix}.$$

(Note that  $\langle \mathbf{o}_{23}, \mathbf{o}_{23} \rangle < 0$  for  $p \geq 5$ .) One easily checks that the eigenvalues are  $\bar{a}^2$  and  $-ia$  respectively. Hence the rotation angle is  $(-4\pi/3) - (2\pi/3p - \pi/2) = (p-4)\pi/2p = 2\pi/2c$ .

For  $p \geq 8$ , the complex line  $m_{1\bar{3}23}$  and the fixed point  $o_{1\bar{3}23}$  of  $R_1R_3^{-1}R_2R_3$  correspond to eigenvectors  $\mathbf{n}_{1\bar{3}23}$  and  $\mathbf{o}_{1\bar{3}23}$  given by:

$$\mathbf{n}_{1\bar{3}23} = \begin{bmatrix} a^2 + \bar{a}\bar{\tau} \\ a^4\tau + a \\ a^3 - \bar{a}^3 - \tau \end{bmatrix}, \quad \mathbf{o}_{1\bar{3}23} = \begin{bmatrix} -a^2\bar{\omega} \\ a \\ \bar{\tau} \end{bmatrix}$$

where  $\omega = e^{2\pi i/3}$ . One easily checks that the eigenvalues are  $\bar{a}^2$  and  $-a\omega$  respectively and so the rotation angle is  $(-4\pi/3) - (2\pi/3p - \pi/3) = (p-6)\pi/3p = 2\pi/3d$ .  $\square$

We now consider the Giraud ridges (see Table 4 for a list of the relevant Giraud intersections, and Section 4.8.4 for the fact that these are indeed ridges of  $E$ ).

**Lemma 5.4** *The images of  $E$  tessellate a neighborhood of  $r_1 \cap P^{-1}r_1^-$ ,  $r_1 \cap P^2s_1$  and  $r_1 \cap s_1$ . Specifically:*

1.  $E, R_1^{-1}E$  and  $P^{-1}R_1E$  cover a neighborhood of the interior of  $r_1 \cap P^{-1}r_1^-$ ;
2.  $E, R_1^{-1}E$  and  $P^2S_1^{-1}E$  cover a neighborhood of the interior of  $r_1 \cap P^2s_1$ ;
3.  $E, R_1^{-1}E$  and  $S_1^{-1}E$  cover a neighborhood of the interior of  $r_1 \cap s_1$ .

PROOF. Using Lemma 3.3, this follows from the fact that these three ridges are contained in the Giraud disks given in Table 4. The bounding bisectors defining these Giraud disks are coequidistant from one of  $y_0, y_1$  or  $y_2$ , as indicated in Table 3. These bisectors divide  $\mathbf{H}_{\mathbb{C}}^2$  into three regions as in Lemma 3.3. We know by Lemma 4.36 that  $E$  is contained in the region containing  $y_j$ . By applying the side pairing maps in the ridge cycle we obtain copies of  $E$  contained in the other two regions.  $\square$

This proves that the side pairings of the polyhedron  $E$  satisfy the cycle conditions of the Poincaré polyhedron theorem.

### 5.3 Hypotheses - consistent horoballs

In order to prove the existence of a consistent system of horoballs (see Corollary 5.6 and Corollary 5.9), we need to study local stabilizers of cusps.

In fact we will determine local stabilizers of all vertices (cusps or not), as well as edges. The techniques are similar to those in Section 18.2 of [Mos80]. The order of these stabilizers will be used when we calculate the orbifold Euler characteristic, see Section 5.5.

**Proposition 5.5** *When  $p = 3$  or  $4$  there is a single-orbit of  $p_*$ -vertices. A representative is  $p_{12}$  and its stabilizer is  $\langle R_1, R_2 \rangle$ . Moreover, there is a single orbit of  $(p_*, p_*)$  edges. A representative is  $(p_{13}, p_{12})$  and its stabilizer is  $\langle R_1 \rangle$ .*

PROOF. Since  $p_{23} = P^{-2}p_{12}$ ,  $p_{13} = P^{-1}p_{12}$ ,  $p_{123\bar{1}} = Pp_{12}$  and  $p_{\bar{3}\bar{2}3123} = P^3p_{12}$  it is clear that all  $p_*$ -vertices lie in the same orbit.

The action of the side pairing maps on the  $p_*$ -vertices may be expressed in terms of  $p_{12}$  as follows. We can write such a vertex as  $p_a = P^i p_{12}$ . The side pairing  $R$  maps  $p_a$  to  $p_b$  and we can write  $p_b = P^j p_{12}$ . This corresponds to an element  $P^j R P^{-i}$  of the stabilizer of  $p_{12}$ .



We list the side pairing, the vertex, its image and the corresponding word in the stabilizer of  $p_{12}$  in terms of  $R_1$  and  $R_2$ . Taking the inverse of a side pairing map (resp. conjugating it by a power of  $P$ ) gives the inverse word (resp. a conjugate word).

	Vertex	Image	Word
$R_1$	$p_{12}$	$p_{12}$	$R_1$
$R_1$	$p_{13} = P^{-1}p_{12}$	$p_{13} = P^{-1}p_{12}$	$PR_1P^{-1} = R_1R_2R_1^{-1}$
$R_1$	$p_{23} = P^{-2}p_{12}$	$p_{123\bar{1}} = Pp_{12}$	$P^{-1}R_1P^{-2} = R_2^{-1}R_1^{-1}$
$S_1$	$p_{23} = P^{-2}p_{12}$	$p_{\bar{3}\bar{2}3123} = P^3p_{12}$	$P^{-3}S_1P^{-2} = R_2^{-1}$
$S_1$	$p_{\bar{3}\bar{2}3123} = P^3p_{12}$	$p_{123\bar{1}} = Pp_{12}$	$P^{-1}S_1P^3 = R_2^{-1}R_1^{-1}R_2$

To show that the stabilizer of  $(p_{13}, p_{12})$  is generated by  $R_1$  we argue in the same way as we did for vertex stabilizers. All edges joining two  $p_*$ -vertices are the images under a power of  $P$  of either the edge  $(p_{13}, p_{12})$  or the edge  $(p_{12}, p_{23}) = R_1^{-1}P(p_{13}, p_{12})$ . We describe each edge  $(p_*, p_*)$  and its image under the side pairing in this way and so obtain an element of the stabilizer of  $(p_{13}, p_{12})$ . We do this for the three  $(p_*, p_*)$  edges in  $r_1$  and the single  $(p_*, p_*)$  edge in  $s_1$ . The others follow by applying powers of  $P$ .

	Edge	Image	Word
$R_1$	$(p_{13}, p_{12})$	$(p_{13}, p_{12})$	$R_1$
$R_1$	$(p_{12}, p_{23}) = R_1^{-1}P(p_{13}, p_{12})$	$(p_{12}, p_{123\bar{1}}) = P(p_{13}, p_{12})$	$id$
$R_1$	$(p_{23}, p_{12}) = P^{-1}(p_{13}, p_{12})$	$(p_{123\bar{1}}, p_{13}) = PR_1^{-1}P(p_{13}, p_{12})$	$R_1^{-1}$
$S_1$	$(p_{23}, p_{\bar{3}\bar{2}3123}) = P^{-2}R_1^{-1}P(p_{13}, p_{12})$	$(p_{\bar{3}\bar{2}3123}, p_{123\bar{1}}) = P^3R_1^{-1}P(p_{13}, p_{12})$	$R_1^{-1}$

In fact no group element interchanges  $p_{12}$  and  $p_{13}$ , and so the stabilizer of the edge  $(p_{13}, p_{12})$  is the intersection of the vertex stabilizers, namely  $\langle R_1 \rangle$ .  $\square$

In Proposition 4.3 we found the structure of  $\langle R_1, R_2 \rangle$ . In particular, for  $p = 3$  it is finite. When  $p = 4$ , the point  $p_{12}$  lies on  $\partial\mathbf{H}_{\mathbb{C}}^2$  and we have just verified the conjectural stabilizer given in [DPP11]. Since there is a single orbit of cusps, a consistent system of horoballs comprises a single horoball at  $p_{12}$  and all its images under the local stabilizer. Since the local stabilizer of  $p_{12}$  is generated by complex reflections, any cycle of side pairing maps or elements of  $\Upsilon$  that maps  $p_{12}$  to itself also maps any horoball at  $p_{12}$  to itself. Thus, we immediately have the following corollary:

**Corollary 5.6** *When  $p = 4$ , the (local) stabilizer in  $\Gamma$  of  $p_{12} \in \partial\mathbf{H}_{\mathbb{C}}^2$  contains no loxodromic maps. In particular, there is a consistent system of horoballs.*

**Proposition 5.7** *When  $p \geq 5$  there are two orbits of  $p_*$ -vertices. Representatives are  $p_{12}^1$  and  $p_{13}^1$  with stabilizers  $\langle R_1, (R_1R_2)^2 \rangle$  and  $\langle R_1, (R_1R_3)^2 \rangle$  respectively. There are two orbits of  $(p_*, p_*)$  edges. Representatives are  $(p_{13}^1, p_{12}^1)$  and  $(p_{12}^1, p_{12}^2)$  with stabilizers  $\langle R_1 \rangle$  and  $\langle (R_1R_2)^2 \rangle$  respectively.*

PROOF. The  $\Gamma$ -orbit of  $p_{12}^1$  in  $E$  comprises  $P$ -orbits of  $p_{12}^1$  and  $p_{12}^{\bar{2}12} = R_2^{-1}p_{12}^1$ .

	Vertex	Image	Word
$R_1$	$p_{12}^1$	$p_{12}^1$	$R_1$
$R_1$	$p_{13}^3 = P^{-1}p_{12}^1$	$p_{13}^{\bar{3}1} = P^{-1}R_2^{-1}p_{12}^1$	$R_2PR_1P^{-1} = (R_1R_2)^2R_1^{-2}$
$R_1$	$p_{23}^2 = P^{-2}R_2^{-1}p_{12}^1$	$p_{123}^{\bar{2}1} = Pp_{12}^1$	$P^{-1}R_1P^{-2}R_2^{-1} = R_1(R_1R_2)^{-2}$
$R_1$	$p_{23}^{\bar{3}23} = P^{-2}p_{12}^1$	$p_{123}^{\bar{3}23\bar{1}} = PR_2^{-1}p_{12}^1$	$R_2P^{-1}R_1P^{-2} = R_1^{-1}$
$S_1$	$p_{23}^{\bar{3}23} = P^{-2}p_{12}^1$	$p_{323}^{\bar{2}32} = P^3R_2^{-1}p_{12}^1$	$R_2P^{-3}S_1P^{-2} = id$
$S_1$	$p_{323}^{\bar{2}32} = P^3R_2^{-1}p_{12}^1$	$p_{123}^{\bar{3}23\bar{1}} = PR_2^{-1}p_{12}^1$	$R_2P^{-1}S_1P^3R_2^{-1} = R_1^{-1}$

Finding the stabilizer of  $p_{13}^1$  is done in a similar way.

The orbit and stabilizer of the edge  $(p_{13}^1, p_{12}^1)$  follow as before. A similar argument shows that no element of the group interchanges  $p_{12}^1$  and  $p_{12}^2$ . Therefore the stabilizer of  $(p_{12}^1, p_{12}^2)$  is the intersection of the vertex stabilizers.  $\square$

Note that, since the stabilizer of  $p_{12}^1$  is generated by the commuting complex reflections  $R_1$  and  $(R_1R_2)^3$ , its order is simply  $2p^2/(p-4)$  which is the product of the orders of these reflections.

**Proposition 5.8** *When  $p \leq 6$  there is a single orbit of  $q_*$ -vertices. A representative is  $q_{123\bar{2}}$  with stabilizer  $\langle R_1, R_2R_3R_2^{-1} \rangle$ . There is a single orbit of  $(q_*, q_*)$  edges. A representative is  $(q_{1\bar{3}23}, q_{123\bar{2}})$  with stabilizer  $\langle S_1 \rangle$ .*

PROOF. This is similar to the constructions of the stabilizers of the  $p_*$ -vertices.

	Vertex	Image	Word
$R_1$	$q_{123\bar{2}}$	$q_{123\bar{2}}$	$R_1$
$R_1$	$q_{1\bar{3}23} = P^{-2}q_{123\bar{2}}$	$q_{1\bar{3}23} = P^{-2}q_{123\bar{2}}$	$P^2R_1P^{-2} = R_1(R_2R_3R_2^{-1})R_1^{-1}$
$S_1$	$q_{123\bar{2}}$	$q_{1\bar{3}23} = P^{-2}q_{123\bar{2}}$	$P^2S_1 = (R_2R_3R_2^{-1})^{-1}$
$S_1$	$q_{1\bar{3}23} = P^{-2}q_{123\bar{2}}$	$q_{123\bar{2}}$	$S_1P^{-2} = R_1(R_2R_3R_2^{-1})$

There is one  $P$ -orbit of  $(q_*, q_*)$  edges. Since  $S_1$  interchanges  $q_{1\bar{3}23}$  and  $q_{123\bar{2}}$  we see that the intersection of the vertex stabilizers, namely  $\langle R_1 \rangle$ , has index two in the stabilizer of the edge  $(q_{1\bar{3}23}, q_{123\bar{2}})$ , which is  $\langle S_1 \rangle$ . This is clear since  $R_1 = S_1^2$ .  $\square$

When  $p \leq 5$ , the stabilizer of  $q_{123\bar{2}}$  has order  $24p^2/(6-p)$  by Proposition 4.6. When  $p = 6$  the point  $q_{123\bar{2}}$  lies on  $\partial\mathbf{H}_{\mathbb{C}}^2$ . Once again its stabilizer agrees with that conjectured in [DPP11] and we have:

**Corollary 5.9** *When  $p = 6$ , the (local) stabilizer in  $\Gamma$  of  $q_{123\bar{2}} \in \partial\mathbf{H}_{\mathbb{C}}^2$  contains no loxodromic maps. In particular, there is a consistent system of horoballs.*

A similar argument gives the following result.

**Proposition 5.10** *When  $p = 8, 12$  there is a single orbit of  $q_*$ -vertices. A representative is  $q_{123\bar{2}}^1$  with stabilizer  $\langle R_1, (R_1R_2R_3R_2^{-1})^3 \rangle$ . There are two orbits of  $(q_*, q_*)$  edges. Representatives are  $(q_{1\bar{3}23}^1, q_{123\bar{2}}^1)$  and  $(q_{123\bar{2}}^1, q_{123\bar{2}}^{\bar{2}32})$  with stabilizers  $\langle S_1 \rangle$  and  $\langle R_1R_2R_3R_2^{-1}R_1 \rangle$  respectively.*

Observe that the stabilizer of  $q_{123\bar{2}}^1$  is generated by the commuting complex reflections  $R_1$  and  $(R_1 R_2 R_3 R_2^{-1})^3$ . Its order is  $2p^2/(p-6)$ , the product of the orders of these reflections.

**Proposition 5.11** *For all values of  $p$  there are two orbits of  $(p_*, q_*)$  edges. Representatives are  $(p_{12}^1, q_{123\bar{2}}^1)$  and  $(p_{13}^1, q_{1\bar{3}23}^1)$ , both with stabilizer  $\langle R_1 \rangle$ . (For low values of  $p$  omit the superscript 1 as appropriate.)*

PROOF. Since the vertices of such an edge are in different orbits, the stabilizer of an the edge must be the intersection of the vertex stabilizers. The only thing to check is that these two edges are in distinct orbits. This may be checked easily as before.  $\square$

For completeness, we end this section with a description of the links of ideal vertices, which describe the structure of cusp neighborhoods (see Figure 17). Note that these are compact, so even for  $p = 4$  and  $p = 6$ , our polyhedron  $E$  has finite volume (see Section 3.2).

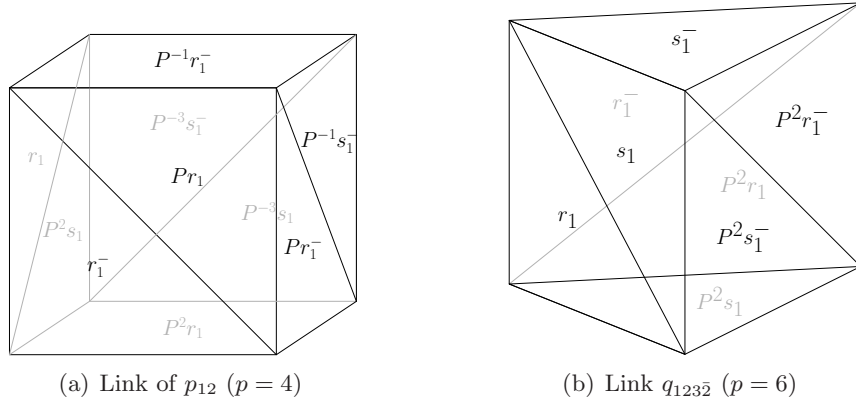


Figure 17: Combinatorics of the links of ideal vertices.

## 5.4 Conclusion - presentation for $\Gamma$

In Section 5.2 we verified that images of  $E$  under the cosets of  $\Upsilon$  in  $\Gamma$  satisfied the local tessellation hypotheses of the Poincaré polyhedron theorem. In Corollaries 5.6 and 5.9 above, we showed that when  $p = 4$  and  $p = 6$  there are consistent horoballs at the cusps. Note that  $E$  has no cusps for the other values of  $p$ . Thus we have verified the hypotheses of the Poincaré polyhedron theorem. Hence we have proved that  $\Gamma$  is discrete and  $E$  is a fundamental polyhedron for the cosets of  $\Upsilon$  in  $\Gamma$ .

We may read off a presentation for  $\Gamma$  directly from the Poincaré polyhedron theorem; compare Section 20 of [Mos80]. The generators of  $\Gamma$  are the side pairing maps  $R_1$  and  $S_1$  of  $E$  together with the generator  $P$  of  $\Upsilon$ . The relations come from the cycle transformations associated to the ridges and the relation from  $\Upsilon$  (there are no reflection relations in this case). For all values of  $p$  we obtain the cycle transformations from Table 7:

$$id = R_1^p = (P^{-1} R_1)^3 = P^2 S_1^{-1} P^2 R_1 P^{-2} R_1 = S_1^{-2} R_1 = (P^2 S_1)^p.$$

In addition, for  $p = 5, 6, 8$  and  $12$ , from Table 8, we obtain  $id = (P^{-3} R_1)^{4p/(p-4)}$  and for  $p = 8, 12$  we obtain  $id = (P^{-2} S_1)^{6p/(p-6)}$ . Finally, we obtain the relation  $id = P^7$  from the

stabilizer of  $\langle P \rangle$  of  $E$ . Thus, the Poincaré theorem gives the presentation:

$$\left\langle R_1, S_1, P \mid \begin{array}{l} id = R_1^p = P^7 = (P^{-1}R_1)^3 = P^2S_1^{-1}P^2R_1P^{-2}R_1 \\ id = S_1^{-2}R_1 = (P^2S_1)^p = (P^{-3}R_1)^{4p/(p-4)} = (P^{-2}S_1)^{6p/(p-6)} \end{array} \right\rangle \quad (29)$$

where we omit the last two relations when the exponent is infinite or negative. Note that for the values of  $p$  where these exponents are negative the two relations still hold and follow from the other relations (compare Corollary 5.6 of [Par06] and Section 2.2 of [Mos80]).

We now simplify the relations and change generators in order to recover the presentation of Theorem 1.2. In particular, we recover the relations found in Section 4.3 only using the cycle relations.

The relation  $id = P^2S_1^{-1}P^2R_1P^{-2}R_1$  clearly implies that  $S_1 = P^2R_1P^{-2}R_1P^2$ ; see (10). Also, Proposition 4.4 implies that  $P^2S_1$  is conjugate to  $R_1^{-1}$ . Hence the relation  $id = (P^2S_1)^p$  is equivalent to  $id = R_1^p$ , and so may be omitted. We now show that the relation  $S_1^2 = R_1$ , which also implies  $S_1R_1 = R_1S_1$ , recovers both the generalized braid relation  $(R_1R_2)^2 = (R_2R_1)^2$  and the braid relation  $R_1(R_2R_3R_2^{-1})R_1 = (R_2R_3R_2^{-1})R_1(R_2R_3R_2^{-1})$ , which were discussed in Section 4.3.

**Lemma 5.12** *Assume that  $P$  has order 7 and that  $J = P^{-1}R_1$  has order 3. Suppose that  $S_1$ ,  $R_2$  and  $R_3$  are defined by*

$$S_1 = P^2R_1P^{-2}R_1P^2, \quad R_2 = JR_1J^{-1} = R_1^{-1}PR_1P^{-1}R_1, \quad R_3 = J^{-1}R_1J = P^{-1}R_1P.$$

*Then, the relation  $S_1^2 = R_1$  is equivalent to  $(R_1R_2)^2 = (R_2R_1)^2$ . Also, the relation  $S_1R_1 = R_1S_1$  is equivalent to  $R_1(R_2R_3R_2^{-1})R_1 = (R_2R_3R_2^{-1})R_1(R_2R_3R_2^{-1})$ .*

PROOF. Using  $P^4 = P^{-3}$ ,  $R_1P^{-1}R_1 = PR_1^{-1}P$  and  $PR_1P^{-1} = R_1R_2R_1^{-1}$ , we have:

$$\begin{aligned} S_1^2R_1^{-1} &= P^2R_1P^{-1}(P^{-1}R_1P^{-1})P^{-1}(P^{-1}R_1P^{-1})P^{-1}R_1P(PR_1^{-1}) \\ &= P(PR_1P^{-1})(R_1^{-1}PR_1^{-1}P^{-1})(R_1^{-1}PR_1^{-1}P^{-1})R_1(PR_1P^{-1})R_1P^{-1} \\ &= P(R_1R_2(R_2R_1)^{-2}R_1R_2)P^{-1}. \end{aligned}$$

Secondly, one easily checks  $R_2R_3R_2^{-1} = R_1^{-1}P^2R_1P^{-2}R_1$ . Therefore

$$\begin{aligned} S_1R_1^{-1}S_1^{-1}R_1 &= P^2R_1P^{-2}R_1P^2R_1^{-1}P^{-2}R_1^{-1}P^2R_1^{-1}P^{-2}R_1 \\ &= R_1(R_2R_3R_2^{-1})R_1(R_2R_3^{-1}R_2^{-1})R_1^{-1}(R_2R_3^{-1}R_2^{-1}). \end{aligned}$$

□

Substituting for  $P^{-1}R_1 = J$ ,  $R_2 = JR_1J^{-1} = R_1^{-1}PR_1P^{-1}R_1$  and  $R_3 = P^{-1}R_1P = J^{-1}R_1J$ , we obtain the presentation given in Theorem 1.2, which agrees with the conjectural presentation given in [DPP11].

## 5.5 Conclusion - orbifold Euler characteristics

In this section we prove Theorem 1.3 which gives the orbifold Euler characteristic of the quotient of  $\mathbf{H}_{\mathbb{C}}^2$  by  $\Gamma$ . We write  $\chi(2\pi/p, \bar{\sigma}_4)$  for the Euler characteristic  $\chi(\Gamma(2\pi/p, \bar{\sigma}_4) \backslash \mathbf{H}_{\mathbb{C}}^2)$  where  $\tau = \bar{\sigma}_4 = -(1 + i\sqrt{7})/2$ .

	Facet	Stabilizer	Order
Vertices	$p_{12}$	$\langle R_1, R_2 \rangle$	$8p^2/(4-p)^2$
	$q_{123\bar{2}}$	$\langle R_1, R_2 R_3 R_2^{-1} \rangle$	$24p^2/(6-p)^2$
Edges	$(p_{12}, p_{13})$	$\langle R_1 \rangle$	$p$
	$(p_{12}, q_{231\bar{2}})$	$\langle R_1 \rangle$	$p$
	$(p_{13}, q_{1\bar{3}23})$	$\langle R_1 \rangle$	$p$
	$(q_{123\bar{2}}, q_{1\bar{3}23})$	$\langle S_1 \rangle$	$2p$
Ridges	$r_1 \cap r_1^-$	$\langle R_1 \rangle$	$p$
	$r_1 \cap P^{-1}r_1^-$	$\langle P^{-1}R_1 \rangle$	3
	$r_1 \cap P^2s_1$	$id$	1
	$r_1 \cap s_1$	$id$	1
	$s_1 \cap P^2s_1^-$	$\langle R_2 R_3 R_2^{-1} \rangle$	$p$
Sides	$r_1$	$id$	1
	$s_1$	$id$	1
Polyhedron	$E$	$\langle P \rangle$	7

Table 9: The Euler characteristic calculation for  $p = 3, 4$ .

We begin by calculating the orbifold Euler characteristic when  $p = 3$  and  $p = 4$ . We choose one representative from each  $\Gamma$ -orbit of facets and give its stabilizer. The stabilizers of vertices and edges, and their orders, were found in Section 5.3. The orders of some vertex stabilizers had also been given in Section 4.3. The ridge cycles described in Section 5.2 give the stabilizers of the ridges. A representative of each orbit of facets and its stabilizer, together with the order of the stabilizer, is given in Table 9. Using these values, the orbifold Euler characteristic is

$$\begin{aligned} \chi(2\pi/p, \bar{\sigma}_4) &= \left( \frac{(4-p)^2}{8p^2} + \frac{(6-p)^2}{24p^2} \right) - \left( \frac{3}{p} + \frac{1}{2p} \right) + \left( \frac{2}{p} + \frac{1}{3} + 2 \right) - 2 + \frac{1}{7} \\ &= \frac{49 - 42p + 9p^2}{14p^2} \end{aligned}$$

Putting in  $p = 3$  and  $p = 4$  we obtain  $\chi(2\pi/3, \bar{\sigma}_4) = 2/63$  and  $\chi(2\pi/4, \bar{\sigma}_4) = 25/224$ .

We now do the same thing for  $p = 5$  and  $p = 6$ . The main difference is that the vertex  $p_{12}$  has become a complex ridge and we introduce several more vertices. The facets, stabilizers and orders in Table 10 imply that the orbifold Euler characteristic is

$$\begin{aligned} \chi(2\pi/p, \bar{\sigma}_4) &= \left( \frac{2(p-4)}{2p^2} + \frac{(6-p)^2}{24p^2} \right) - \left( \frac{3}{p} + \frac{p-4}{2p} + \frac{1}{2p} \right) \\ &\quad + \left( \frac{2}{p} + \frac{1}{3} + 2 + \frac{p-4}{4p} \right) - 2 + \frac{1}{7} \\ &= \frac{15p^2 - 140}{56p^2}. \end{aligned}$$

Putting in  $p = 5$  and  $p = 6$  we obtain  $\chi(2\pi/5, \bar{\sigma}_4) = 47/280$  and  $\chi(2\pi/6, \bar{\sigma}_4) = 25/126$ .

Finally, we consider the cases  $p = 8$  and  $p = 12$ . The facets, stabilizers and orders are given in Table 11, and show that the orbifold Euler characteristic is

	Facet	Stabilizer	Order
Vertices	$p_{12}^1$	$\langle R_1, (R_1 R_2)^2 \rangle$	$2p^2/(p-4)$
	$p_{13}^1$	$\langle R_1, (R_1 R_3)^2 \rangle$	$2p^2/(p-4)$
	$q_{123\bar{1}}$	$\langle R_1, R_2 R_3 R_2^{-1} \rangle$	$24p^2/(6-p)^2$
Edges	$(p_{12}^1, p_{13}^1)$	$\langle R_1 \rangle$	$p$
	$(p_{12}^1, p_{12}^2)$	$\langle (R_1 R_2)^2 \rangle$	$2p/(p-4)$
	$(p_{12}^1, q_{123\bar{2}})$	$\langle R_1 \rangle$	$p$
	$(p_{13}^1, q_{1\bar{3}23})$	$\langle R_1 \rangle$	$p$
	$(q_{123\bar{2}}, q_{1\bar{3}23})$	$\langle S_1 \rangle$	$2p$
Ridges	$r_1 \cap r_1^-$	$\langle R_1 \rangle$	$p$
	$r_1 \cap P^{-1} r_1^-$	$\langle P^{-1} R_1 \rangle$	3
	$r_1 \cap P^2 s_1$	$id$	1
	$r_1 \cap s_1$	$id$	1
	$s_1 \cap P^2 s_1^-$	$\langle R_2 R_3 R_2^{-1} \rangle$	$p$
	$r_1 \cap P^{-3} r_1^-$	$\langle R_2 R_3 \rangle$	$4p/(p-4)$
Sides	$r_1$	$id$	1
	$s_1$	$id$	1
Polyhedron	$E$	$\langle P \rangle$	7

Table 10: The Euler characteristic calculation for  $p = 5, 6$ .

	Orbit	Stabilizer	Order
Vertices	$p_{12}^1$	$\langle R_1, (R_1 R_2)^2 \rangle$	$2p^2/(p-4)$
	$p_{13}^1$	$\langle R_1, (R_1 R_3)^2 \rangle$	$2p^2/(p-4)$
	$q_{123\bar{2}}^1$	$\langle R_1, (R_1 R_2 R_3 R_2^{-1})^3 \rangle$	$2p^2/(p-6)$
Edges	$(p_{12}^1, p_{13}^1)$	$\langle R_1 \rangle$	$p$
	$(p_{12}^1, p_{12}^2)$	$\langle (R_1 R_2)^2 \rangle$	$2p/(p-4)$
	$(p_{12}^1, q_{123\bar{2}}^1)$	$\langle R_1 \rangle$	$p$
	$(p_{13}^1, q_{1\bar{3}23}^1)$	$\langle R_1 \rangle$	$p$
	$(q_{123\bar{2}}^1, q_{1\bar{3}23}^1)$	$\langle S_1 \rangle$	$2p$
	$(q_{123\bar{2}}^1, q_{123\bar{2}}^{232})$	$\langle R_1 R_2 R_3 R_2^{-1} R_1 \rangle$	$4p/(p-6)$
Ridges	$r_1 \cap r_1^-$	$\langle R_1 \rangle$	$p$
	$r_1 \cap P^{-1} r_1^-$	$\langle P^{-1} R_1 \rangle$	3
	$r_1 \cap P^2 s_1$	$id$	1
	$r_1 \cap s_1$	$id$	1
	$s_1 \cap P^2 s_1^-$	$\langle R_2 R_3 R_2^{-1} \rangle$	$p$
	$r_1 \cap P^{-3} r_1^-$	$\langle R_2 R_3 \rangle$	$4p/(p-4)$
	$s_1 \cap P^{-2} s_1^-$	$\langle R_1 R_3^{-1} R_2 R_3 \rangle$	$6p/(p-6)$
Sides	$r_1$	$id$	1
	$s_1$	$id$	1
Polyhedron	$E$	$\langle P \rangle$	7

Table 11: The Euler characteristic calculation for  $p = 8, 12$ .

$$\begin{aligned}
\chi(2\pi/p, \bar{\sigma}_4) &= \left( \frac{2(p-4)}{2p^2} + \frac{(6-p)^2}{24p^2} \right) - \left( \frac{3}{p} + \frac{p-4}{2p} + \frac{1}{2p} + \frac{p-6}{4p} \right) \\
&\quad + \left( \frac{2}{p} + \frac{1}{3} + 2 + \frac{p-4}{4p} + \frac{p-6}{6p} \right) - 2 + \frac{1}{7} \\
&= \frac{-98 + 21p + 2p^2}{14p^2}.
\end{aligned}$$

Putting in  $p = 8$  and  $p = 12$  gives  $\chi(2\pi/8, \bar{\sigma}_4) = 99/448$  and  $\chi(2\pi/12, \bar{\sigma}_4) = 221/1008$ .

## 6 Arithmeticity and Galois theory

### 6.1 Trace fields and commensurability

Recall from [PP09] that we can adjust the generators  $R_1$ ,  $J$  and the Hermitian form  $H$  so that their entries lie in

$$\mathbb{L} = \mathbb{Q}(\tau, e^{2\pi i/p}).$$

Note that after making this adjustment,  $R_1$  no longer has unit determinant.

In this section, we consider the adjoint trace field  $k = \mathbb{Q}(\text{tr Ad } \Gamma)$  for the relevant sporadic triangle groups, i.e. the ones with  $\tau = \bar{\sigma}_4 = -(1 + i\sqrt{7})/2$ , and  $p = 3, 4, 5, 6, 8$  or  $12$ . Recall from [DM86], [Mos80] and [Pau10] that:

**Lemma 6.1** *The field  $\mathbb{Q}(\text{tr Ad } \Gamma)$  is a commensurability invariant of subgroups  $\Gamma < \text{U}(n, 1)$ , where  $\text{tr Ad}(\gamma) = |\text{tr}(\gamma)|^2$  for  $\gamma \in \text{U}(n, 1)$ .*

Since we have arranged for  $R_1$  and  $J$  (as well as the matrix of the Hermitian form  $H$ ) to have entries in  $\mathbb{L} = \mathbb{Q}(\tau, e^{2\pi i/p})$ , the adjoint trace field is contained in  $\mathbb{R} \cap \mathbb{Q}(\tau, e^{2\pi i/p})$ .

In fact it is easy to see by computing the trace of a handful of group elements that  $k$  contains  $\mathbb{Q}(\cos \frac{2\pi}{p}, \sqrt{7} \sin \frac{2\pi}{p})$ . Note that the adjustment indicated above changes the trace of elements of  $\Gamma$ , but the absolute values of these traces remain the same. In fact the following two traces suffice:

$$\begin{aligned}
|\text{tr}(R_1)|^2 &= |e^{4i\pi/3p} + 2e^{-2i\pi/3p}|^2 \\
&= 5 + 4 \cos(2\pi/p), \\
|\text{tr}(JR_1JR_1^{-1})|^2 &= |e^{-2\pi i/3p} - \bar{\tau}e^{4i\pi/3p}|^2 \\
&= 3 - 2\Re(\tau e^{2\pi i/p}) \\
&= 3 + \cos(2\pi/p) + \sqrt{7} \sin(2\pi/p).
\end{aligned}$$

Now clearly we can go from  $k$  to  $\mathbb{L}$  simply by adjoining  $\sqrt{-7}$ , so  $\mathbb{L}$  has degree 2 over  $k$ . This shows that  $k$  is equal to  $\mathbb{R} \cap \mathbb{L}$ , and

$$k = \mathbb{Q}(\cos(2\pi/p), \sqrt{7} \sin(2\pi/p)).$$

More specifically, for the relevant values of  $p$ , we find the fields given in Table 12. This shows that the corresponding six lattices are in different commensurability classes; indeed there is only one pair having the same adjoint trace field, but  $\Gamma(2\pi/3, \bar{\sigma}_4)$  is cocompact whereas  $\Gamma(2\pi/6, \bar{\sigma}_4)$  is not. For completeness, we also recall the following result from [Pau10].

$p$	$k$	Degree
3	$\mathbb{Q}(\sqrt{21})$	2
4	$\mathbb{Q}(\sqrt{7})$	2
5	$\mathbb{Q}(\sqrt{14}\sqrt{5+\sqrt{5}})$	4
6	$\mathbb{Q}(\sqrt{21})$	2
8	$\mathbb{Q}(\sqrt{2}, \sqrt{7})$	4
12	$\mathbb{Q}(\sqrt{3}, \sqrt{7})$	4

Table 12: The list of the adjoint trace fields of the lattices  $\Gamma(2\pi/p, \bar{\sigma}_4)$  shows that these 6 lattices lie in different commensurability classes.

**Theorem 6.2** *None of the six lattices  $\Gamma(2\pi/p, \bar{\sigma}_4)$  is commensurable to any Deligne-Mostow lattice.*

Indeed, the adjoint trace fields of the lattices in [DM86] are all of the form  $\mathbb{R} \cap \mathbb{Q}(\zeta_n) = \mathbb{Q}(\cos \frac{2\pi}{n})$ , and only certain values of  $n$  actually appear in that list. More specifically, each Deligne-Mostow group in  $\text{PU}(2, 1)$  is described by a 5-tuple of rational numbers, and  $n$  is simply the least common denominator of these rational numbers (see [DM86], Section 12). Note that if  $n = 2k$  where  $k$  is odd, then  $\mathbb{Q}(\zeta_n) = \mathbb{Q}(\zeta_k)$ .

Given the degrees that appear in Table 12, it is enough to check the cyclotomic fields of degree 4 or 8. The relevant values of  $n$  are listed in Table 13. Since all groups except the one with  $p = 3$  are non-arithmetic, we only look at the non-arithmetic Deligne-Mostow groups in  $\text{PU}(2, 1)$ . We list the corresponding adjoint trace fields in Table 13. This proves Theorem 6.2.

$n$	$\mathbb{Q}(\zeta_n) \cap \mathbb{R}$	Degree
5 or 10	$\mathbb{Q}(\sqrt{5})$	2
8	$\mathbb{Q}(\sqrt{2})$	2
12	$\mathbb{Q}(\sqrt{3})$	2
15 or 30	$\mathbb{Q}(\sqrt{3}\sqrt{\frac{5+\sqrt{5}}{2}})$	4
16	$\mathbb{Q}(\sqrt{2+\sqrt{2}})$	4
20	$\mathbb{Q}(\sqrt{\frac{5+\sqrt{5}}{2}})$	4
24	$\mathbb{Q}(\sqrt{2}, \sqrt{3})$	4

Table 13: The list of cyclotomic fields whose totally real field has degree 2 or 4.

## 6.2 Arithmeticity

In this section we apply the Mostow–Vinberg arithmeticity criterion (Proposition 3.1) to study arithmeticity. The result (Proposition 6.4) follows from Theorem 4.1 of [Pau10], but for completeness we provide details for this special case. In the coordinates used in the



previous section  $H$  is the following

$$H = \begin{bmatrix} \alpha & \beta & \gamma \\ \bar{\beta} & \alpha & \beta \\ \bar{\gamma} & \bar{\beta} & \alpha \end{bmatrix}$$

where  $\alpha = 2 - e^{2\pi i/p} - e^{-2\pi i/p}$ ,  $\beta = (e^{-2\pi i/p} - 1)\tau$  and  $\gamma = (1 - e^{-2\pi i/p})\bar{\tau}$ . In particular, all entries of  $H$  lie in  $\mathbb{L} = \mathbb{Q}(\tau, e^{2\pi i/p})$ . Observe also that  $\tau = \bar{\zeta}_7 + \bar{\zeta}_7^2 + \bar{\zeta}_7^4$  for  $\zeta_7 = e^{2\pi i/7}$ , so that  $\mathbb{L} \subset \mathbb{Q}(\zeta_7, \zeta_p) = \mathbb{Q}(\zeta_{7p})$ , where the last equality follows from the fact that 7 is coprime to  $p$ .

Let  $k \in \mathbb{N}$ . By the Chinese remainder theorem, there exists  $l \in \mathbb{N}$  such that  $l \equiv 1 \pmod{7}$  and  $l \equiv k \pmod{p}$ . In particular, if  $k$  is coprime to  $p$ ,  $\zeta_{7p} \mapsto \zeta_{7p}^l$  induces an automorphism of  $\mathbb{Q}(\zeta_{7p})$  which fixes  $\zeta_7$  and sends  $\zeta_p$  to  $\zeta_p^k$ ; hence  $\mathbb{L} = \mathbb{Q}(\tau, e^{2\pi i/p})$  has an automorphism fixing  $\tau$  and sending  $\zeta_p$  to  $\zeta_p^k$ . Similarly, there is an automorphism of  $\mathbb{L}$  fixing  $\zeta_p$  and sending  $\tau$  to  $\bar{\tau}$ .

Note that all these automorphisms clearly commute with complex conjugation, so that for any  $\sigma \in \text{Gal}(\mathbb{L}/\mathbb{Q})$ ,  $H^\sigma$  is a Hermitian form. Although  $H$  has signature  $(2, 1)$ , its Galois conjugates  $H^\sigma$  may have various signatures for different  $\sigma$ 's. With the current notation, Proposition 3.1 translates into the following.

**Proposition 6.3** *The lattice  $\Gamma(2\pi/p, \tau)$  is arithmetic if and only if for any  $\sigma \in \text{Gal}(\mathbb{L}/\mathbb{Q})$  not inducing the identity on  $k = \mathbb{R} \cap \mathbb{L}$ , the form  $H^\sigma$  is definite.*

Since the diagonal elements of  $H^\sigma$  are all positive, it is indefinite (i.e it has signature  $(1, 2)$  or  $(2, 1)$ ) precisely when  $\det(H^\sigma) < 0$ . We list values of  $\det(H)$  and all  $\sigma$  with  $\det(H^\sigma) < 0$  in Table 14 (for  $p = 5$  there are two non-trivial Galois automorphisms for which  $\det(H^\sigma) < 0$ , we list both of them). It is quite clear from Table 12 that these automorphisms act non-trivially on the adjoint trace field  $k$ .

$p$	$\tau^\sigma, \zeta_p^\sigma$	$\Gamma^\sigma$	$\det(H)$	$\det(H^\sigma)$
3			$-\frac{1}{2}(9 + 3\sqrt{21})$	
4	$\bar{\tau}, \zeta_4$	$\Gamma(2\pi/4, \sigma_4)$	$-6 - 2\sqrt{7}$	$-6 + 2\sqrt{7}$
5	$\bar{\tau}, \zeta_5$	$\Gamma(2\pi/5, \sigma_4)$	$-\frac{\sqrt{5}}{4}(5 + \sqrt{5} + \sqrt{14}\sqrt{5 - \sqrt{5}})$	$-\frac{\sqrt{5}}{4}(5 + \sqrt{5} - \sqrt{14}\sqrt{5 - \sqrt{5}})$
	$\tau, \zeta_5^2$	$\Gamma(4\pi/5, \bar{\sigma}_4)$		$\frac{\sqrt{5}}{4}(5 - \sqrt{5} + \sqrt{14}\sqrt{5 + \sqrt{5}})$
6	$\bar{\tau}, \zeta_6$	$\Gamma(2\pi/6, \sigma_4)$	$-\frac{1}{2}(5 + \sqrt{21})$	$-\frac{1}{2}(5 - \sqrt{21})$
8	$\tau, \zeta_8^3$	$\Gamma(6\pi/8, \bar{\sigma}_4)$	$-1 + \sqrt{7} - \sqrt{14}$	$-1 - \sqrt{7} - \sqrt{14}$
12	$\tau, \zeta_{12}^5$	$\Gamma(10\pi/12, \bar{\sigma}_4)$	$\frac{3}{2} - \sqrt{3} - \sqrt{7} + \frac{1}{2}\sqrt{21}$	$\frac{3}{2} + \sqrt{3} - \sqrt{7} - \frac{1}{2}\sqrt{21}$

Table 14: Computation of  $\det(H)$  for various values of  $p$ ; when there is one, we list an automorphism  $\sigma$  such that  $H^\sigma$  is indefinite.

**Proposition 6.4** *Consider the groups  $\Gamma(2\pi/p, \bar{\sigma}_4)$ ,  $p = 3, 4, 5, 6, 8$  and 12. Then  $\Gamma(2\pi/p, \bar{\sigma}_4)$  is arithmetic if and only if  $p = 3$ .*

## 7 Appendix: combinatorial data

In this section we gather together the data about the facets of  $E$  and their orbits under  $P$ .

$m_1$	$\xrightarrow{P}$	$m_{12\bar{1}}$	$\xrightarrow{P}$	$m_{123\bar{2}\bar{1}}$	$\xrightarrow{P}$	$m_{1231\bar{3}\bar{2}\bar{1}}$	$\xrightarrow{P}$	$m_{\bar{3}\bar{2}123}$
			$\xrightarrow{P}$	$m_{\bar{3}23}$	$\xrightarrow{P}$	$m_3$	$\xrightarrow{P}$	$m_1$
$m_2$	$\xrightarrow{P}$	$m_{13\bar{1}}$	$\xrightarrow{P}$	$m_{\bar{2}12}$	$\xrightarrow{P}$	$m_{1\bar{3}23\bar{1}}$	$\xrightarrow{P}$	$m_{\bar{3}12\bar{1}3}$
			$\xrightarrow{P}$	$m_{23\bar{2}}$	$\xrightarrow{P}$	$m_{\bar{3}13}$	$\xrightarrow{P}$	$m_2$

Table 15:  $P$ -orbits of mirrors of  $R_1$  and  $R_2$ .

Suppose that  $u$  and  $v$  are words so that  $uv$  is conjugate to 12. If the mirrors of  $m_u$  and  $m_v$  intersect in  $\overline{\mathbf{H}}_{\mathbb{C}}^2$  then their intersection point is denoted  $p_w$ . The relationship between  $u$ ,  $v$  and  $w$  is slightly subtle. The easiest situation is when  $uv = w$ , such as  $m_1 \cap m_2 = p_{12}$ . However, any mirror in the group generated by  $u$  and  $v$  also passes through this point. So, for example,  $m_1 \cap m_{12\bar{1}} = m_{12\bar{1}} \cap m_{\bar{2}12} = p_{12}$ .

$p_{12}$	$\xrightarrow{P}$	$p_{123\bar{1}}$	$\xrightarrow{P}$	$p_{1231\bar{2}\bar{1}}$	$\xrightarrow{P}$	$p_{\bar{3}\bar{2}3123}$	$\xrightarrow{P}$	$p_{\bar{3}123}$
			$\xrightarrow{P}$	$p_{23}$	$\xrightarrow{P}$	$p_{13}$	$\xrightarrow{P}$	$p_{12}$

Table 16:  $P$ -orbits of  $p_*$  vertices, for  $p = 3$  or 4.

If  $m_u$  and  $m_v$  are ultraparallel then we denote their common perpendicular by  $m_w$  where  $u$ ,  $v$  and  $w$  are related as above. In this case the  $P$ -orbit of  $m_w$  may be found using the same subscripts as appear in the  $P$ -orbit of  $p_w$  in the Table 16. In this case,  $m_u$  and  $m_v$  intersect in  $p_w^u$ . The  $P$ -orbits of these points are given in Table 17.

$p_{12}^1$	$\xrightarrow{P}$	$p_{123\bar{1}}^{12\bar{1}}$	$\xrightarrow{P}$	$p_{1231\bar{2}\bar{1}}^{123\bar{2}\bar{1}}$	$\xrightarrow{P}$	$p_{\bar{3}\bar{2}3123}^{1231\bar{3}\bar{2}\bar{1}}$	$\xrightarrow{P}$	$p_{\bar{3}123}^{\bar{3}\bar{2}123}$
			$\xrightarrow{P}$	$p_{23}^{\bar{3}23}$	$\xrightarrow{P}$	$p_{13}^3$	$\xrightarrow{P}$	$p_{12}^1$
$p_{12}^2$	$\xrightarrow{P}$	$p_{123\bar{1}}^{13\bar{1}}$	$\xrightarrow{P}$	$p_{1231\bar{2}\bar{1}}^{\bar{5}12}$	$\xrightarrow{P}$	$p_{\bar{3}\bar{2}3123}^{1\bar{3}23\bar{1}}$	$\xrightarrow{P}$	$p_{\bar{3}123}^{\bar{3}12\bar{1}3}$
			$\xrightarrow{P}$	$p_{23}^{23\bar{2}}$	$\xrightarrow{P}$	$p_{13}^{\bar{3}13}$	$\xrightarrow{P}$	$p_{12}^2$
$p_{12}^{\bar{2}12}$	$\xrightarrow{P}$	$p_{123\bar{1}}^{1\bar{3}23\bar{1}}$	$\xrightarrow{P}$	$p_{1231\bar{2}\bar{1}}^{\bar{3}12\bar{1}3}$	$\xrightarrow{P}$	$p_{\bar{3}\bar{2}3123}^{23\bar{2}}$	$\xrightarrow{P}$	$p_{\bar{3}123}^{\bar{3}13}$
			$\xrightarrow{P}$	$p_{23}^2$	$\xrightarrow{P}$	$p_{13}^{13\bar{1}}$	$\xrightarrow{P}$	$p_{12}^{\bar{2}12}$
$p_{12}^{12\bar{1}}$	$\xrightarrow{P}$	$p_{123\bar{1}}^{123\bar{2}\bar{1}}$	$\xrightarrow{P}$	$p_{1231\bar{2}\bar{1}}^{1231\bar{3}\bar{2}\bar{1}}$	$\xrightarrow{P}$	$p_{\bar{3}\bar{2}3123}^{\bar{3}\bar{2}123}$	$\xrightarrow{P}$	$p_{\bar{3}123}^{\bar{3}23}$
			$\xrightarrow{P}$	$p_{23}^3$	$\xrightarrow{P}$	$p_{13}^1$	$\xrightarrow{P}$	$p_{12}^{12\bar{1}}$

Table 17: For  $p = 5$  or 6, there are four  $P$ -orbits of  $p_*$  vertices.

Similarly, suppose  $u$  and  $v$  are words in  $\Gamma$  so that  $uv$  is conjugate to  $123\bar{2}$ . If  $m_u$  and  $m_v$  intersect in  $\overline{\mathbf{H}}_{\mathbb{C}}^2$  then we denote their intersection point by  $q_w$ , where  $u$ ,  $v$  and  $w$  where  $w$  is conjugate in the group generated by  $u$  and  $v$  to  $uv$ . These vertices are listed in Table 18.

If  $m_u$  and  $m_v$  are ultraparallel then we denote their common perpendicular by  $m_w$ , where  $u$ ,  $v$ ,  $w$  are related as before. The intersection point of  $m_u$  and  $m_w$  is denoted  $q_w^u$ ; see Table 19.

$q_{123\bar{2}}$	$\xrightarrow{P}$	$q_{12\bar{1}\bar{3}13}$	$\xrightarrow{P}$	$q_{2\bar{3}\bar{2}123}$	$\xrightarrow{P}$	$q_{13\bar{1}\bar{3}23}$	$\xrightarrow{P}$	$q_{\bar{2}123}$
			$\xrightarrow{P}$	$q_{1\bar{3}23}$	$\xrightarrow{P}$	$q_{12\bar{1}\bar{3}}$	$\xrightarrow{P}$	$q_{123\bar{2}}$

Table 18:  $P$ -orbits of  $q_*$  vertices, for  $3 \leq p \leq 6$ .

$q_{1\bar{3}23}^1$	$\xrightarrow{P}$	$q_{12\bar{1}\bar{3}}^{1\bar{2}}$	$\xrightarrow{P}$	$q_{123\bar{2}}^{1\bar{2}\bar{3}\bar{1}}$	$\xrightarrow{P}$	$q_{12\bar{1}\bar{3}13}^{1\bar{2}\bar{3}\bar{1}\bar{2}}$	$\xrightarrow{P}$	$q_{\bar{2}\bar{3}\bar{2}123}^{\bar{3}\bar{2}\bar{1}}$
			$\xrightarrow{P}$	$q_{13\bar{1}\bar{3}23}^{\bar{3}\bar{2}\bar{3}}$	$\xrightarrow{P}$	$q_{\bar{2}123}^{\bar{3}}$	$\xrightarrow{P}$	$q_{1\bar{3}23}^1$
$q_{1\bar{3}23}^{\bar{3}\bar{2}\bar{3}}$	$\xrightarrow{P}$	$q_{12\bar{1}\bar{3}}^3$	$\xrightarrow{P}$	$q_{123\bar{2}}^1$	$\xrightarrow{P}$	$q_{12\bar{1}\bar{3}13}^{1\bar{2}\bar{1}}$	$\xrightarrow{P}$	$q_{\bar{2}\bar{3}\bar{2}123}^{1\bar{2}\bar{3}\bar{2}\bar{1}}$
			$\xrightarrow{P}$	$q_{13\bar{1}\bar{3}23}^{1\bar{2}\bar{3}\bar{1}\bar{2}\bar{3}}$	$\xrightarrow{P}$	$q_{\bar{2}123}^{\bar{3}\bar{2}\bar{1}}$	$\xrightarrow{P}$	$q_{1\bar{3}23}^{\bar{3}\bar{2}\bar{3}}$
$q_{1\bar{3}23}^{1\bar{3}\bar{2}\bar{3}\bar{1}}$	$\xrightarrow{P}$	$q_{12\bar{1}\bar{3}}^{\bar{3}\bar{1}\bar{2}\bar{1}\bar{3}}$	$\xrightarrow{P}$	$q_{123\bar{2}}^{2\bar{3}\bar{2}}$	$\xrightarrow{P}$	$q_{12\bar{1}\bar{3}13}^{\bar{3}\bar{1}\bar{3}}$	$\xrightarrow{P}$	$q_{\bar{2}\bar{3}\bar{2}123}^2$
			$\xrightarrow{P}$	$q_{13\bar{1}\bar{3}23}^{1\bar{3}\bar{1}}$	$\xrightarrow{P}$	$q_{\bar{2}123}^{\bar{2}\bar{1}\bar{2}}$	$\xrightarrow{P}$	$q_{1\bar{3}23}^{1\bar{3}\bar{2}\bar{3}\bar{1}}$

Table 19: For  $p = 8$  or  $12$ , there are three  $P$ -orbits of  $q_*$  vertices.

## References

- [ACT02] D. Allcock, J. A. Carlson, and D. Toledo. The complex hyperbolic geometry of the moduli space of cubic surfaces. *J. Algebraic Geom.*, 11(4):659–724, 2002.
- [BHH87] G. Barthel, F. Hirzebruch, and T. Höfer. *Geradenkonfigurationen und Algebraische Flächen*. Aspects of Mathematics, D4. Friedr. Vieweg & Sohn, Braunschweig, 1987.
- [CJ76] J. H. Conway and A. J. Jones. Trigonometric diophantine equations (on vanishing sums of roots of unity). *Acta Arithmetica*, 30:229–240, 1976.
- [Coh93] H. Cohen. *A course in computational algebraic number theory*, volume 138 of *Graduate Texts in Mathematics*. Springer-Verlag, Berlin, 1993.
- [Cor92] K. Corlette. Archimedean superrigidity and hyperbolic geometry. *Ann. of Math. (2)*, 135(1):165–182, 1992.
- [CS10] D. I. Cartwright and T. Steger. Enumeration of the 50 fake projective planes. *C. R. Math. Acad. Sci. Paris*, 348(1-2):11–13, 2010.
- [Der05] M. Deraux. Dirichlet domains for the Mostow lattices. *Experiment. Math.*, 14(4):467–490, 2005.
- [Der06] M. Deraux. Deforming the  $\mathbb{R}$ -Fuchsian  $(4,4,4)$ -triangle group into a lattice. *Topology*, 45:989–1020, 2006.
- [DFP05] M. Deraux, E. Falbel, and J. Paupert. New constructions of fundamental polyhedra in complex hyperbolic space. *Acta Math.*, 194:155–201, 2005.
- [DM86] P. Deligne and G. D. Mostow. Monodromy of hypergeometric functions and non-lattice integral monodromy. *Inst. Hautes Études Sci. Publ. Math.*, 63:5–89, 1986.
- [DM93] P. Deligne and G. D. Mostow. *Commensurabilities among lattices in  $PU(1, n)$* , volume 132 of *Annals of Mathematics Studies*. Princeton Univ. Press, Princeton, 1993.

- [DPP11] M. Deraux, J. R. Parker, and J. Paupert. Census for the complex hyperbolic sporadic triangle groups. *Experiment. Math.*, 20:467–486, 2011.
- [FP06] E. Falbel and J. Parker. The geometry of the Eisenstein-Picard modular group. *Duke Math. J.*, 131:249–289, 2006.
- [Gir21] G. Giraud. Sur certaines fonctions automorphes de deux variables. *Ann. Sci. École Norm. Sup.*, 38:43–164, 1921.
- [Gol99] W. M. Goldman. *Complex Hyperbolic Geometry*. Oxford Mathematical Monographs. Oxford University Press, 1999.
- [GPS88] M. Gromov and I. Piatetski-Shapiro. Nonarithmetic groups in Lobachevsky spaces. *Inst. Hautes Études Sci. Publ. Math.*, 66:93–103, 1988.
- [GS92] M. Gromov and R. Schoen. Harmonic maps into singular spaces and  $p$ -adic super-rigidity for lattices in groups of rank one. *Inst. Hautes Études Sci. Publ. Math.*, 76:165–246, 1992.
- [Hir83] F. Hirzebruch. Arrangements of lines and algebraic surfaces. In *Arithmetic and Geometry, Vol. II*, volume 36 of *Progr. Math.*, pages 113–140. Birkhäuser Boston, Mass., 1983.
- [HP96] S. Hersonsky and F. Paulin. On the volumes of complex hyperbolic manifolds. *Duke Math. J.*, 84(3):719–737, 1996.
- [Hsi03] P.-H. Hsieh. Cotranchal bisectors in complex hyperbolic space. *Geom. Dedicata*, 97:93–98, 2003. Special volume dedicated to the memory of Hanna Miriam Sandler (1960–1999).
- [Kat08] F. Kato. On the Shimura variety having Mumford’s fake projective plane as a connected component. *Math. Z.*, 259:631–641, 2008.
- [Kli03] B. Klingler. Sur la rigidité de certains groupes fondamentaux, l’arithmécité des réseaux hyperboliques complexes, et les “faux plans projectifs”. *Invent. Math.*, 153(1):105–143, 2003.
- [KM12] A. Kappes and M. Möller. Lyapunov spectrum of ball quotients with applications to commensurability questions. Preprint, [arXiv:1207.5433](https://arxiv.org/abs/1207.5433), 2012.
- [Kon00] S. Kondo. A complex hyperbolic structure for the moduli space of curves of genus three. *J. Reine Angew. Math.*, 525:219–232, 2000.
- [Mar75] G. A. Margulis. Discrete groups of motions of manifolds of nonpositive curvature. In *Proceedings of the International Congress of Mathematicians (Vancouver, B.C., 1974)*, Vol. 2, pages 21–34. Canad. Math. Congress, Montreal, Que., 1975.
- [Mar91] G. A. Margulis. *Discrete subgroups of semisimple Lie groups*, volume 17 of *Ergebnisse der Mathematik und ihrer Grenzgebiete*. Springer-Verlag, Berlin, 1991.
- [McM13] C. T. McMullen. The Gauss-Bonnet theorem for cone manifolds and volumes of moduli spaces. Preprint, 2013.

- [McR06] D. B. McReynolds. Finite subgroups of arithmetic lattices in  $U(2, 1)$ . *Geom. Dedicata*, 122:135–144, 2006.
- [Mos80] G. D. Mostow. On a remarkable class of polyhedra in complex hyperbolic space. *Pacific J. Math.*, 86:171–276, 1980.
- [Par06] J. R. Parker. Cone metrics on the sphere and Livne’s lattices. *Acta Math.*, 196:1–64, 2006.
- [Par08] J. R. Parker. Unfaithful complex hyperbolic triangle groups I: Involutions. *Pacific J. Math.*, 238:145–169, 2008.
- [Par] J. R. Parker. *Complex Hyperbolic Kleinian Groups*. Cambridge University Press, To appear.
- [Pau10] J. Paupert. Unfaithful complex hyperbolic triangle groups III: arithmeticity and commensurability. *Pacific J. Math.*, 245:359–372, 2010.
- [Pic81] E. Picard. Sur une extension aux fonctions de deux variables du problème de Riemann relatif aux fonctions hypergéométriques. *Ann. Sci. École Norm. Sup. (2)*, 10:305–322, 1881.
- [PP09] J. R. Parker and J. Paupert. Unfaithful complex hyperbolic triangle groups II: Higher order reflections. *Pacific J. Math.*, 239:357–389, 2009.
- [PY07] G. Prasad and S.-K. Yeung. Fake projective planes. *Invent. Math.*, 168(2):321–370, 2007.
- [Rag72] M. S. Raghunathan. *Discrete subgroups of Lie groups*. Springer-Verlag, New York, 1972. *Ergebnisse der Mathematik und ihrer Grenzgebiete, Band 68*.
- [Rez95] A. Reznikov. Simpson’s theory and superrigidity of complex hyperbolic lattices. *C. R. Acad. Sci. Paris Sér. I Math.*, 320(9):1061–1064, 1995.
- [Sau90] J. K. Sauter. Isomorphisms among monodromy groups and applications to lattices in  $PU(1, 2)$ . *Pacific J. Math.*, 146(2):331–384, 1990.
- [Sch02] R. E. Schwartz. Complex hyperbolic triangle groups. In *Proceedings of the International Congress of Mathematicians, Vol. II (Beijing, 2002)*, pages 339–349, Beijing, 2002. Higher Ed. Press.
- [Sch03] R. E. Schwartz. Real hyperbolic on the outside, complex hyperbolic on the inside. *Inv. Math.*, 151(2):221–295, 2003.
- [Shv92] O. V. Shvartsman. An example of a nonarithmetic discrete group in the complex ball. In *Lie groups, their discrete subgroups, and invariant theory*, volume 8 of *Adv. Soviet Math.*, pages 191–196. Amer. Math. Soc., Providence, RI, 1992.
- [Sto12] M. Stover. Arithmeticity of complex hyperbolic triangle groups. *Pacific J. Math.*, 257(1):243–256, 2012.
- [Tho10] J. M. Thompson. *Complex hyperbolic triangle groups*. PhD thesis, Durham University, 2010.

- [Thu98] W. P. Thurston. Shapes of polyhedra and triangulations of the sphere. *Geometry and Topology Monographs*, 1:511–549, 1998.
- [Tit66] J. Tits. Classification of algebraic semisimple groups. In *Algebraic Groups and Discontinuous Subgroups (Proc. Sympos. Pure Math., Boulder, Colo., 1965)*, pages 33–62. Amer. Math. Soc., Providence, R.I., 1966.
- [Vin68] E. B. Vinberg. Discrete groups generated by reflections in Lobačevskiĭ spaces. *Math. USSR Sb.*, 1:429–444, 1968.
- [Wei60] A. Weil. Algebras with involutions and the classical groups. *J. Indian Math. Soc.*, 24:589–623 (1961), 1960.
- [Yeu04] S.-K. Yeung. Integrality and arithmeticity of co-compact lattice corresponding to certain complex two-ball quotients of Picard number one. *Asian J. Math.*, 8(1):107–129, 2004.
- [Zha12] T. Zhao. New construction of fundamental domains for certain Mostow groups. *Pacific J. Math.*, 259(1):209–256, 2012.

MARTIN DERAUX  
INSTITUT FOURIER, UNIVERSITÉ DE GRENOBLE 1  
deraux@ujf-grenoble.fr

JOHN R. PARKER  
DEPARTMENT OF MATHEMATICAL SCIENCES, DURHAM UNIVERSITY  
j.r.parker@durham.ac.uk

JULIEN PAUPERT  
SCHOOL OF MATHEMATICAL AND STATISTICAL SCIENCES, ARIZONA STATE UNIVERSITY  
paupert@asu.edu